Iron Homeostasis in Neuron-Glia Interaction

Dissertation

for the award of the degree

Doctor rerum naturalium

of the Georg-August University Göttingen

within the program Genes and Development

of the Georg-August University School of Science (GAUSS)

submitted by

Tina Kling

born in

Pforzheim, Germany

Göttingen, 2016

Members of the Thesis Committee:

Supervisor

Prof. Dr. Mikael Simons

Max Planck Institute for Experimental Medicine, Göttingen

Department of Molecular Neurobiology, Technical University of Munich

Second member of the thesis committee

Prof. Dr. Christian Klämbt

Institut für Neurobiologie, Westfälische Wilhelms Universität, Münster

Third member of the thesis committee:

Prof. Dr. Jörg Großhans

Institut für Entwicklungsbiochemie, Universiätsmedizin, Göttingen

Extended Thesis Committee:

Prof. Dr. Gregor Bucher, Georg-August University Göttingen

Prof. Dr. Ralf Heinrich, Georg-August University Göttingen

PD Dr. Hauke Werner, Max Planck Institute for Experimental Medicine, Göttingen

Date of Disputation: 19.09.2016

Affidavit

I hereby declare that this PhD thesis “Iron Homeostasis in Neuron-Glia Interaction” has been written independently with no other aids or sources than quoted.

Tina Kling

July 2016

Göttingen, Germany

All religions, arts and sciences are branches of the same tree. All these aspirations are directed toward ennobling man's life, lifting it from the sphere of mere physical existence and leading the individual towards freedom.

Albert Einstein'Moral Decay', Out of My Later Years (1937, 1995)

Contents

List of Figures

List of Tables

Abbreviations

A1	abdominal segment 1
AD	Alzheimer's disease
AEL	after egg lay
ANOVA	Analysis of variance
Appl	Amyloid precursor protein like
APS	Ammonium persulfate
ATP	Adenosine triphosphate
BBB	blood-brain barrier
BPS	Bathophenanthrolinedisulfonic acid disodium
Brp	Bruchpilot
BSA	Bovine serum albumin
CD8	cluster of differentiation
cDNA	Complementary DNA
Cni	Cornichon
CNS	Central nervous system
D. viri	*Drosophila virilis*
D.m.	*Drosophila melanogaster*
ddH_2O	double-distilled water
DFO	Deferoxamine
DIV	days in vitro
Dlg	Disc large
DMT1	Divalent metal transporter 1
DNA	Deoxyribonucleoteic acid
Dpr-2	Defective proboscis extension response 2
dsRNA	double stranded RNA
EGFR	Epidermal growth factor receptor
elav	embryonic lethal abnormal vision
ER	Endoplasmic reticulum
ERES	ER intermediate compartment
FAC	ferric ammonium citrate
Fas2	Fasciclin 2
Fe^{2+}	ferrous iron
Fe^{3+}	ferric iron
Fer1HCH	Ferritin 1 heavy chain
Fer2LCH	Ferritin 2 light chain

FGF	Fibroblast growth factor
FRDA	Friedreich's ataxia
Fth	Ferritin 1 heavy chain, mouse
Ftl	Ferritin light chain, mouse
g = RCF	relative centrifugal force
Gbb	Glass bottom boat
gcm	glia cell missing
GFP	Green fluorescent protein
Glaz	Glial lazarillo
Gli	Gliotactin
GOLD	Golgi dynamics
Golgi	Golgi apparatus
GPI	Glycosylphosphatidyinositol
h	Hour
HRP	Horseradish peroxidase
IgSF	Immunoglobulin superfamily
IRE	iron responsive element
IRP	iron responsive protein
ISC	iron-sulfur (Fe-S) cluster
ISF	interstitial fluid
L	Liter
LIP	labile iron pool
Loco	Locomation defects
Lpp	Lipophorin
M	Mole
MCO	multi copper oxidase
MCS	Multiple cloning site
MCT1	Monocarboxylate transporter 1
min	Minute
mRNA	messenger RNA
NADH	Nicotinamide adenine dinucleotide
NCC69	sodium chloride cotransporter 69
NL	Neural lamina
NMJ	neuromuscular junction
NPC	neuroepithelial progenitor cell
Nrg	Neuroglian
Nrg-1	Neuregulin-1
Nrv2	Nervana 2
NrxIV	NeurexinIV
n-syb	neuronal synaptobrevin

OPC	oligodendrocyte precursor cell
opm	opossum
ORF	open reading frame
PAGE	Polyacrylamide gel electrophoresis
PBS	Phosphate buffered saline
PCR	Polymerase chain reaction
PD	Parkinson's disease
PDGF	Platelet-derived growth factor
PFA	Paraformaldehyde
PG	Perineurial glia
PNS	Peripheral nervous system
Ppk	Pickpocket
pSJ	Pleated septate junction
QUAS	QF upstream activating sequence
repo	reverse polarity
RfA	Reading frame A
Robo	Roundabout
ROS	reactive oxygen species
RT	Room temperature
RT-PCR	Reverse transcription polymerase chain reaction
Scara-5	Scavenger receptor class A, member 5
SDS	sodium dodecyl sulfate
sec	Second
SEM	Standard error of the mean
shRNA	Short hairpin RNA
SN	Substantia nigra
SPG	Subperineurial glia
TCA	tricarboxylic acid cycle
TEMED	N'N'N'-tetramethylethylene diamine
Tf	Transferrin
TGF	Transforming growth factor
Tim-2	T-cell immunoglobulin and muncin domain protein 2
TUNEL	Terminal deoxynucleotidyl transferase dUTP nick end labeling
U	unit
UAS	Upstream activating sequence
unc5	uncoordinated 5
Unc-5	Uncoordinated 5
UTR	untranslated region
VNC	ventral nerve cord
WG	Wrapping glia

Wg	Wingless
Yp-2	Yolk protein 2
Zip13	zinc and iron-regulated transporter protein 13

Acknowledgements

I would like to take the opportunity to thank the people who significantly contributed to this work and to the invaluable experiences I made during my time in Göttingen. I thank my supervisor Mikael Simons for giving me the chance to work in his lab. Thank you Mika for giving me freedom in performing experiments, for trusting in me, for introducing me to the world of science, and for guiding my project in the right direction.

I appreciate the important suggestions, time and support of my thesis committee members Prof. Jörg Großhans and Prof. Christian Klämbt. I am especially grateful to Christian's unlimited help and mentorship. I always look up to you as a great scientist and person.

Furthermore, I thank Prof. Gregor Bucher, Prof. Ralf Heinrich and PD Hauke Werner for being part of my examination board.

I sincerely acknowledge our collaborators Prof. Moritz Rossner and PD Dr. Olaf Jahn for their efforts. I thank Dr. Ginger Carney and Prof. Susan Eaton for providing reagents and fly lines and Prof. Herbert Jäckle's laboratory for their measureless support in providing fly food, without which the project would have been impossible. My further gratitude goes to the Vienna *Drosophila* RNAi Center and the Bloomington Stock Center for providing transgenic fly lines, to the Developmental Hydridoma Bank for antibodies and to Addgene for sharing plasmids. I also want to thank the students, who helped me with the maintenance of the fly stocks as well as Nicola and Nic for taking EM pictures.

I want to appreciate the Göttingen Graduate School for Neuroscience, Biophysics and Molecular Biosciences for making us PhD students a little more skilled and for providing an excellent scientific environment for its members.

I would like to mention all former and actual lab members of AG Simons, who provided such a pleasant work environment: Aniket Ghosh, Basti Schmitt, Mostafa Bakhti, Natalia Manrique, Shweta Aggarwal, Shima Safaiyan, Uli Weickert, Sebastian Timmler, Caro Velte, Nicola

Schwedhelm, Minhui Su, Dirk Fitzner, Caroline Bergner, Nils Halbsgut, Ludovico Cantuti, Schanila Nawaz, Nicolas Snaidero, Maryam Khojasteh and Giselheid Schulz.

I am grateful, particularly to Beate Koch, Anne Stündl and Marcel Kunadt from AG Schneider for housing me during the writing of this thesis and for all their kindness, mental support and corrections of the drafts.

Especially I want to thank my friends in the institute making the lab a second home: Shima not only for being my “PhD sister” and bench mate, but also for her endless support; Caro for all chats during good and bad times, sport sessions and long party nights; Mostafa for teaching me how to play football and much more; Aniket for many scientific discussions; Marcel for little delights when visiting AG Simons; Uli for numerous boulder evenings; Arwed for good music in the fly lab; Anne, not only for sharing the office but also a part of our lives; Petra for endless talks, skiing trips and for always being there. I will really miss all the Christmas cookie-baking nights, sport events, Christmas market evenings, movie sessions, coffee breaks and barbecues with all of you.

Finally yet importantly, I want to acknowledge my friends outside the lab for distracting me on the weekends and bringing me down after long lab days.

I thank my parents and family for their unconditional love and support, for giving me freedom in my choices and for accepting that they had to do without me many times. I thank Benni for his love and for being my safe harbor.

Thank you.

Summary

One major function of glial cells is to support neurons and create an environment that allows fast signal propagation. However, when neurons are ensheathed, they also get isolated from the extracellular environment and can no longer take up factors required for growth and function. Hence, glial cells have to regulate the neurons' metabolic and trophic support. To identify candidate genes that are necessary for this support, we initiated a RNA interference screen in *Drosophila* peripheral nerves.

In a screen for highly conserved molecules, we could successfully detect genes that are both required in glial cells and important for neuronal architecture and function. We found that pan-glial inhibition of p24-1 resulted in axonal loss, changed nerve architecture, transportation failure of axonal vesicles, migration defects of photoreceptor cells and swellings of neuronal mitochondria. p24 proteins act in the secretory pathway to shuttle cargo molecules through the biosynthetic pathway. A second p24 family member, opossum, reproduced the p24-1 phenotype revealing that they act in concert. Thus, we tried to identify the p24-1 cargo in a secondary RNAi screen. The iron binding protein Ferritin1 heavy chain was identified which displayed the same peripheral nerve phenotype as p24-1 knockdown. By *in vivo* and *in vitro* studies, we could show that Fer1HCH is released from glia cells and taken up by neurons. The inhibition of glial iron release caused accumulations of toxic ferrous iron resulting in ferroptosis. The application of inhibitors, which chelate iron or inhibit ferroptosis, reduced glial and axonal phenotypes. However, the transport defect of axonal vesicles was not recovered. As iron is essential for mitochondrial function, we assumed that iron import is required in neurons for energy production. Thus, we aimed to measure the effect of iron deprivation on neurons. Therefore, two binary expression systems were combined allowing for manipulations on glial cells and contemporaneous isolation of translating ribosomes from neurons. We found that several iron responsive transcripts are down-regulated upon blockage of glial Fer1HCH secretion. Hence, we identified a route for iron import into the nervous system of *Drosophila* and could show that blockage of this transport caused glial ferroptosis.

1 Introduction

Higher organisms are equipped with a complex nervous system, which consists only of the two cell types neurons and glia.

Neurons transduce information through electrical and chemical signals. They connect to each other and thereby form a network, which is capable to compute complex inputs and permits the organism to adapt by a changed behavior.

The glia was long time considered to be the glue that keeps the brain together (Virchow, 1871). In fact, these cells have vital roles in development, health and function of the nervous system. They insulate axons by forming a multi-layered membrane structure (Bhat et al., 2001; Salzer et al., 2008; Snaidero et al., 2014) and protect them by maintaining a constant ionic milieu through control of the blood-brain barrier (Abbott et al., 2006; Stork et al., 2008). Glial cells direct the outgrowth of axons during development (Gilmour et al., 2002; Sepp et al., 2001) and they control synapse formation and maturation (Allen and Barres, 2005). They carry out the metabolic support of the neuron by providing lactate (Saab et al., 2013; Tsacopoulos and Magistretti, 1996; Volkenhoff et al., 2015). They respond to neural stimuli with calcium waves (Schummers et al., 2008), are involved in synaptic transmission (Fields, 2002) and even modify neuronal signals by releasing gliotransmitters (Volterra and Meldolesi, 2005).

All these assignments are based on multiple reciprocal interactions between neuronal and glial cells. Thus, they need to communicate, which is mediated either by release of molecules or by direct cell contacts. Studies, mostly analyzing developmental nervous system processes showed that glia and neuron depend on each other (Ghosh et al., 2011; Hidalgo et al., 2006, 2011; Stratoulias and Heino, 2015). Later, during maturation a spatial tight interaction between the two cell types is set, which is difficult to investigate *in vivo* and thus poorly understood. To examine this interaction process *Drosophila* serves as an favored model

organism because of the lower glia/neuron ratio compared to vertebrates (Herculano-Houzel, 2014). The advantage of the more simple structure paired with a high degree of conserved characteristics makes the *Drosophila* nervous system an ideal system to also gain relevant insights into glial functions in mammals (Stork et al., 2012).

1.1 Morphological classes of glia cells

To be able to fulfill complex functions glia cells needed to specialize. This is reflected in a variety of different morphologies. In the next section, I want to summarize different classes of glial cells in the vertebrate and invertebrate system.

1.1.1 Origin and function of glia cells in the vertebrate system

In the vertebrate nervous system, we mainly find four glial cell types: astrocytes, oligodendrocytes, Schwann cells and microglia.

Astrocytes and oligodendrocytes are resident in the central nervous system (CNS). In the embryo, neuroepithelial progenitor cells (NPC) develop to radial glia which first give rise to neurons and then to astrocytes and oligodendrocyte precursor cells (OPC) (Rowitch and Kriegstein, 2010). Astrocytes represent the most frequent glial cell type in the CNS. These cells are of great importance because they have both regulatory roles and are necessary for the neuronal survival (Allen, 2014). In addition to many other tasks, astrocytes mediate metabolic support of CNS cells through coupling to the vascular system (Pellerin et al., 2007). They control the formation, function and turnover of synapses for instance by removal of neurotransmitter, by pruning synapses and by buffering potassium levels (Allen, 2014; Clarke and Barres, 2013).

Oligodendrocytes form myelin around axons of the CNS, which consists of multi-layered wraps of compacted membrane (Simons and Nave, 2015). This serves as an electric insulator and allows saltatory nerve conduction between the nodes of Ranvier (Seidl, 2014). Myelination in the CNS begins within the first weeks after birth. Thereby OPCs undergo morphological changes and send processes to enwrap multiple axons simultaneously (Snaidero et al., 2014). Recent studies suggest that myelination is not terminated after

development but rather adapts to neuronal activity for example during the acquisition of new motor skills (Gibson et al., 2014; Mckenzie et al., 2014).

Microglia, the third class of glial cell in the CNS, arise from mesodermal erythromyeloid stem cells which have a yolk sac origin (Aguzzi et al., 2013; Ginhoux et al., 2013). They are mainly described to be the tissue-resident immune cells of the brain and come into action when apoptotic cells and pathogens need to be removed (Casano and Peri, 2015). Recent work suggests that microglia are also involved in neurogenesis and wiring of the brain by secreting neurotrophic factors (Shigemoto-Mogami et al., 2014; Squarzoni et al., 2014) as well as by participating in synaptic refinement (Holtmaat and Svoboda, 2009).

Schwann cells, the main glial type in the peripheral nervous system (PNS), arise from cells of the neural crest (Jacob, 2015). Comparable to CNS progenitor cells, neural crest cells give first rise to neurons and later to glia. They generate two populations: Schwann cell precursors and satellite glia. The latter stay associated with the cell neuronal body where they probably regulate the metabolic support (Huang et al., 2013). Schwann cell precursors migrate along the peripheral nerve and form myelin around thick caliber axons. As in the CNS this ensures rapid signal conduction but in comparison to oligodendrocytes, they only form one internode (Salzer, 2015). During nerve injury, Schwann cells can remove dead cells and mediate repair (BrosiusLutz and Barres, 2014; Jessen and Mirsky, 2016).

1.1.2 Glial cell types in *Drosophila*

In the *Drosophila* nervous system, we find three main classes of glial cells: surface-associated glia, cortex-associated glia and neuropil-associated glia.

Surface-associated glia has epithelial character and can be further subdivided based on morphological features (Stork et al., 2012). Perineurial glia represents the outermost glial layer. Together with macrophages they are thought to build the neural lamella and serve as a first physical barrier to protect the nervous system (Carlson et al., 2000; Leiserson et al., 2000), but they do not form stable cell contacts (Stork et al., 2008). They also were described to be responsible for the import of the sugar trehalose from the hemolymph (Volkenhoff et al., 2015). Subperineurial glia cells, the second class of surface glia, lie underneath perineurial

glia cells and enclose the nervous system. They form a thin monolayer with stable contacts between the cells. These contacts consist of pleated septate junction (pSJ), which prevent para-cellular diffusion and thereby seal the nervous system forming the blood brain barrier (BBB) (Auld et al., 1995; Baumgartner et al., 1996; Stork et al., 2008).

The cortex-associated glia is restricted to the CNS, where it ensheathes neuroblasts as well as neuronal cell bodies, and makes contacts to the blood-brain barrier and the tracheal system (Pereanu et al., 2005). Cortex glial cells are most likely also responsible to for the metabolic support of neuronal cell bodies.

The neuropil-associated glia can be separated in three sub-classes. Wrapping glia cells, primarily in the PNS, have a tight interaction with axons and enwrap single axons during larval stages (Stork et al., 2008). The ensheathing glia resides in the CNS, where it sends processes around the synaptic neuropil and subdivides brain regions (Awasaki et al., 2008; Hartenstein, 2011). Astrocyte-like glia cells, in contrast to the ensheathing glia, infiltrate the neuropil. Cells of this type are closely associated to synapses (Freeman, 2015; Stork et al., 2012). *Drosophila* astrocytes ensure signal transduction at the synapse by regulating the neurotransmitter homeostasis and even modulate neuronal transmission (Freeman, 2015).

Most of the above-described so-called lateral glia cells arise during embryonic stages 8-12 from neural precursor cells termed neuroglioblast, which produce ganglion mother cells giving rise to neurons and glia. Another type of stem cells are glioblasts, which produce solely glial progeny (Altenhein et al., 2015). The switch between neuronal and glial cell fate is mediated by the transcription factor *glial cells missing* (*gcm*), which is expressed in all glial cells (except midline glia) (Jones et al., 1995). Known target genes of gcm are *reverse polarity* (*repo*), *poinedP1* and *tramtrack p69* (Jones, 2005). The best studied glial transcription factor is repo, which is expressed in the longitudinal glia pattern throughout the fly life (Campbell et al., 1994; Xiong et al., 1994). Repo has a dual role in glial differentiation: Tramtrack p69 together with repo represses neuronal differentiation (Yuasa, 2003), while repo in combination with pointedP1 drives glial differentiation by activating downstream genes like *loco defects* (*loco*) and *Dead ringer* (Granderath et al., 2000; Klaes et al., 1994; Shandala et al., 2003).

1.1.3 Layout of the larval nervous system of *Drosophila*

The Drosophila embryonic as well as the larval nervous systems has been a favored model to study neural development and function over the last decades. The advantage of these models is particularly the easy accessibility and the translucent cuticle. Combined with versatile genetic tools, the system has been used by researchers to identify molecular programs and basic principles of neural development (Doherty et al., 2009; Gerber and Stocker, 2007; Lee and Luo, 1999; Lee et al., 1999; Silies et al., 2014; Stork et al., 2008).

The larval behavior is quite simple. Locomotion includes bending, peristalsis, turning and feeding (Green et al., 1983). The sensory organs perceive thermal, chemical and light stimuli (Gomez-Marin and Louis, 2012). During larval stages new connections are made, neuronal cells form and the sensory organs develop (Hartenstein, 1993).

The larva is structured in eleven segments. Beside the specialized head structure, there are three thoracic segments and eight abdominal segments (A1-A8) (Keshishian et al., 1996). In each abdominal segment, one can find ~60 body-wall muscles (30 per hemi-segment) which are innervated by the segmental nerves. The synaptic connections they make with muscles are termed neuro muscular junctions (NMJs).

The larval nervous system can be divided in a central and peripheral part (Figure 1). The CNS consists of two brain lobes and the ventral nerve cord (VNC). Around 90% of all cells are of neuronal fate (Rodrigues et al., 2011). The cell bodies reside in the neuronal cell cortex. This structure can be distinguished from the neuropil, in which the axons and dendrites form connections (Freeman, 2015). The PNS comprises two segmental nerves per segment (one per hemi-segment) which results in a total number of 16 segmental nerves. The detailed structure of the peripheral nerves will be discussed in the following section. The length of a larva at the beginning of the first larval stage is ~0.5 mm and increases over the larval stages to a length of 7-8 mm. The longest peripheral nerve at the end of the third larval stage reaches 3 mm (Matzat et al., 2015).

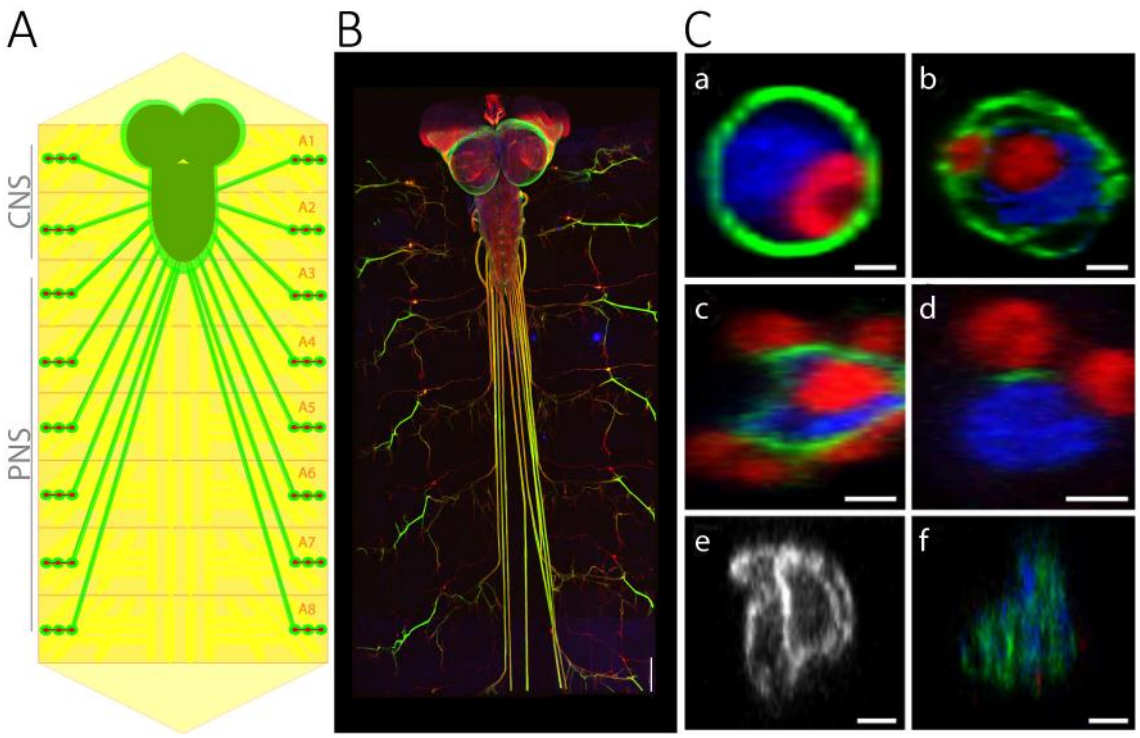

Figure 1: Layout of the larval nervous system. Overview over the complete nervous system of a third instar larva. Glial layers can be labeled with different sub-type specific markers. (**A**) Schematic overview of the nervous system. Muscles are depicted in yellow, glia in green and neurons in red. The nervous system can be divided in a central (CNS) and a peripheral part (PNS). The abdominal nerves A1 – A8 connect muscles and sensory organs with the VNC. Note that glia membrane covers all nerves. (**B**) Confocal maximum intensity projection of the whole nervous system. Glia are labeled in green by repo CD8GFP expression, neurons with anti-HRP antibody and glial nuclei with anti-repo antibody stain. Scale bar 150 µm. (**C**) Orthogonal section through peripheral nerves reveals cell sub-types, which can be labeled with different markers (green). Axons are depicted in blue, glial nuclei in red. (a) Viking-GFP trap labels the neural lamella around the nerve. (b) Perineurial glia cells can labeled by GFP expression with the C527Gal4 line or with the Jupiter-GFP trap. (c) Subperineurial glia can be labeled by GFP expression with gliotactinGal4 or with the 261-GFP trap. (d) Septate junctions appear as a thin line along the nerve. They can be labeled by a GFP-trap insertion in *neurexinIV*. (e) All glia can be labeled by GFP expression with repoGal4. (f) Wrapping glia can be labeled with the GFP-trap in the *nervana2* gene or by GFP expression with nervana2Gal4. Scale bar 2 µm. (c) Reproduced from Stork et. al. 2008 with permission from Society of Neuroscience.

1.1.4 Development of axonal ensheathment in the PNS

The peripheral nerves of the *Drosophila* larva have a quite simple structure compared to the nerves of the CNS. The peripheral nerve consists of the segmental (or abdominal) nerve and a smaller transverse nerve. Each abdominal nerve comprises efferent motor axons and afferent

sensory axons. Approximately 36 motor neurons are born at the dorsal site of the VNC and project their axons to innervate the muscles in a highly stereotypic manner (Bate and Arias, 1993; Keshishian et al., 1996; Kohsaka et al., 2012). Around 42 sensory neurons are located in the body wall, which project their axons to the ventral site of the VNC. Thus, the motor output and sensory input are clearly segregated (Landgraf et al., 2003; Mahr and Aberle, 2006). Motor and sensory axons fasciculate and are ensheathed by glia. Seven glia cells are generated in the VNC migrating along the nerve and five glia cells are born in the periphery. At the end of embryogenesis, twelve glial cells reside in every nerve (von Hilchen et al., 2013). All glial layers can be distinguished by expression of different maker genes (compare Figure 1 C) (Stork et al., 2008). The outermost layer, as in the CNS, is comprised of perineurial glia cells. These cells divide post-embryonically (Leiserson et al., 2000) enabling them to cover the whole nerve during the extensive larval growth phase (Figure 2). In contrast, the underlying subperineurial glia does not proliferate but accommodates nerve growth by extending the cell surface (Sepp et al., 2000). Subperineurial cells in the PNS form a thin epithelial-like monolayer around the axons. Thereby the cell enwraps the axons completely and forms an auto-cellular connection. In this ~4.7 µm long overlap the septate junctions are located (Matzat et al., 2015), which consist of components such as NeurexinIV, Gliotactin, Nervana2 and Coiled and exhibit a ladder–like structure (Auld et al., 1995; Baumgartner et al., 1996; Genova and Fehon, 2003; Limmer et al., 2014). As mentioned before, these cell junctions seal the nerve and represent the hemolymph-nerve barrier. Only this protection against the high potassium concentration in the hemolymph allows a normal electrical conductance (Carlson et al., 2000; Stork et al., 2008). Septate junctions are set up at embryonic stage 17 and maintained during longitudinal and radial extension of the nerve (Limmer et al., 2014). Another task is fulfilled by the subperineurial glia. Inhibition of the kinase Fray or its downstream target sodium-potassium-chloride transporter NCC69 leads to nerve swellings and suggests that the glia functions in the control of the ionic balance within the nerve (Leiserson and Keshishian, 2011; Leiserson et al., 2000). The innermost glial layer is termed wrapping glia. Three to four wrapping glia cells reside in each nerve. They develop their characteristic morphology during larval stages by producing vast amounts of membrane

(Figure 2). At the end of the third larval stage, they terminate their differentiation and separate all peripheral axons (Stork et al., 2008). Gap junctions between glial cells are formed by Innexin proteins in early larval stages and interconnect the glial layers (Spéder and Brand, 2014; Stebbings et al., 2002).

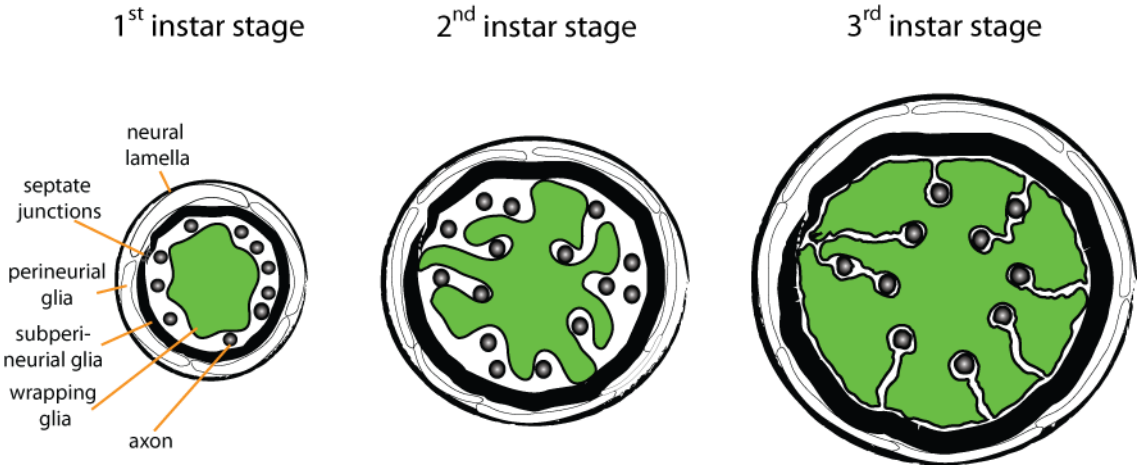

Figure 2: Development of larval peripheral nerves. Schematic overview over the development of a peripheral nerve. Cross section view. In first instar larvae three glial cell type are present in the PNS: perineurial glia, which is surrounded by neural lamella, subperineurial glia, and wrapping glia (green). Note that wrapping glia produces large membrane amounts to separate all axons until the end of the third instar stage. Subperineurial glia constitutes an impermeable barrier by forming auto-cellular septate junctions already during embryonic stages. SPG grow in size to cover the radial nerve growth and maintain BBB integrity. Perineurial glia divide to cover nerve growth.

1.1.5 Comparing axonal ensheathment between Vertebrates and Invertebrates

Vertebrate peripheral axons are tightly associated with Schwann cells (Taveggia, 2016). As described before, they form myelin around the axon allowing saltatory nerve conduction. However, only thick caliber axons are myelinated (Gillespie and Stein, 1983). The myelin thickness is regulated by the release of the axonal factor Neuregulin-1 (Nrg1). While overexpression of Nrg1 leads to hyper-myelination, reduced NRG1 expression causes hypo-myelination (Michailov et al., 2004). Nrg1 binding to the glially expressed EGF receptor

complex ErbB2/ErbB3 activates signaling cascades (PI3 Kinase/AKT-1 and MAPK/ERK) driving myelination (Taveggia, 2016). Thinner axons stay unmyelinated and lay in pockets of Remak fibers (Nave and Trapp, 2008). These Remak fibers arise from Schwann cell precursors and resemble quite strongly *Drosophila* wrapping glia cells (Rodrigues et al., 2011). Comparing the vertebrate and invertebrate ensheathing process, not only the appearance of the cells but also the molecular mechanisms seems to be similar. In the *Drosophila* compound eye for instance, proliferation and migration but also differentiation of retinal glia cells is regulated by the fibroblast growth factor (FGF) receptor Heartless (Silies et al., 2014). The wrapping process around photoreceptor axons is triggered by the neuronally derived FGF8-like ligand Thisbe which activate Heartless (Franzdóttir et al., 2009). In *Drosophila* segmental nerves differentiation of the wrapping process is regulated by the activation of the epidermal growth factor receptor (EGFR). Binding of the neuregulin-like protein Vein regulates extension of glial membrane around peripheral axons. However, this seems to be an autocrine mechanism since Vein is derived from wrapping glia cells themselves (Matzat et al., 2015). Although *Drosophila* does not form myelin, the wrapping process in both vertebrates and invertebrates is controlled by the activation of receptor tyrosine kinases (Rodrigues et al., 2011).

1.2 Modes of neuron-glia interactions

Development and function of the nervous system are not only based on performance but rather on the interactions between neurons, glia and the environment. Many examples can be found in higher organism: intercellular signaling is needed for the neural specification and differentiation (Urbán and Guillemot, 2014); shaping of the dendritic tree is influenced by the target field (Jan and Jan, 2010); the establishment of synapses requires a close interplay between pre- and post-synapse (Margeta and Shen, 2010); axon pathfinding relies on neuron-glia interactions (Chotard and Salecker, 2004). Interestingly, the relation of neurons and glia seems to get more sophisticated the more complex the nervous system is developed. In *Drosophila* only 10% of the cells within the nervous system are of glial fate, whereas in mammals the ratio is ~50 % (Herculano-Houzel, 2014). The fact that the neuron-glia unit is relatively simple combined with the advantages of *Drosophila* as a genetically powerful model

system, makes *Drosophila* nerves an ideal system to study cell interaction and communication within the nervous system (Edenfeld et al., 2005).

1.2.1 Signaling between neurons and glia

Much of our knowledge about signaling mechanisms between neuron and glia derives from studying the embryonic nervous system development. In the embryonic brain, glia guide the fasciculation of pioneer axons and ablating peripheral glia cells causes defasciculation and projection failure of sensory neurons (Klämbt and Goodman, 1991; Sepp et al., 2001; Tessier-Lavigne and Goodman, 1996). One example for direct cell contact has been described between commissural axons and midline glia, where the Immunoglobulin superfamily (IgSF) members Wrapper and NeurexinIV mediate adhesion. Wrapper, which is attached to differentiating midline glia cells via a glycosylphosphatidylinositol (GPI) anchor, can bind to NeurexinIV presented on the axonal surface. Wrapper mutants fail to ensheath the commissural axons and the positioning of glial cells is disturbed (Noordermeer et al., 1998; Stork et al., 2009). A second IgSF member has been described to be important for early glial migration of PNS glia along axons of motor neurons. Fasciclin2 (Fas2) is expressed by motor neurons and glia cells to mediate cell adhesion in a homophilic manner. The local down-regulation of the axonal Fas2 by the Fizzy-related/Cdh1 complex then initiates migration of the glia. Hence, axonal signals control the onset of glial migration (Silies and Klämbt, 2010). Third, the IgSF member Neuroglian (Nrg) is required for a homophilic cell interaction. Neuronal and glial cells each express a distinct isoform, which contains different intracellular domains allowing linkage to the cytoskeleton via Ankyrin (Hortsch et al., 1990, 2009). Beside axon sprouting and dendrite branching, Nrg is also involved in septate junction formation and synaptic stability (Enneking et al., 2013; Genova and Fehon, 2003).

1.2.2 Secreted molecules in the nervous system

Many of the molecules regulating neuron-glia communication are secreted factors. The already mentioned EGF receptor, for instance, is not only important for wrapping glia differentiation (Franzdóttir et al., 2009; Matzat et al., 2015) but also for the cell number

control in the *Drosophila* embryo (Silies and Klämbt, 2011). The axonally derived factors Spitz and Vein activate the EGF receptor of midline and longitudinal glia respectively, to prevent cell death (Bergmann et al., 2002; Hidalgo et al., 2001). Glia can also regulate neuronal proliferation by reacting on fat body derived signal triggering a release of insulin-like peptides. Neuroblasts perceive this insulin signals and exit quiescence (Chell and Brand, 2010).

During embryonic development of the ventral nerve cord axons grow in a highly stereotypic manner. The pattern they create during this process is guided by repulsive and attractive signals (Jacobs, 2000). Netrin, for example, is secreted by the midline glia and attracts motor axons, which express the receptor Frazzled (Kolodziej et al., 1996). Slit is a repulsive cue and retracts axons expressing the receptor Roundabout (Robo) (Kidd et al., 1999; Seeger et al., 1993). Migrating peripheral glia express the Netrin receptor Uncoordinated5 (Unc5) which acts repulsive when detecting the Netrin signal from the ventral midline. Interestingly, in the CNS neuronally derived Netrin directs longitudinal glioblasts towards the midline (von Hilchen et al., 2010).

Another migratory cue, which can be found in the vertebrate and invertebrate system, is regulated via the platelet derived growth factor (PDGF) receptor. Activation of its *Drosophila* homolog PVR through neuronally secreted PVF ligands can trigger migration of midline glia cells in the embryo and in glia of the optic stalk in the *Drosophila* larva (Kim et al., 2014; Learte et al., 2008). Likewise in vertebrates, binding of PDGFα to the PDGF receptor activates proliferation of OPCs (Zuchero and Barres, 2013).

Another example for glia-axon interaction involves the transforming growth factor (TGF) signaling. During metamorphosis, γ neurons of the mushroom body have to be remodeled. Therefore, a pruning process is started, which is controlled by the hormone ecdysone (Lee et al., 2000). Cortical and astrocyte-like glia regulate this step by secreting the TGFβ ligand myoglianin, which activates the receptor Baboon causing intrinsic TGFβ signaling in mushroom body neurons. The effect of this signaling is the up-regulation of the ecdysone receptor in neurons (Awasaki et al., 2011). Signaling between neurons and glia is also described during NMJ formation and function (Ou et al., 2014). Peripheral glia secrete the TGFβ ligand Maverick, which binds to the post-synapse and in turn activates *glass bottom*

boat (gbb) transcription inducing synapse growth (Ball et al., 2010; Fuentes-Medel et al., 2012). Another TGF ligand, which acts at the NMJ, is the TNFα ligand Eiger. Upon glial secretion, Eiger binds to the neuronally presented TNFα receptor Wengen, which activates caspases and causes axonal and synaptic degeneration (Keller et al., 2011). Another interesting study showed the involvement of the morphogen wingless (Wg) at the NMJ. Glial cells secrete Wg, which induces glutamate receptor clustering at the post-synaptic site. This mechanism enables glia cells to regulate synaptic functionality (Kerr et al., 2014).

1.2.3 Metabolic support in the nervous system of Vertebrates and Invertebrates

A tight neuron-glia interaction is required to respond to the metabolic needs of the nervous system. In both, flies and humans, the nervous system is shielded from the blood and nutrient circulation. Hence, all metabolites required for the nervous system have to be shuttled over the blood-brain barrier. In the PNS of *Drosophila* and mice, we find especially long nerve tracts. Still, the metabolic needs of these nerves need to be satisfied. Constant energy supply is needed for the axonal transport, to maintain the ion gradient but also to synthesize and send synaptic and structural proteins along these nerves (Nave, 2010). Energy in form of ATP could be generated in the cell body, however it is likely that only local energy supply can ensure the integrity of the axonal function (Morrison et al., 2013).

In vertebrates, access to nutrients for neurons is restricted in two ways: first by the blood-brain barrier, which is set up by impermeable tight junctions of the endothelial cells in brain capillaries (Reese and Karnovsky, 2005) and second by the myelin membrane covering large parts of the axons. Astrocytes form connections between neuronal cell bodies and blood capillaries to ensure the metabolic import of nutrients (Abbott et al., 2006; Bélanger et al., 2011; Kasischke et al., 2004). Glucose is transferred to oligodendrocytes via gap junctions to be used for glycolysis. Lactate can then diffuse through cytoplasmic channels and be released by the monocarboxylate transporter 1 (MCT1) (Saab et al., 2013). Subsequently, axons take up the lactate with help of MCT2 and use it for their mitochondrial energy production (Suzuki et al., 2011).

In *Drosophila,* the blood-brain barrier is established by surface glia cells. Hence, import of nutrients has to be accomplished by transport through these cells. It has been shown that the sugar trehalose is taken up from the hemolymph and processed by perineurial glia cells to alanine and lactate. Possibly, products can be shuttled over gap junctions to other glia cells in order to be released to neurons. Inhibition of glycolytic genes in glia cause neuronal death. Neurons take up lactate, which is further used for ATP production over the TCA cycle (Volkenhoff et al., 2015). Expression of glycolytic genes in neurons seems dispensable for energy supply, but required for longevity (Miller et al., 2012).

1.3 Iron homeostasis

Iron is an essential metabolite ensuring survival of almost all eukaryotic and prokaryotic organisms. As part of heme, iron-sulfur clusters (ISC) and as a cofactor iron is involved in vital processes like DNA synthesis, oxygen transport, metabolic energy production and cellular respiration (Gozzelino and Arosio, 2016). Although iron has various functions, its ability to exchange electrons with many substrates can also be toxic for cells (Harrison and Arosio, 1996). In the presence of hydrogen peroxide, free iron can cause the production of reactive oxygen species (ROS) such as hydroxyl radicals via the Fenton reaction (Dixon and Stockwell, 2014). This leads to oxidative stress, lipid peroxidation and DNA damage, which will comprise cell viability. To prevent these toxic effects, organisms developed a fine-tuned regulatory mechanisms, which allow binding, uptake, storage, mobilization and recycling of iron (Arosio et al., 2009; Connor et al., 1990; Rouault, 2006).

1.3.1 Distribution and storage of iron

In vertebrates, systemic iron supply is regulated over the iron level of the blood plasma. The glycoprotein Transferrin (Tf) can bind two molecules of ferric iron and circulates in the plasma in order to deliver iron to cells. The transferrin receptor is expressed in target cells, which can take up iron bound transferrin via clathrin-dependent endocytosis (Harding et al., 1983). Body iron is released from duodenal enterocytes and macrophages. Thereby, in humans the majority of iron (20-25 mg per day) is coming from recycled senescent cells (erythrocytes)

and only 1-2 mg iron per day has to be taken up by nutrition (Hentze et al., 2010). Gut cells absorb dietary iron with help of the divalent metal transporter (DMT1) (Gunshin et al., 1997). The hormone hepcidin, released by hepatocytes, plays a crucial role in the systemic iron supply. It binds to the iron exporter ferroportin of iron releasing cells, triggers its internalization and leads to a reduction of iron efflux (Nemeth et al., 2004). Upon cellular internalization of Tf-Fe_2 via the transferrin receptor, early endosomes are acidified which causes a conformational change and release of iron (Dautry-Varsat et al., 1983). Iron is then reduced to Fe^{2+} by metalloreductases (Ohgami et al., 2006) and shuttled via DMT1 into the cytosol, whereas Tf is recycled back to the cell surface. The cytoplasmic so-called *labile iron pool* (LIP) can be used directly for iron based reactions or stored within the Ferritin complex (Arosio et al., 2009). The complex is built of 24 subunits of Ferritin 1 heavy chains (FTH1) and Ferritin light chains (FTL) and generates a nano cavity, which can accommodate up to 4500 iron atoms (Tandara and Salamunic, 2012). Ferritin has been described to protect cells from iron toxicity and oxidative stress. FTH1 harbors a ferroxidase domain, which can induce the oxidation of ferrous (Fe^{2+}) to ferric (Fe^{3+}) iron and the deposition into the complex core. This stored iron is kept in a redox inactive form that is unaffected by Fenton chemistry (Arosio et al., 2009). Although Ferritin is mainly localized in the cytosol, it is probably also secreted (Meyron-Holtz et al., 2011). Two surface receptors for Ferritin have been identified: Scara-5 and Tim-2. Scara-5 is involved in kidney organogenesis and preferentially binds Ferritin light chain circulating in the blood serum. Subsequently, iron-loaded Ferritin can be taken up by cells via receptor-mediated endocytosis. In contrast, T cell immunoglobulin-domain and muncin-domain 2 receptor (Tim-2) mainly binds H Ferritin, which causes its internalization into endosomes (Chen et al., 2005). It is expressed on B-cells, kidney cells and oligodendrocytes (Han et al., 2011; Todorich et al., 2008). Beside transferrin iron transport, the mechanism of Ferritin uptake represents an alternative way to deliver iron to cells (Wang et al., 2010).

1.3.2 Regulation of iron consumption

The best-described functions of iron are the participation in the prosthetic group heme and in iron-sulfur clusters (ISC). Though in higher organisms they are also synthesized in the cytoplasm (Lill and Mühlenhoff, 2006), the majority of iron is consumed by the heme and ISC machinery inside of mitochondria (Rouault, 2015). Proteins, which use heme as a prosthetic group, are for instance hemoglobin, myoglobin, cytoglobin, cytochrome c-oxidase, NO-synthase, lactoperoxidase and catalase. NADH-dehydrogenase, succinate dehydrogenase, aconitase are examples for enzymes with ISC (Tandara and Salamunic, 2012). The import of iron into mitochondria is accomplished by transporters termed mitoferrins (Paradkar et al., 2009).

Inside the cell, the expression of iron-binding proteins is regulated on a post-translational level over the IRE/IRP system (iron response element / iron response protein). Ferritins and other transcripts of the iron metabolism contain an iron responsive element in their 5' untranslated region (UTR) or, like Ferroportin in the 3' UTR (Figure 3). Under iron deprivation, the iron responsive proteins IRP1 and IRP2 bind with high affinity to the 5' located IRE blocking ribosome binding and translation. In case the IRP binds to a 3' IRE site, the transcript will be stabilized (Rouault, 2006; Tandara and Salamunic, 2012). High cellular iron levels cause a conformational change of the IRP, which can no longer bind to the IRE. Now translation can proceed for transcripts with 5' IRE and degradation is triggered of the transcript with 3'IRE (Subbarao et al., 2006). With this iron-sensing system, the cell can quickly react to iron excess by translating iron storage molecules. Vice versa during iron deprivation, the translation of iron internalization proteins like TfR ensures the cellular demands (Gozzelino and Arosio, 2016).

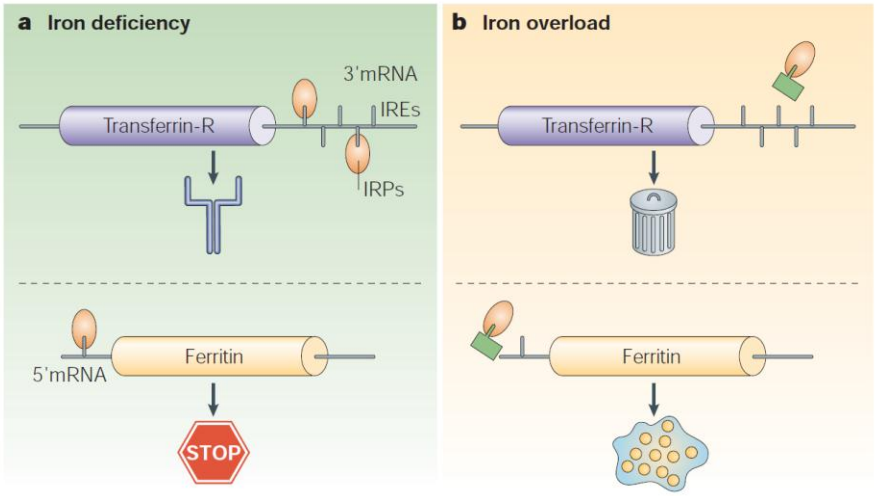

Figure 3: Regulation of iron storage and export with the IRE/IRP system. Iron-responsive protein amounts are regulated on a translational level. Iron regulatory proteins (IRPs) bind to 3' or 5' untranslated regions in the mRNA. (**a**) In iron deficiency, IRPs bind to the 3' UTR of TfR, which protects mRNA from degradation. Binding of IRP to the 5' UTR of Ferritin however inhibits translation by block of ribosome binding. (**b**) If iron is present in cells, IRPs cannot bind to IREs and TfR mRNA allowing the degradation, whereas Ferritin mRNA can be translated. Adapted from Iron brain ageing and neurodegenerative disorders. Reproduced from Zecca et. al. 2004 with permission from Nature Publishing Group.

1.3.3 Iron metabolism in the brain

Iron is required for many brain functions such as myelin synthesis, neurotransmitter production, synaptic plasticity and neural mitochondrial respiration and metabolism (Moos, 2002). Disturbed iron homeostasis is linked to neural dysfunction (Salvador, 2010): iron deficiency during development causes impaired cognitive abilities whereas iron overload leads to neuronal death (Ghosh et al., 2015). The challenge for the body is to provide the brain with iron, which is per se disconnected from the systemic circulation because of the blood-brain-barrier. To bypass this barrier, cells of the brain exhibit all components of the iron transport and storage system but the expression varies between the cell types. Iron enters the brain over the transferrin receptor expressed on endothelial cells of the BBB (Figure 4) and is released into the interstitial fluid (ISF) by ferroportin (McCarthy and Kosman, 2013; Moos, 2002). Astrocytes, which are over their end-feet in contact to the endothelium, can

shuttle iron and express the ferroxidase ceruloplasmin. This enzyme, as well as the oligodendroglial ferroxidase hephaestin oxidizes iron to Fe^{3+}, which facilitates ferroportin mediated iron export (Patel et al., 2002). In the CNS transferrin is mainly synthesized by oligodendrocytes (Bloch et al., 1985). After iron entered the brain, it can bind to Apo-transferrin and circulate in the ISF. Ultimately, holo-transferrin can be internalized from cells that express the TfR. Neurons stain strongly for TfR whereas microglia are characterized by a strong Ferritin staining (Rouault, 2013).

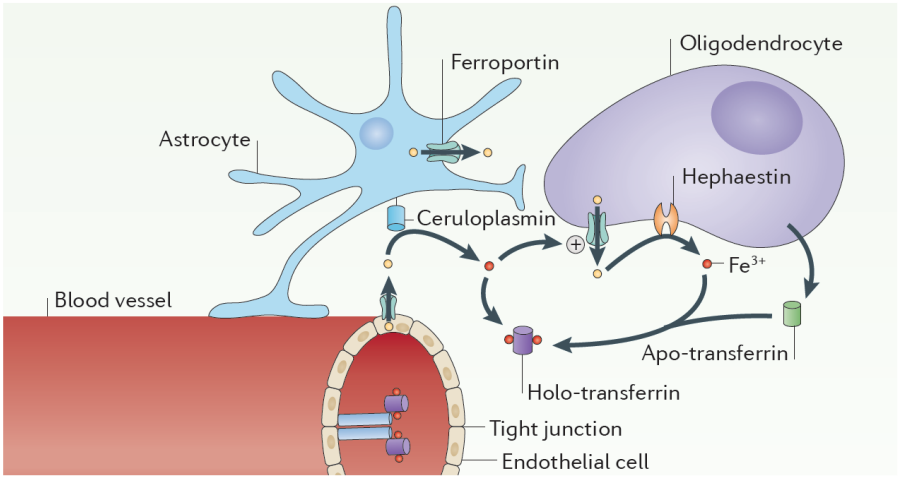

Figure 4: Iron metabolism in the mammalian CNS. Iron can cross the BBB by uptake of circulating holo-transferrin from the blood with help of the Transferrin receptor. The iron exporter Ferroportin helps to release iron to the interstitial fluid. The astrocytic ferroxidase Ceruloplasmin oxidizes Fe^{2+} to Fe^{3+}, which can bind to apo-transferrin secreted from oligodendrocytes. Probably, neurons and glia acquire the majority of iron from iron-loaded transferrin in the interstitial fluid. Reproduced from Rouault et. al. 2013 with permission from Nature Publishing Group.

1.3.4 Iron homeostasis in *Drosophila*

Much less is known about the iron metabolism in *Drosophila melanogaster*. Although there are conserved iron regulatory proteins in flies and mammals, other molecules either do not have a functional homolog or are not described yet. As in vertebrates, iron is required for the functionality of proteins in form of a cofactor, bound to heme or as part of ISC (Tang and

Zhou, 2013a). In *Drosophila*, dietary iron is absorbed by the cells of the midgut, which express the DMT1 homolog *Malvolio* (Rodrigues et al., 1995). However, no molecule with a similar function as ferroportin, which is able to release iron has been identified yet (Tang and Zhou, 2013b). Two multi copper oxidases (MCO) have been described to have a potential regulatory oxidase function similar to hephastin in vertebrates. MCO3 contains a putative iron-binding site and gene mutation leads to iron accumulation in the gut (Bettedi et al., 2011). For MCO1 it is known that it has multi copper ferroxidase activity but the exact function remains unclear (Lang et al., 2012). Insect and mammalian Ferritins have a conserved structure of 12 heavy and 12 light chains but the intercellular localization differs (Pham and Winzerling, 2010). While vertebrate Ferritin is mainly found in the cytosol, in many invertebrate species Ferritin localizes to the biosynthetic vesicular pathway (Nichol et al., 2002). In fact, insect Ferritin is secreted and present in the hemolymph. In *Drosophila*, we also find a set of transferrin genes (Yoshiga et al., 1999). Transferrin 1 (Tsf1) is the counterpart of the mammalian iron transporter and is secreted into the hemolymph as well (Yoshiga et al., 1999). There is evidence that it is involved in the immune response but so far the exact function of Tf1 concerning the distribution of iron remains elusive (Levy et al., 2004). Although Tsf1 and Ferritin are secreted so far no iron receptor like TfR or Ferritin receptor could be identified (Mandilaras et al., 2013). The iron loading of Ferritin is dependent on the delivery of cytosolic iron into the endoplasmic reticulum, which is most likely fulfilled by the zinc regulated iron transporter 13 (Zip13, also known as Zip99C). Zip13 mutants fail to transport iron to ER-Golgi compartment. Supposedly Zip13 can act as an iron exporter (Xiao et al., 2014).

1.4 Aim of this work

The aim of this work is to identify molecules, which are involved in neuron-glia interaction and communication. We set out to search for glial proteins, which can influence the neuronal integrity. To find new glial molecules, which are needed for the neuronal function we selected the *Drosophila* peripheral nerve as a model. The superiority of this model is its simplicity combined with the genetic tools available. Only three glial sub-types are present in the peripheral nerves and the axo-glial structure has a highly stereotypical pattern. We conducted a cell type specific RNA interference screen of conserved molecules, which might have glial function in vertebrates and invertebrates. RNA interference was induced in all glial cells using a pan-glial activator line. Neuronal and glial membranes were labeled with specific markers. As readout for the screen, we used confocal microscopy to detect changes of the axo-glial unit in the peripheral nervous system.

2 Material and Methods

The listed chemicals used to prepare buffers, media and solutions were purchased in *pro analysis* or cell culture grade quality from the following companies:

AppliChem	Merck	Stratec
Carl Roth	New England Biolabs	Sigma Aldrich
Life Technologies	Promega	Thermo Fisher Scientific
Machery Nagel	Roche	Vector Laboratories
Serva	5Prime	PeqLab

The solutions were prepared with ultrapure water and autoclaved or sterile filtered before use.

2.1 Buffer, Media and Solutions

4% PFA	heat 300 ml ddH_2O to 60°C, dissolve 20 g PFA, add 1N NaOH until solution is transparent; add 50 ml 10x PBS, adjust pH to 7.2, add ddH_2O to final volume of 500 ml; aliquot and store at -20°C until use.
5% Milk	5% non-fat milk powder in PBS-Tween

10% APS	10% ammonium persulfate in ddH_2O, store at -20°C
10% GS	10% goat serum in PBT
10% SDS	10% sodium dodecyl sulfate in ddH_2O
50% Chlorix	50% Chlorix cleaning agent in ddH_2O
70% Ethanol	70% Ethanol in ddH_2O
Apple juice agar	dissolve 18 g agar in 500 ml ddH_2O, autoclave, store until use. Add 150 ml ddH_2O, heat in microwave; add 3 ml glacial acetic acid
DNA loading buffer 10x	4 M urea 50% sucrose 50 mM EDTA Spatula tip of bromphenol blue and xylene cyanol
Lämmli buffer (4x)	0.25M Tris/HCl pH6.8 8% SDS 40% Glycerol 0.02% bromphenol blue 200 mM DTT or 0.8% β mercaptoethanol
LB agar plates	18 g agar per 1 L LB medium
LB medium	10 g tryptone 5 g yeast extract

	10 g NaCl Fill up to 1 L with ddH_2O, adjust pH to 7 and autoclave
Mowiol	dissolve 12 g Mowiol in 30 g Glycerol; add 30 ml ddH_2O and mix for 5 min; add 60 ml Tris-HCl pH8.5, centrifuge at 5.000/ 5 min; store at -20°C
PBS	130 mM NaCl 7 mM Na2HPO4 3 mM KH2PO4 2.7 mM KCl Adjust to pH 7.4
PBT	PBS and 0.3% Triton X-100
PBS-T	PBS and 0.05% Tween 20
Protein lysis buffer	5 x IP buffer (Life Technologies) 150 mM NaCl 2 mM MgCL2 1 mM DTT 1x cOmplete Protease Inhibitor (Roche)
Polysome extraction buffer	20mM Hepes, pH7.5 150 mM KCl 5mM $MgCl_2$ 1% Triton X-100 0.5 mM DTT 100 µg/ml Cycloheximide

	100 U/ml RNAse OUT
	1x cOmplete Protease Inhibitor (Roche)
Polysome wash buffer	150 mM NaCl
	0.05% Triton X-100
	50 mM Tris
	5 mM MgCl2
	40 U/ml RNAse OUT
Running buffer (SDS-Page)	25 mM Tris base
(10x)	192 mM glycine
	0.1% SDS
Resolving gel buffer	375 mM Tris HCl, pH 8.8
Stacking gel buffer	125 mM Tris HCl, pH 6.8
TAE buffer (10x)	400 mM Tris-acetate
	10 mM EDTA
Western blot transfer buffer	20mM Tris base
	153 mM glycine
	20% Methanol

2.2 Fly Genetics

2.2.1 Maintenance and Crossing of Flies

Fly lines were kept in plastic vials with Standard *Drosophila* food and maintained on 18°C, 21°C or 25°C. For crossings, virgin female and 2-5 days old male flies were used.

2.2.2 Germline transformation

ϕC31 mediated germline transformation is a method to create a transgenic fly line. Therefore, a plasmid containing the gene of interest and a visible marker is injected into an early embryo that can integrate into the germline. The integration event is mediated by the ϕC31 integrase. The integration site is predefined by using intergenic landing sites that carry an attP attachment element, which can recombine with the attB site of the plasmid (Bischof, 2006).

To use the ϕC31 mediated germline transformation plasmid DNA was prepared with the Machery-Nagel Endotoxin-free Midi Kit. The landing site was selected upon expression strength. The microinjection procedure was performed by BestGene Inc. After receiving the F2 generation of transformants, the flies were crossed to balancer lines and a stable transgenic fly line was established.

2.2.3 Generation of recombinant fly lines

For some experiments, it was necessary to create recombinant fly lines. First, flies were bred which were heterozygous for the two genes of interest (gene A and B). Female offspring was then crossed to a balancer line. Single offspring of the second crossing was again crossed to balancer animals and tested for recombination by PCR or marker gene expression.

2.2.4 Inhibitor Test of Ferroptosis inhibiting drugs

Ferroptosis is a form of iron dependent cell death, which can be inhibited by applying iron chelators or the compound Ferrostatin-1. To test whether the genotypes of interest display ferroptosis dependent cell death, larvae were treated with a series of iron chelators and inhibitors: Deferoxamine salt (DFO, 50 µM), Cyxlopirox olamine (CPX, 4 mM),

Bathophenanthroline disulfonic acid (BPS, 50 µM) as well as with Ferrostatin-1 (Fer-1, 150 µM) and ferric ammonium citrate (FAC, 25mM). To treat animals, crossings of Gal4 driver and UAS-RNAi line were set up and embryos were collected for 1h on agar plates containing standard fly food mixed with inhibitor solutions at 25°C. After hatching, the larvae were counted and selected for the right genotype. Every two days the animals were transferred to new plates containing the food inhibitor mixture. At the indicated time points, several animals were dissected and stained for axon defects with the HRP and Bruchpilot antibody.

2.2.5 Isolation of primary cells from *Drosophila* Embryos

To prepare a mixed culture of primary *Drosophila* cells, crossings of around 100 virgins of the Gal4 driver line repoCD8/GFP with 30 males of the UAS effector line UAS-Ferritin1HCH-HA or wildtype males for control was set up in a large embryo collection cages on agar plates containing fresh backer's yeast. The flies were allowed to lay eggs for 4-6 hours at 25°C. Then the apple juice agar plate was changed and the collected embryos were kept at 4°C until further processing. The embryos were washed off the agar plate with tap water and help of a sieve. Now, the embryos were placed in 50% Chlorix solution for 3 minutes to remove the chorion. After rinsing with excess tap water the embryos were carefully transferred to a dounce homogenizer and homogenized with 7-8 strokes in 1ml Schneider's medium. The cell suspension was transferred to a sterile 1.5 ml reaction tube and centrifuged at 500 g for 5 minutes at room temperature. The pellet was resuspended in 1ml Schneider's medium containing 1 mg/ml elastase and incubated for 30 minutes at room temperature. Now the cell-elastase mix was transferred to a 15 ml Falcon tube containing 4 ml Schneider's medium with 10% fetal bovine serum (FBS) to inactivate the enzyme. The solution was filtered through a 50 µm syringe filter and centrifuged at 400 g for 5 minutes. The cells were carefully resuspended in 1 ml Schneider's medium with 10 % FBS and 0.01% Penicillin/Streptomycin (Gibco) and seeded in different densities.

2.2.6 List of fly lines

2.2.6.1 Wild-type and balancer stocks

Table 1: *Drosophila* wild-type and balancer stocks used in this study.

fly sock	comment	source / reference
OregonR	Wild-type	Lindsyley and Zimm, 1992
w^{1118}	white^{-}, wild-type	Lindsyley and Zimm, 1992
w^{1118};;TM3,e,Sb/TM6b,e	balancer III.chromosome	Bloomington Stock Center
w^{1118};Tft/CyO	balancer II.chromosome	Bloomington Stock Center
w^{1118};Tft/CyO;TM2,e/TM6b,e	Balancer II+III.chromosome	Klämbt, unpublished

2.2.6.2 Exon traps and other transposon insertions

Table 2: *Drosophila* mutants and transposon insertions used in this study.

fly sock	comment	source / reference
Ferritin1HCH^{451}	Lethal P-element insertion in *fer1hch*	Bloomington Stock Center
NeurexinIV$^{]454[}$	GFP-trap in *neurexinIV*	(Edenfeld et al., 2006)
Nrv2$^{]GFP[}$	GFP-trap in *nervana2*	Bloomington Stock Center
261]GFP[	GFP-trap expressed in subperineurial glia	C. Klämbt, unpublished
Jupiter$^{]GFP[}$	GFP-trap insertion in *jupiter*	Bloomington Stock Center
p24-1^{EY12314}	Viable P-element insertion in *p24-1*	Bloomington Stock Center
P24-1^{KG09084}	Viable P-element insertion in *p24-1*	Bloomington Stock Center

2.2.6.3 Gal4 activator lines

Table 3: *Drosophila* Gal4 activator lines used in this study.

fly sock	comment	source / reference
Act5CGal4	Gal4 actin 5 C promoter fusion	Bloomington Stock Center
N-sybGal4 (#51635)	Neuronal synaptobrevin Gal4	Bloomington Stock Center
elav^{C155} Gal4	Gal4 neuronal expression	Bloomington Stock Center
Nrv2Gal4	Gal4 expression in wrapping glia	Bloomington Stock Center
GliGal4	Gal4 expression in subperineurial glia	(Sepp and Auld, 1999)
c527Gal4	Gal4 expression in perineurial glia	(Hummel et al., 2002)
RepoGal4	Gal4 expression in glia	Bloomington Stock Center
Repo4.3 Gal4	Gal4 expression in glia	(Lee and Jones, 2005)
LppGal4	Gal4 expression in fat body	(Brankatschk and Eaton, 2010)

2.2.6.4 UAS effector lines

Table 4: *Drosophila* UAS effector lines used in this study.

fly sock	comment	source / reference
UAS-CD8GFP	Membrane GFP expression	Bloomington Stock Center
UAS-Ferritin1HCH-HA	Ferritin1HCH-HA expression	This work
UAS-p24-1[D.viri]-3xHA	p24-1 from D. virilis expression	This work
UAS-24-1[stringDNA]	Synthetic p24-1 expression	This work
UAS-24-1[stringDNA]-GFP	Synthetic p24-1-GFP expression	This work
UAS-Rpl10ab-HA	Rpl10ab-HA expression	(Bischof et al., 2013)

2.2.6.5 Recombinants

Table 5: *Drosophila* recombinants generated in this study.

fly sock	comment	source
repoGal4, CD8mCherry, ppkGFP	repoGal4 and ppkGFP on third chromosome	This work
repoGal4, n-sybQF.2	repoGal4 and nsybQF.2 on third chromosome	This work

2.2.6.6 Q-System stocks

Table 6: *Drosophila* Q system lines used in this study.

fly sock	comment	source / reference
QF.2-Act5C	Actin 5 C promoter fusion	Bloomington Stock Center
QF.2-N-syb	QF.2 expression in neurons	Bloomington stock center
QUAS-GFP-Rpl10ab	Expression of GFP-Rpl10ab with Q system	This work
QUAS-HA-Rpl10ab	Expression of HA-Rpl10ab with Q system	This work

2.3 Immunohistochemistry

2.3.1 Fixation and antibody staining of *Drosophila* primary cells

The fixation protocol was performed at room temperature. Cells were grown in 24-well or 48-well plates. First, the cell culture medium was removed and 4% PFA was added for 15 minutes at room temperature. Then the PFA was removed and the fixed cells were washed three times for 5 minutes each with PBS. The permeabilization as performed by adding PBS with 0.1% Triton X-100 for two minutes followed by three washes with PBS. Now, the cells were blocked with 3% BSA in PBS for 30 minutes. The primary antibody was diluted in 3% BSA/PBS and the cells were either incubated for four hours at room temperature or overnight on 4°C. Afterwards, the coverslips were washed four times for 5 minutes with PBS. Now the secondary antibody was diluted 3% BSA and incubated on the cells for 2 h at room temperature. Upon three washes with PBS (5 min each), coverslips were briefly washed in ddH_2O and mounted on objective slides with a drop of Mowiol.

2.3.2 Dissection, fixation and antibody staining of larval nervous system

To analyze the larval nervous system as a whole filet preparation of the 3rd instar larvae was performed. The larvae of the right genotype were collected in PBS on a silica gel preparation plate. One larva was transferred to a drop of ice cold PBS and pinned on the plate, dorsal site up, with minutiae needles on the most anterior and posterior ends. Several washes with cold PBS helped to anesthetize the animal. Now a small cut at the dorsal posterior end and a long cut at the midline until the mouth hawks opened the animal. After removal of trachea and gut tissue with help of fine forceps, the preparation could be opened and fixed on 4 outer sides with needles. After 30 minutes of dissection, the filet preparations should be fixed.

For fixation, Bouin's solution (3 min fixation) or 4 % PFA was used (20 min fixation) was used depending on the antibody. Fixation was followed by three short washes and transfer of the filet preparations into a 1.5 ml reaction tube. Additional three 15 min washes with PBT were performed. Tissue was blocked at least 1 h with 10% goat serum at room temperature or at 4°C over night. Primary antibody was diluted in 10% goat serum and incubated with the

preparations at 4°C for 16 h. Antibody was removed and two short and three long washing steps (15 min each) was performed. Secondary antibody was again diluted in 10% goat serum and incubated with the preparations for 4 h at room temperature under agitation. Again, stained tissue was washed adequately. All liquid was removed and replaced by 2 drops of Vecta Shield mounting medium (Vector Laboratories). Tissue was stored several days until it was mounted.

The preparations were mounted on an objective slide in a drop of Vecta Shield. As a small spacer for the cover slip a bit of modeling clay was used. The cover slip was attached with 4 drops of transparent nail polish.

2.3.3 Staining of iron in the larval tissue

Iron can be found in two oxidation states, ferrous (Fe^{2+}) and ferric (Fe^{3+}) iron. To stain ferric iron the Perl's stain was applied; to stain ferrous iron the Turnbull's blue stain was used.

Third instar larvae were collected and dissected as described in 2.3.2. The tissue was fixed for 20 minutes in 4% Paraformaldehyde (PFA). The samples were washed three times with PBS. Before iron staining, the samples were incubated for 15 minutes in 2% H2O2 in Methanol. Then they rinsed well several times with distilled water. Now the staining working solutions could be prepared. For Perl's stain one part of 10% potassium ferrocyanide solution was mixed with one part of 10% hydrochloric acid. For Turnbull's blue stain one part of 2% ferricyanide solution was mixed with one part of 2% hydrochloric acid. The samples were immersed for 1 hour in the corresponding working solution. After removing the staining solution, the samples were washed 6 times with distilled water. To enhance the blue iron stain, a 3.3'-diaminobenzidine (DAB) enhancement was carried out with the ImmPACT DAB Peroxidase Substrate Kit (Cat.No. SK-4105, Vector Laboratories). The samples were covered with DAB working solution according to manufacturer's instructions. Afterwards the samples were washed for 5 minutes in distilled water. Before mounting on an objective slide, the samples were dehydrated with an ethanol series and cleared with 2 washes of xylene. Finally, the preparations were embedded in DePeX (Serva).

2.3.4 List of antibodies used for immunohistochemistry

2.3.4.1 Primary antibodies

Table 7: Primary antibodies used in this study.

Antibody	origin	Dilution	source / reference
α-Repo (8D12)	mouse IgG	1 : 200	Developmental Studies Hybridoma Bank
α-GFP	rabbit IgG	1 : 1000	Life Technologies
α-GFP	mouse IgG	1 : 1000	Life Technologies
α-HA (F7)	Mouse IgG	1 : 100	Santa Cruz
α-HA	Rabbit IgG	1 : 250	abcam
α-Bruchpilot	mouse IgG	1 : 300	Developmental Studies Hybridoma Bank
α-Elav	rat IgG	1 : 50	Developmental Studies Hybridoma Bank
α-Futsch	mouse IgG	1 : 200	Developmental Studies Hybridoma Bank
α-24B10	mouse IgG	1 : 100	Developmental Studies Hybridoma Bank
α-E06	mouse IgM	1 : 500	Avanti
α-ATP5α	mouse IgG	1 : 1000	abcam
α-HRP-Cy3	rabbit	1 : 200	Jackson ImmunoResearch
α-HRP-Alexa647	goat	1 : 200	Jackson ImmunoResearch

2.3.4.2 Secondary Antibodies and dyes

Table 8: Secondary antibodies used in this study.

Antibody	Conjugation	origin	Dilution	source / reference
α-Mouse IgG	Alexa 488, 555, 647	goat	1:1000	Life Technologies
α-Rabbit IgG	Alexa 488, 555, 647	goat	1:1000	Life Technologies
α-Rat IgG	Alexa 488, 555, 647	goat	1:1000	Life Technologies
α-Mouse IgM	Alexa 488, 555, 647	goat	1:1000	Life Technologies
ToPro3	-	-	1:10000	Life Technologies

2.4 Molecular biology

2.4.1 Bacteria strains

Table 9: Bacterial strains used for cloning in this study.

Strain	source
E. coli DH5α Max Efficiency competent cells	Thermo Fisher Scientific
E. coli OneShot Top10 chemically competent cells	Thermo Fisher Scientific
E. coli OneShot ccdB Survival 2T1 chemically competent cells	Thermo Fisher Scientific

2.4.2 Plasmids

Table 10: DNA plasmids used in this study.

Plasmid	Description	Reference
pUAST	P-element mediated germline transformation	(Brand and Perrimon, 1993)
pUASTattB	ϕC31 mediated germline transformation	(Bischof et al., 2007)
pUASTattB-RfA	ϕC31 vector combined with Gateway system	(Stephan, 2008)
pUASTattB-RfA-GFP	ϕC31 vector combined with Gateway system and c-terminal eGFP tag	(Stephan, 2008)
pUASTattB-RfA-3xHA	ϕC31 vector combined with Gateway system and c-terminal 3 x HA tag	(Stephan, 2008)
pUASTattB-Myc-RfA	ϕC31 vector combined with Gateway system and n-terminal Myc tag	(Stephan, 2008)
pQUAST	Q system germline transformation vector	(Potter et al., 2010)

pUAST-GFP-Rpl10ab	Transformation vector to express n-terminal GFP tagged Rpl10ab	(Thomas et al., 2012)
pUAST-HA-Rpl10ab	Transformation vector to express n-terminal HA tagged Rpl10ab	(Thomas et al., 2012)
pENTR/D-TOPO	Cloning vector, Gateway system	Life Technologies Inc.

2.4.3 Transformation of DNA

Transformation of plasmid DNA into chemically competent DH5α, TOP10 or *ccdB* Survival 2T1 *E. coli* cells was performed according to manufacturer's instructions. Upon heat-shock, 250 µl warm SOC medium was added and cells were incubated at 37°C for 1 hour under agitation. Finally, cells were spread on LB agar plates containing 100 µg/ml ampicillin or 50 µg/ml kanamycin according to the antibiotic resistance of the plasmid DNA and incubated for 16-18 h at 37°C.

2.4.4 DNA restriction

For DNA restriction, usually 1µg DNA was used. Restriction was performed as recommended by manufacturer's instructions (NEB). DNA and restriction enzyme mix was incubated for 2-3 hours at 37°C.

2.4.5 Mini plasmid purification

Single bacteria clones were inoculated in 4 ml LB medium containing the corresponding antibiotic and incubated for 16-18 h at 37°C under constant shaking. Medium was centrifuged at 10000g for 5 minutes. The isolation of plasmid DNA was performed with NucleoSpin Plasmid purification kit (Machery-Nagel) following manufacturer's instructions. DNA was eluted with 50 µl warm, sterile ddH_2O.

2.4.6 Midi plasmid purification

50 ml LB medium was inoculated with bacterial mini cultures of single clones and incubated under constant shaking overnight at 37°C. Cultures were centrifuged at 4000 g for 15 min at 4°C. Plasmid extraction was performed using NucleoBond Xtra Midi EF Kit (Machery-Nagel) followed by manufacturer's instructions. DNA was eluted using 250 µl warm, sterile ddH_2O. Concentration was determined with a NanoDrop2000c measuring the 260 nm absorbance of 1 µl DNA solution.

2.4.7 Isolation of genomic DNA from tissue

Isolation of genomic DNA from single flies was performed using the Invisorb Mini Tissue Kit (Invitek) according to manufacturer's instructions. Fly tissue was lysed overnight at 52°C and isolated DNA was reconstituted in 15 µl H_2O and stored at -20°C.

2.4.8 Polymerase Chain Reaction

Specific DNA sequences for cloning or genotyping were amplified by polymerase chain reaction (PCR). For cloning purposes, the Phusion High-Fidelity DNA polymerase Kit (NEB) was used. For conventional genotyping, the GoTag Flexi DNA polymerase Kit (Promega) was used. The PCR mix contained 1 x Polymerase buffer, 1.25 mM $MgCl_2$, 0.2 mM dNTPs, 0.5 mM of each primer, 1-5 µl of template DNA and 1.25 U of DNA polymerase. The mixture was filled up to 20 µl with ddH_2O and incubated in a Thermocycler with an adapted temperature profile as indicated in Table 11.

Table 11: Exemplary temperature profile for GoTaq and Phusion based PCR.

Temperature profile GoTag PCR		
95°C	3 min.	
95°C	30 sec.	39 cycles
64°C	30 sec.	
72°C	1 min.	
72°C	8 min.	
4°C	∞	

Temperature profile Phusion PCR		
95°C	30 sec.	
95°C	10 sec.	35 cycles
68°C	15 sec.	
72°C	15 sec.	
72°C	8 min.	
4°C	∞	

2.4.9 Agarose gel electrophoresis

To visualize PCR products or restriction enzyme digested products, DNA was separated by agarose gel electrophoresis and stained with the fluorescent DNA binding dye SybrSafe (Life Technologies). 1% agarose was mixed with 1 x TAE buffer and heated for 3 minutes in a microwave. SybrSafe (1 to 10 diluted) was added and the gel was cast in a gel chamber. 10-30 µl of DNA mixed with 10 x DNA loading dye was loaded in gel pockets and gel was run at 120V for 30-60 minutes. Finally, DNA was visualized with an INTAS UV system and the INTAS capture software.

2.4.10 Molecular Cloning

For cloning of most DNA plasmids, Life Technology's Gateway system was used. First, pENTR clones were generated using the pENTR/D-TOPO cloning Kit according to manufacturer's instructions. Plasmids were amplified by transformation in chemically competent E. coli Top10 cells. Screening for correct clones was performed by restriction enzyme digestion of plasmid mini preparations (MiniSpin Kit, Machery-Nagel) and sequencing followed by large scale DNA isolations via Midi preparations (Nucleobond Midi Kit EF, Machery-Nagel). To generate expression plasmids the Gateway LR clonase enzyme kit was used according to manufacturer's instructions. 100 ng pENTR containing the gene of interest was incubated wit 150 ng of expression vector containing the Gateway cassette (RfA). Correct clones were negatively selected in the presence of *ccdB* gene and by antibiotics resistance.

For integration of short sequences into a DNA plasmid site directed mutagenesis PCR was used (Liu and Naismith, 2008). PCR was performed as described with *Pfu* DNA polymerase (Promega). Integration was verified by sequencing.

2.4.11 Sequencing and primer design

Primers were designed with the DNAStar8 software SeqBuilder. Primer synthesis as well as sequencing was performed by the AGCTLab (core facility, MPI for experimental medicine). Sequences were evaluated with DNAStar8 software SeqMan.

2.5 Biochemical methods

2.5.1 Protein extraction from *Drosophila* larvae

Third instar larvae of the correct genotype were collected and washed in PBS. If brain extracts were needed, larvae were dissected in ice cold PBS. Brains were collected on ice in a fresh 1.5 ml reaction tube with protein lysis buffer. Depending on the downstream application either 2-3 µl of lysis buffer was used per brain. If whole larval extracts were needed, the larvae were transferred directly to a pre chilled dounce homogenizer. 10-15 µl of lysis buffer was used per larva. The tissue or the larvae were homogenized on ice with a pestle, passed through a 27 gauge needle and if needed, sonicated for 1 minute (Branson type sonicator) with 30% power. The crude lysate was cleared by centrifugation at 10000 g, 4°C for 20 minutes. The liquid phase (between the pellet and the lipid phase) was transferred to a fresh reaction tube

2.5.2 SDS polyacrylamide gel electrophoresis

Proteins of tissue lysates were separated by size on a sodium dodecyl polyacrylamide gel electrophoresis (SDS page) (Laemmli, 1970). To cast the polyacrylamide gels the Bio-Rad mini gel system was used. The composition of a 10 % mini gel is indicated in Table 12 . Prior to loading equal amounts of protein lysate on the gel, 4x Laemmli buffer was added to the protein lysate and samples were heated for 10 min at 70°C. For non-reducing gel electrophoresis no reducing agent (DTT or β mercaptoethanol) was added to the sample buffer. Empty gel pockets were loaded with Laemmli buffer only and one pocket was loaded with 5 µl of pre-stained protein ladder (Thermo Fisher Scientific). Electrophoresis was performed at 100 V in running buffer.

Table 12: Recipe for polyacrylamide mini gels.

Stacking Gel		Resolving Gel 10%	
H_2O	1.21 ml	H_2O	1.66 ml
30% Acrylamide solution	0.27 ml	30% Acrylamide solution	2.04 ml
Stacking buffer	0.5 ml	Resolving buffer	1.3 ml
10% SDS solution	20 µl	10% SDS solution	50 µl
10% APS solution	20 µl	10% APS solution	50 µl
TEMED	3 µl	TEMED	2 µl

2.5.3 Western blot and protein detection

Upon separation of proteins Western blot was performed (Burnette, 1981). The mini gel (only the resolving gel part) was incubated for 5 minutes in transfer buffer. Then, the gel together with Whatman filter papers and nitrocellulose membrane was assembled in a blotting cassette (Bio-Rad). Blotting was performed at 4°C with a cooling pack at 30 V for 16 h. After transfer, the nitrocellulose membrane was transferred to a 50 ml tube and blocked with 5% milk in PBS-T for 60 min under agitation. Then, the first antibody was added and the membrane was incubated on 4°C overnight. After washing with PBS-T, the second HRP-coupled antibody was added and incubated for 60 min at room temperature followed by 30 min washing with PBS-T. Proteins were detected by adding Pierce ECL Western Blotting substrate. The light emission was detected with X-ray films.

2.5.4 Cell type specific affinity isolation of translating Ribosomes (TRAP)

For this method flies were bred expressing the ribosomal Protein RPL10 tagged with the HA protein label. The UAS- or QUAS-HA-Rpl10ab construct was either expressed in glial cells (with repoGal4) or in neurons (with n-syb QF.2). Around 200 3rd instar larvae of the corresponding genotype were collected and washed in PBS. All the following steps were performed on ice.

3 ml of polysome extraction buffer per genotype was prepared freshly by adding 0.5 mM DTT, 100 µg/ml cycloheximide, 1x Complete Protease Inhibitor and 100 U/ml RNAse OUT. For dissection, 10 ml polysome extraction buffer was prepared without RNAse OUT. Larval nervous systems were dissected and collected in 500 µl cold extraction buffer. Homogenization was conducted with a pre-cooled pestle and by passing the lysate through needles (20 gauge, 23 gauge, 27 gauge). Lysates were incubated for 30 min on ice and finally centrifuged at 10000 g for 30 min at 4°C. In the meantime, magnetic α-HA beads (F-7, Santa Cruz) were washed two times with 900 µl extraction buffer by collecting the beads for 1 min on a magnet. The liquid phase was transferred to a fresh 1.5 ml reaction tube and incubated with the magnetic beads overnight at 4°C under agitation.

4 ml of wash buffer was prepared. The supernatant was removed from the beads and three washes with gentle resuspending followed. Beads were transferred to a fresh RNAse free 1.5 ml reaction tube and resuspended in 400 µl wash buffer. 5 µl 10% RNAse-free SDS solution and 5 µl of Proteinase K (RNAse-free, PeqLab) were added followed by an incubation at 55°C for 30 min. For RNA extraction, 400 µl Phenol/Chloroform/Isoamylalcohol (acidic, C. Roth) was added and vortexed for 30 sec. Mixture was transferred to Phase Lock Gel tube (5Prime), mixed by handshaking for 5 min and centrifuged at 14000 g for 5 min at RT. The upper phase was transferred to a fresh Phase Lock Gel tube, 400 µl Phenol/Chloroform/Isoamylalcohol was added and extraction was repeated. The upper phase was transferred to a fresh 1.5 ml reaction tube. RNA was precipitated by adding 0.1 x volumes of 8M LiCl, 0.007 x volumes of Glycoblue (15mg/ml) and 3 x volumes of 100% ice cold Ethanol. Mix was inverted and incubate for 8-15 hours on -20°C. The sample was centrifuged at 16000 g for 45 min at 4°C. The pellet was washed carefully with 500 µl 70% Ethanol and 5 min centrifugation at 4°C. After removal of the Ethanol the pellet was dried for 30 to 45 min at 4°C, resuspended in 20 µl RNAse-free water and stored at -80°C.

2.5.5 DNAse treatment of RNA

Before starting, the complete work place as well as pipettes and devices were cleaned with RNAseZAP or with an Ethanol/ 2% SDS mixture to avoid RNAse contamination.

RNA was thawed slowly on ice and filled up to 50 µl volume by adding 5 µl 10 x DNAse reaction buffer, 1 µl DNAse I (10 U/µl, Roche), 0.5 µl RNAse OUT and RNAse-free ddH_2O. The mix was incubated at 37°C for 20 min. Then, 150 µl ddH_2O and 200 µl P/C/I was added. After mixing for 30 sec on a vortex, the liquid was transferred to a Phase Lock Gel tube and mixed by hand shaking for 5 min. Upon centrifugation at 14000 g for 5 min at RT, the upper phase was transferred to a fresh 1.5 ml reaction tube. 200 µl P/C/I was added and mixed on a vortex followed by centrifugation. The upper phase was transferred to a fresh reaction tube. RNA was precipitated by adding 0.1 x volumes of 3 M NaAcetate, pH4.8, 0.007 x volumes of GlycoBlue (15 mg/ml) and 1 x volume of isopropanol on -20°C for at least 1 h. The mixture was centrifuged at 16000 g for 30 min at 4°C. The supernatant was removed carefully and the pellet was washed with 1 ml 75% Ethanol and 5 min centrifugation at 4°C. After removing the supernatant, the pellet was dried for 30 to 45 min and resuspended in 20 µl RNAse-free ddH_2O. The concentration was determined using a NanoDrop. RNA was stored at -80°C.

2.6 Image acquisition, processing and equipment

2.6.1 Equipment used for image acquisition

Table 13: List of microscopes used in this study.

Equipment	Company
LSM 510 Confocal Microscope	Carl Zeiss
Stereo Discovery V8 Microscope	Carl Zeiss
Axiovert 100 M Fluorescent Microscope	Carl Zeiss

2.6.2 Software

Table 14: List of software and online resources used in this study.

Name of the Software	Application	Source
Adobe Illustrator CS4	Image processing	*www.**adobe**.com/products/**illustrator**.html*
Adobe Photoshop CS4	Image Processing	*www.**adobe**.com/products/**photoshop**.html*
DNASTAR Lasergene 8	DNA analysis and editing	*www.**dnastar**.com/t-**dnastar**-**lasergene**.aspx*
Zen Software	Image acquisition	*www.**zeiss**.com/microscopy/en_de/products/.../**zen**-lite.htm*
Mendeley	Bibliography manager	*https://www.**mendeley**.com/*
Graphpad Prism	Statistical analysis	*www.**graphpad**.com/scientific-software/**prism**/*
Bitplane Imaris	Image processing and analysis	*www.**bitplane**.com/*
Flybase	Genomic annotations in *D.m.*	*http://**flybase**.org/*
Bloomington	Fly line distributor	*http://**flystocks**.bio.indiana.edu/*
VDRC	RNAi lines distributor	*http://stockcenter.**vdrc**.at/*
DPiM	Protein interaction map	*https://**interfly**.med.harvard.edu*
Uniprot	Protein database	*www.**uniprot**.org/*
Signal P 4.1	Protein prediction tool	*www.cbs.dtu.dk/services/**SignalP**/*
Panther	Gene list analysis	*http://**panther**db.org/*

2.6.3 Statistical analysis

The statistical analysis was performed with the Graphpad prism software. To compare two groups a Student's t-test was used. For the comparison of tree or more groups the one-way ANOVA was performed. The post-hoc Bonferroni test was applied for a pairwise comparison. A p value of smaller than 0.05 was considered statistically significant for all tests. Results were expressed as standard error of the mean (SEM).

3 Results

3.1 Screening of conserved glial proteins

To study neuron-glia interactions, we used the *Drosophila* peripheral nerves as a model system. The fly's peripheral nerves have a simple structure, are easy to access and versatile genetic tools make them suitable for a screening approach. To identify glial genes, which are important for neurons, we designed a screen in which we inhibited a set of genes in the glia and searched for neuropathies. The technique of RNA interference combined with the UAS/Gal4 expression system allows tissue specific gene silencing.

3.1.1 Selecting candidates that are necessary in vertebrates and invertebrates

We were interested to identify candidates, which are conserved between vertebrates and invertebrates. As a basis for the selection of candidates, a proteome analysis of axo-glial fractions from human and mouse central nervous system has been used (Manrique-Hoyos, 2012). With the help of the NCBI search tool HomoloGene (www.ncbi.nlm.nih.gov/homologene), we selected those proteins, which had a homolog, or a similar protein in *Drosophila*. The UAS-RNAi fly lines for the selected 141 candidates were provided by VDRC (Table 18). As a glia specific driver line repo4.3;repoGal4,CD8GFP was used also expressing a membrane bound GFP. Most analyses in this study were performed with the repoGal4 line harboring two Gal4 insertions (also referred to as repoGal4,CD8GFP).

3.1.2 Screening concept and results

For the screening procedure, crossings of repoGal4,CD8GFP virgins and UAS-RNAi males were incubated at 25°C (Figure 5 A). The nervous system of third instar larvae was dissected and immunohistochemically stained for glial (anti-repo, anti-GFP) and neuronal markers (anti-HRP,

anti-Futsch). A confocal analysis revealed that 40.14% of all candidates (56 lines) showed changes of the peripheral nerves after glia specific knockdown (Figure 5 B). The alterations included defasciculated and destabilized axons, axonal swellings, glial swellings, glial wrapping failure and faint glial signal.

To categorize the positive candidates, we used the Panther gene list analysis tool (Mi et al., 2013). The majority of the identified gene functions included binding (24%), catalytic activity (24%) and transporter activity (14%) (Figure 5 C).

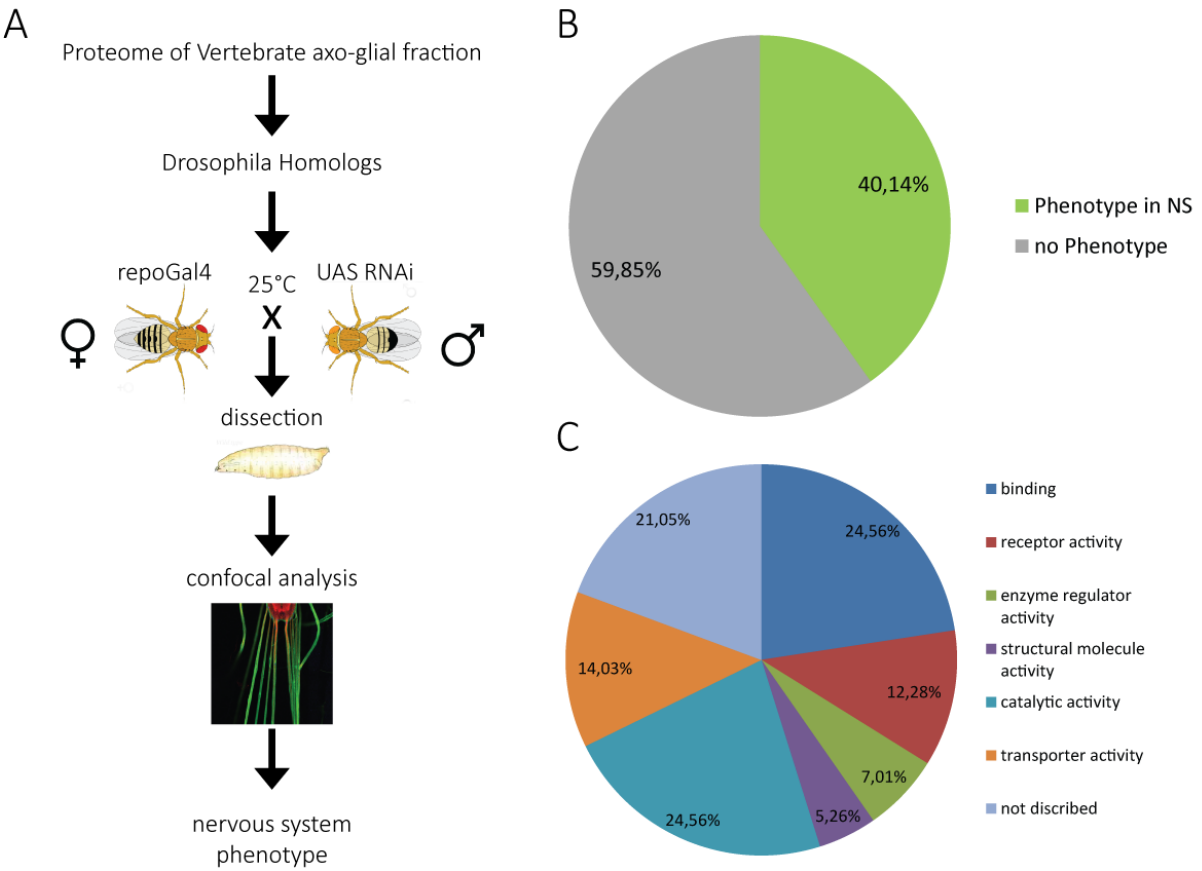

Figure 5: Scheme and results of glial specific RNAi screen. (**A**) The screening procedure is depicted. *Drosophila* RNAi of the selected candidates was expressed with the glial-specific repoGal4 driver line. Third instar larval PNS were scored after confocal analysis for PNS changes. (**B**) Results from screening. 141 RNAi lines were analyzed. 56 lines showed defects in the nervous system upon glial inhibition. (**C**) Panther gene list analysis. Positive candidates were grouped by gene function.

3.2 p24-1 is crucial for the axon-glial architecture

3.2.1 p24-1 expression is essential for glial cells

Regarding the screening outcome, the candidate p24-1 displayed the strongest effect on peripheral nerves upon knockdown in the glia. Therefore, we subjected p24-1 to a more elaborate investigation.

Inhibition of p24-1 in glial cells with VDRC line p24-1$^{GD\ 12196}$ resulted in lethality of the animals during late larval stages. Observations of the animals' behavior indicated no effect in first and second instar larval stage. Third instar larvae, in contrast, developed crawling problems. The motor defects became more prominent in older animals. In comparison to wild-type larvae, p24-1 RNAi expressing larvae were not able to crawl up the walls of housing vials (during wandering larval stage). In addition, the larvae could not enter pupal stage and remained up to several days in third instar stage until they died.

The confocal analysis of third instar larval nervous system upon glial p24-1 inhibition showed severe malformations of the peripheral nerves (Figure 6 B). The glia membrane was visualized by antibody staining of the membrane bound GFP. Neurons were stained with the pan-neuronal marker anti-HRP as well as with a sensory neuron specific antibody against Futsch.

The confocal pictures revealed that glia and axons generated swellings along the nerve, which never occurred in wild-type control nerves. The glia cell seemed disassembled in swelling regions. In some parts of the nerve, the glial GFP signal appeared faint, whereas in other parts it appeared similar to wild-type nerves.

3.2.2 p24-1 inhibition has an strong effect on axons

Glial p24-1 RNAi expression however had a much more remarkable effect on the axon morphology. The axons formed protrusions, which were in parts not ensheathed by glia membrane (Figure 6 B, C). Before and after this local out-foldings, the axons appeared normal which was in contrast to wild-type axons that were completely covered by glia membrane (Figure 6 A). To be able to distinguish between axonal membrane and cytoskeleton we used a

neuronal membrane marker (HRP) and an antibody against the microtubule associated protein Futsch. With both markers, we were able to detect the characteristic bulging phenotype. This antibody combination also allowed us to distinguish between motor and sensory axons since Futsch is only expressed in sensory neurons (Hummel et al., 2000). The pictures showed that not only Futsch-positive but also all other HRP labeled axons undergo morphological alterations, meaning that sensory and motor axons are affected (Figure 6 C).

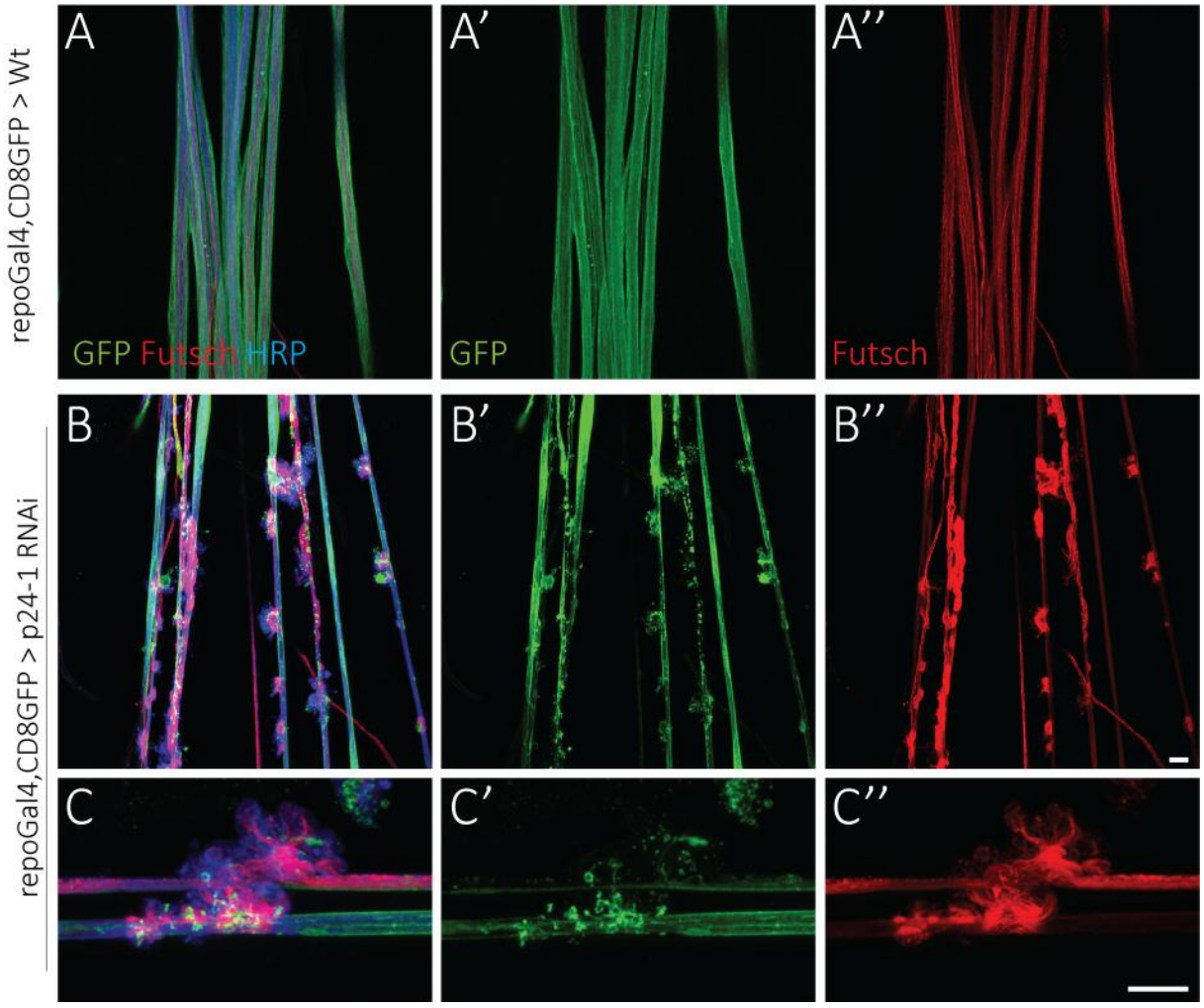

Figure 6: Glial inhibition of p24-1 gene function shows out-foldings in PNS. (**A**) Along peripheral nerves glial damage (green) and axonal out-foldings were observed upon expression of p24-1 RNAi in the glia. (**B**) repo4.3;repoGal4>CD8GFP/+ was used as control. (**C**) Futsch labeled sensory neurons and other HRP marked neurons are affected by the out-foldings. Glia membrane is not ensheathing the out-folded areas. Scale bar 10 µm.

3.2.3 Weak glial defects after p24-1 inhibition in glial sub-classes

To dertermine in which glial cell type p24-1 function was required, we induced RNA interference in the three glial subtypes seperately. Glial membrane was labeled by expression of a membrane bound CD8GFP. Neurons were visualilzed with the HRP antibody. Inhibition of p24-1 in the wrapping glia with nervana2Gal4 did not cause lethality in third instar larvae, but the evaluation of the confocal images revealed strong wrapping defects (Figure 7 A). Membranes of wrapping glia cells were not evenly distributed along the nerve or were even missing (compared to control Figure 8 B). In some nerves, deposits of CD8GFP labeled membrane could be found, which indicates rather a degenerating than a developmental defect. An axonal phenotype was not detectable after p24-1 inhibition in the wrapping glia. Inhibition in the subperineurial glia with gliotactinGal4 (Figure 7 B) and in the perineurial glia with C527Gal4 (Figure 7 C) neither displayed the out-folding phenotype nor lethality. The only defect observed was a faint GFP signal after p24-1 inhibition in subperineurial glia (Figure 7 B) indicating mild defects. To conclude the analysis of the glial sub-classes, p24-1 seems to have a function in wrapping and subperineurial glia.

Because of the strong axonal phenotype after inhibition with repoGal4, we wondered if p24-1 function is also required in neuronal cells. Therefore we expressed p24-1 RNAi with the neuron specific Gal4 driver n-syb (neuronal synaptobrevin). As shown in Figure 7 D, there was no defect visible after neuronal inhibition. Hence, p24-1 seems to have no or minor functions in neurons during larval stages.

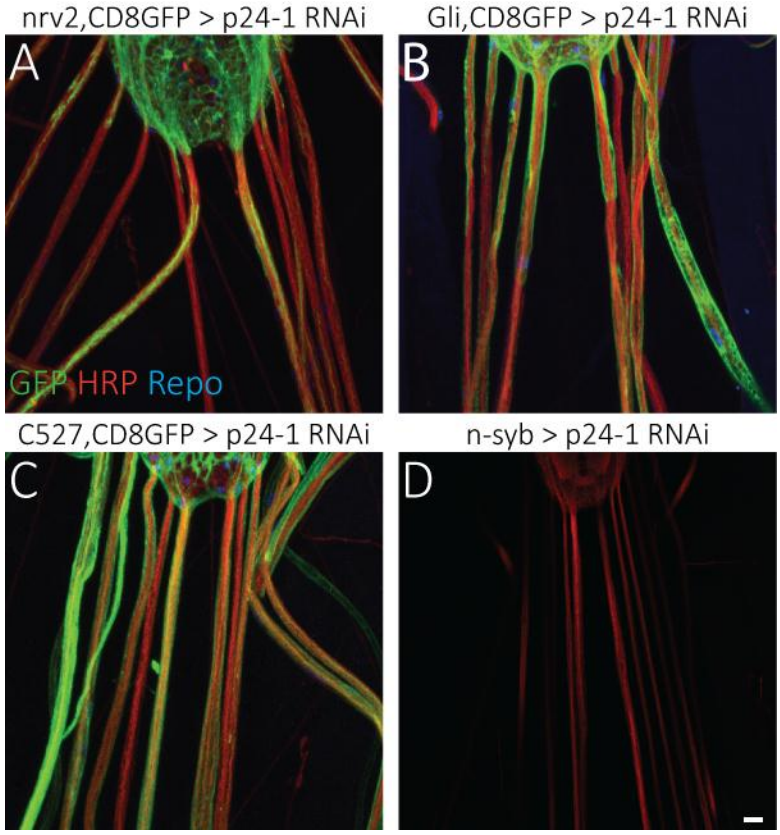

Figure 7: p24-1 inhibition in glial subclasses and neurons. Glia membrane was labeled with anti-GFP (green), glial nuclei with anti-Repo (blue) and neurons with anti-HRP (red). (**A**) p24-1 RNAi was expressed in wrapping glia with nervana2 Gal4. Wrapping defects were observed. (**B**) Expression in subperineurial glia with gliotactin Gal4, (**C**) in perineurial glia with C527 Gal4 and (**D**) in neurons with n-syb Gal4. No neuronal out-foldings were detected. Scale bar 10 µm.

3.2.4 p24-1 is required in wrapping and subperineurial glia

Because the axonal out-folding phenotype was not detectable after p24-1 inhibition in the different glial sub-classes, we repeated the analysis of the sub-classes by using GFP exon trap lines, which allow Gal4 independent labeling of glia sub-types. The wrapping glia was marked with a GFP insertion into the *nervana2* gene (BL #6828). The subperineurial glia was labeled by a GFP insertion in a not-yet defined gene (Piggy Bac #261, C. Klämbt unpublished). Septate junctions were labeled by a GFP insertion (#454) into the *neurexinIV* gene (Edenfeld et al.,

2006) and perineurial glia by a GFP insertion into the *jupiter* gene (Bl #6836). The marker lines were combined with the pan-glial driver line repoGal4.

When examining the wrapping glia, we could detect strong wrapping defects (Figure 8 A) compared to control nerves (Figure 8 B). In some parts the wrapping glia cells were present but did not enwrap the axons, in other areas the cell looked fragmented. In the protrusion, the wrapping glia appeared disassembled. These observations are in accordance to the phenotype generated by p24-1 RNAi expression with nervana2 Gal4 (Figure 7 A).

The subperineurial glia seemed to be present surrounding the nerve (Figure 8 C) as in control images (Figure 8 D), but the GFP signal in the PNS was faint, which indicated a defect in this cell type. As described in 1.1.3, the most important feature of the subperineurial glia is formation and maintenance of the BBB, which is based on auto-cellular septate junctions. To investigate the integrity of the BBB, we used the *neurexinIV*$^{\#454}$ GFP trap line as a marker for septate junctions. In control animals, the NeurexinIV signal formed one straight line along the nerve and a ring-like structure at the sites where two subperineurial cells met (Figure 8 F). Inhibition in the glia led to a disturbed NeurexinIV pattern. In nerves not displaying out-foldings the signal was diffuse, whereas in nerves with axonal out-foldings the signal was interrupted (Figure 8 E).

Perineurial glia cells surrounded the nerve as in control animals (Figure 8 G, H). In some cases, they covered the out-folded areas but in others not (Figure 8 G). To summarize the analysis of the glial sub-types, we found that the wrapping glia and the subperineurial glia were affected upon pan-glial p24-1 inhibition.

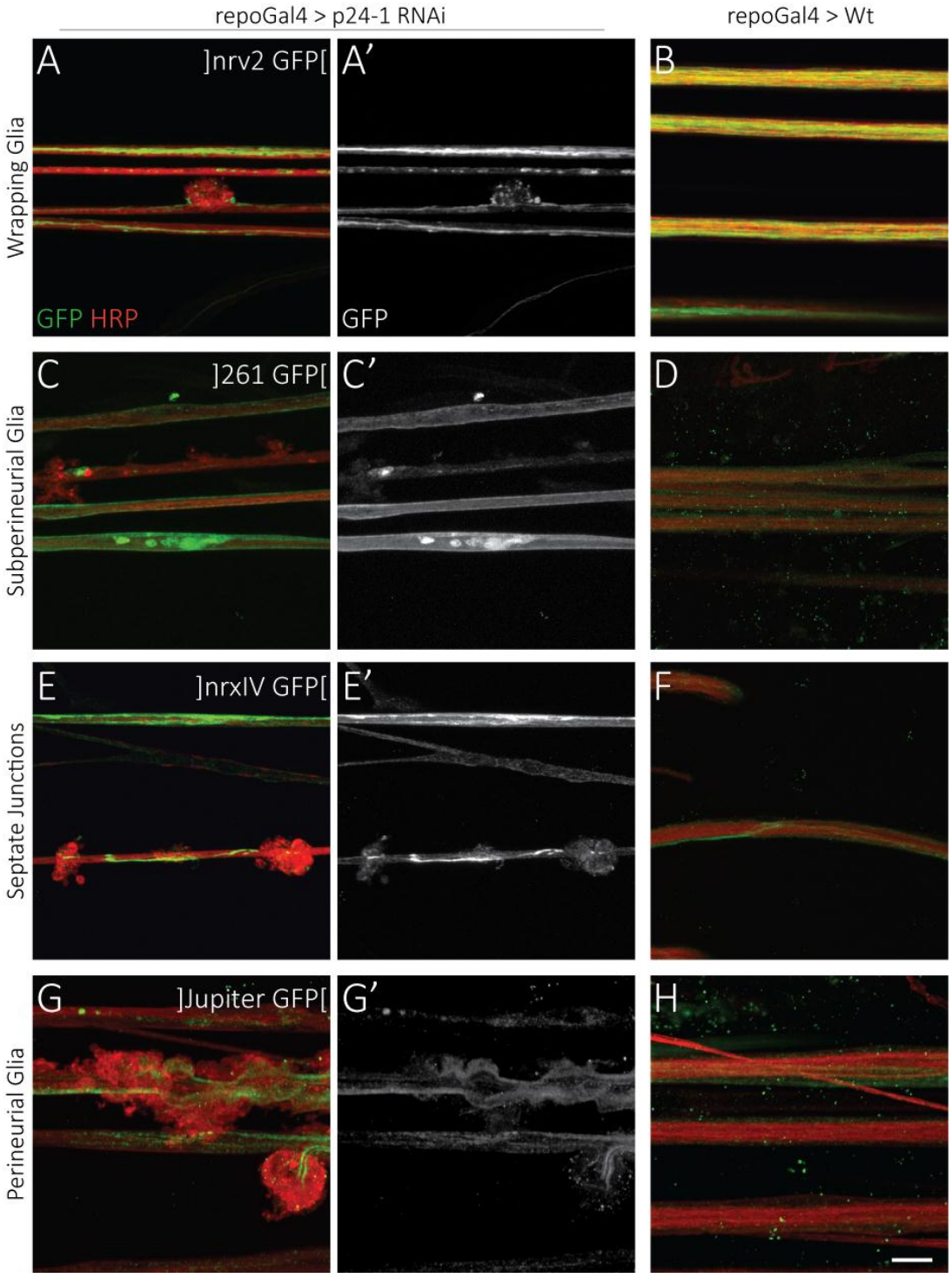

Figure 8: Gal4 independent analysis of glial sub-classes after p24-1 inhibition in glial cells. GFP marks glial structure (green), HRP stains neurons (red). (**A**, **B**) wrapping glia was labeled with the nrv2GFP trap. (**C**, **D**) subperineurial glia was labeled with the #261-GFP trap. E, F septate junctions were labeled with the nrx IV 454 GFP trap. (**G**, **H**) perineurial glia was labeled with the Jupiter GFP trap. Genotypes of GFP-trap;repoGal4/p24-1 RNAi (**A**, **C**, **E**, **G**) was compared to GFP-trap;repoGal4/+ (**B**, **D**, **F**, **H**). Scale bar 10 µm.

3.2.5 Ultrastructure reveals massive glial defects and axonal loss

Transmission electron microscopy (TEM) was used to analyze the details of the cellular structure of glial cells upon p24-1 inhibition. In control nerves of third instar larvae, we could clearly distinguish between perineurial, subperineurial and wrapping glia cells. Wrapping glia was separating all the axons at the end of the larval stage (Figure 9 C). Upon p24-1 RNAi expression with repoGal4, the glia seemed disorganized (Figure 9 A, B). In non-protrusion areas perineurial glia and subperineurial was present and surrounded the axons. However, there was no separation of axons by wrapping glia (Figure 9 B). We also found vesicular structures and signs of degradation. The neural lamella was thinner compared to wild-type nerves. In the out-folded areas, the structure seemed severely destructed. Discrimination between the glial sub-types was not possible (Figure 9 B). Quantifications of the axon number revealed 76 axons (SEM ± 0.8) wild-type segmental nerves A4-A6. After inhibition of p24-1 in glial cells we found significantly less axons per nerve (mean = 55.3 SEM ± 1.66, Figure 9 C).
The TEM data show that upon p24-1 inhibition, degradation occurred in peripheral nerves causing disassembly of glial cells and loss of axons.

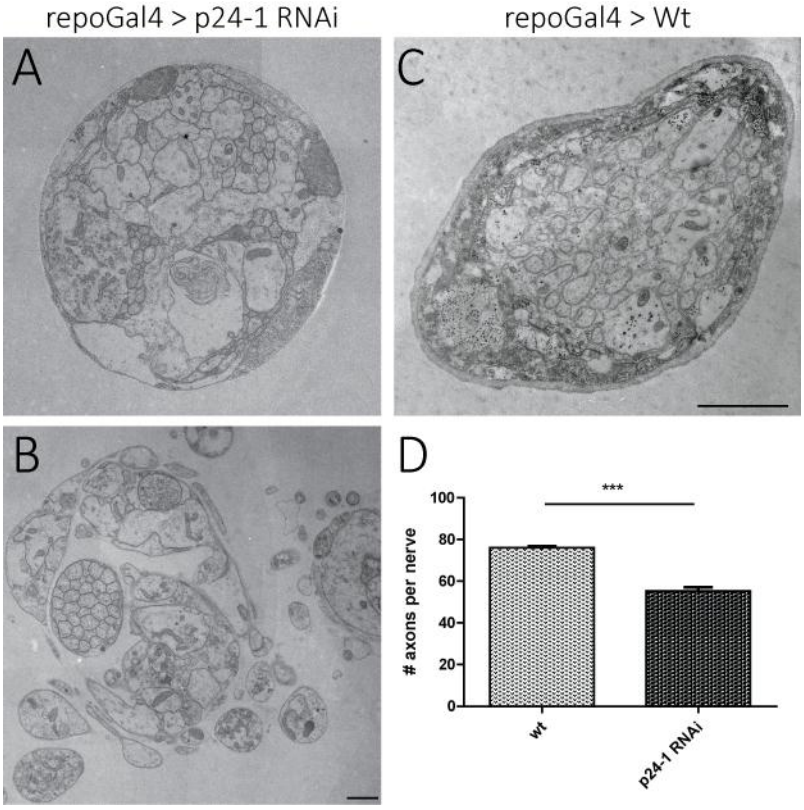

Figure 9: Ultrastructural analysis of the p24-1 phenotype in the PNS. TEM micrograph of third instar larval peripheral nerves, cross sections. (**A**, **B**) Nerve sections upon p24-1 inhibition in glia, genotype repoGal4/p24-1 RNAi, display massive disassembly in non-protrusion (**A**) as well as in protrusion areas (**B**). (**C**) Control nerve, genotype repoGal4/+. All glial sub-types can be identified. (**D**) Quantification of axon number reveals axonal loss upon p24-1 inhibition. Scale bar 2 µm.

3.2.6 No apoptosis detectable upon p24-1 inhibition

Regarding the massive glial and axonal defects observed in the ultrastructural analysis, we expected glial and neuronal cell death. To monitor cell death, the terminal deoxynucleotidyl transferase dUTP nick end labeling (TUNEL) assay was performed, which can detect fragmented DNA resulting from apoptotic nuclei. For the assay, glial membrane was labeled by expression of membrane bound mCD8Cherry red-fluorescent protein (red). TUNEL positive cells were detected by green fluorescence and all nuclei were labeled with the DNA

intercalating dye ToPro3. Glial inhibition of p24-1 did not result in TUNEL positive cells (Figure 10 A). In control nerves there was, as well no TUNEL staining detectable (Figure 10 B). DNase treated tissue served as positive control in which TUNEL staining was observed in all nuclei of the PNS and CNS (Figure 10 C).

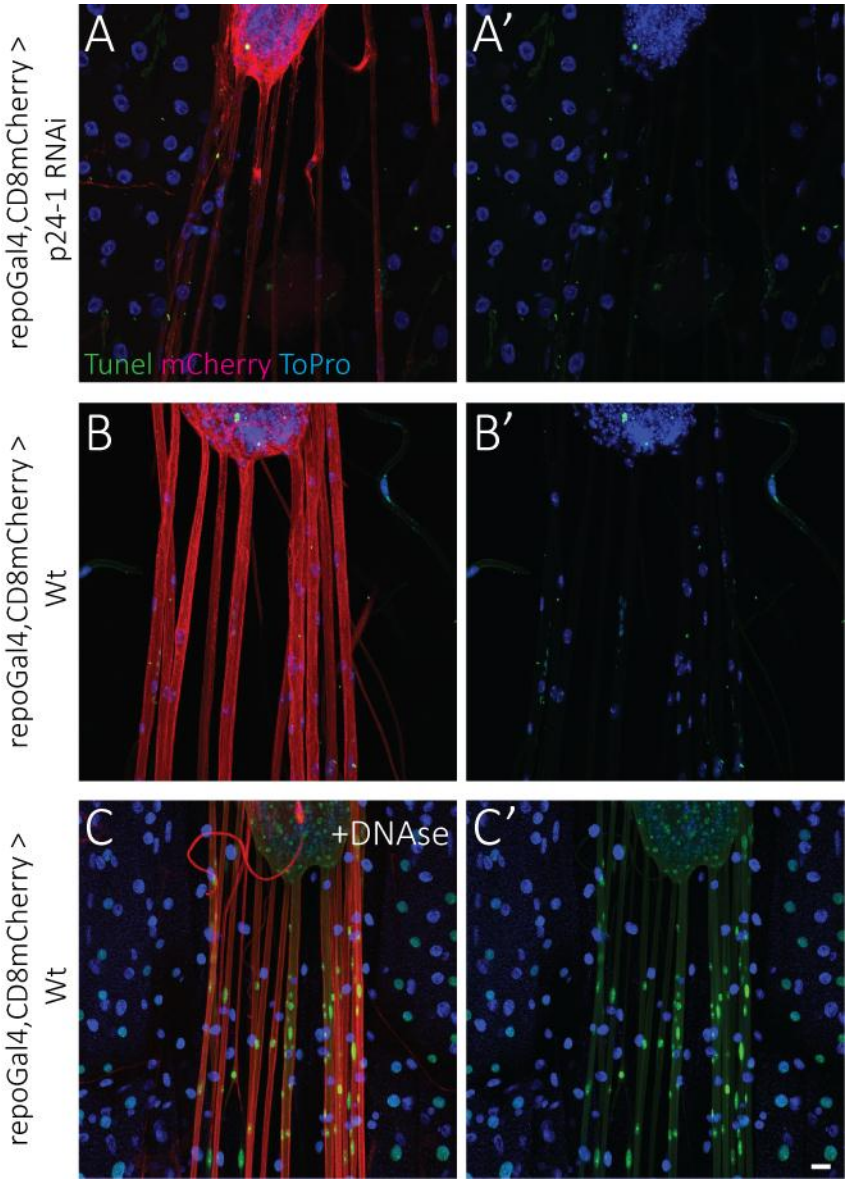

Figure 10: Tunel assay is negative upon p24-1 inhibition. Tunel assay in third instar PNS. Glia membrane was labeled by mCD8Cherry expression (red), TUNEL positive cells (green) and all nuclei with ToPro dye (blue). (**A**) Inhibition of p24-1 in glial cells did not show TUNEL positive cells. (**B**) Control nerves were negative for TUNEL stain. (**C**) DNase treated control nerves with nerves were positive for TUNEL stain. Scale bar 10 µm.

3.3 Non-cell autonomous effects of p24-1 inhibition

3.3.1 Single axon labeling illustrates local instabilities

Regarding the initial experiments, we deduced that p24-1 RNAi expression in glial cells had a strong non-cell autonomous effect on axons. To clarify what happens to the neuron, we made use of the fly line pickpocket-GFP expressing a GFP fusion protein of the sodium channel pickpocket (ppk), which labels two to four axons per nerve. This fly line was combined with the pan-glial driver line repoGal4 and a membrane bound CD8mCherry insertion (red). In control nerves, the axons were aligned straightly throughout the nerve (Figure 11 C). In contrast, inhibition of p24-1 in the glia displayed local axonal instabilities. Before and after the out-folding the axons run straight, but in the area of the protrusion, it made a loopy structure (Figure 11 A). Exemplarily, the dimension of the out-folding was 23 µm in length and 20 µm in height.

The single axon labeling revealed another characteristic. Upon inhibition of p24-1, we observed small swellings of the axon itself (Figure 11 B). The swellings were found all along the nerve, in the out-folded areas and in the straight parts.

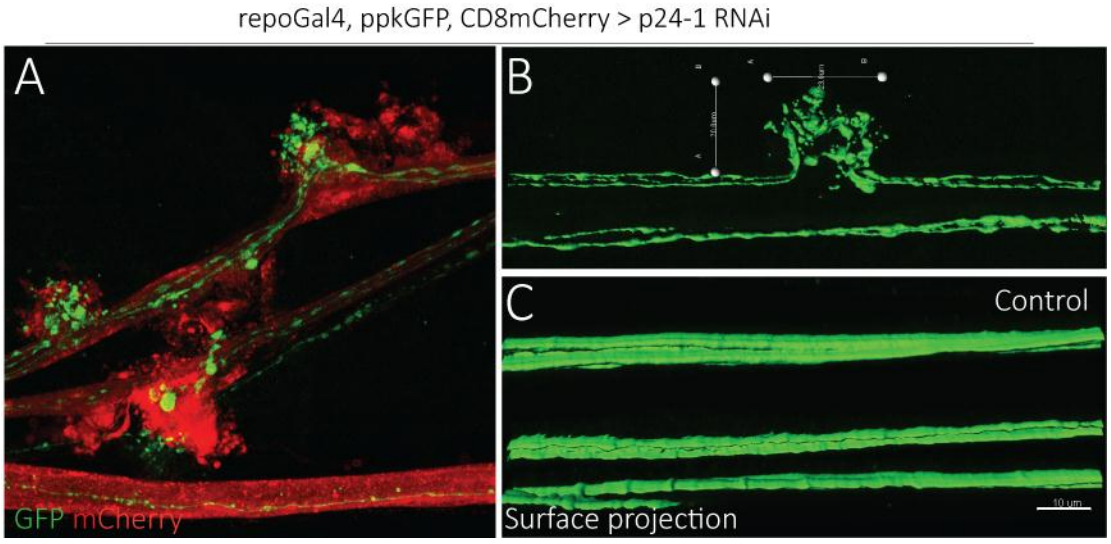

Figure 11: Single axon labeling shows local instabilities. Glia membrane was labeled by CD8mCherry expression (red) and axons by ppk-GFP expression (green). (**A**) Expression of ppk-GFP allowed single axon labeling of 2 to 4 axons per nerve. Upon pan-glial p24-1 inhibition, local axonal instabilities and axonal swellings were visible. (**B**) Imaris 3D reconstruction of ppkGFP expressing axons reveals out-foldings of ~20 x 23 µm length. In addition, axonal swellings are visible. (**C**) Projections of control axons do not show swellings or alterations. Scale bar 10 µm.

3.3.2 Axonal transport defects after p24-1 inhibition

One feature of axonal integrity is fast axonal transport. Synaptic proteins synthesized in the cell body need to be transported along the axon to the synapse (anterograde transport), and other proteins need to be transferred back from the periphery to the cell body (retrograde transport). Because we observed swellings in the axon upon p24-1 inhibition in larval nerves, we wondered if axonal transportion is affected. For the analysis, we used an antibody against the synaptic protein Bruchpilot (Brp). Brp-positive vesicles are transported from the neuronal cell body in the CNS to the motor synapse. In third instar larval nerves of control animals, only few vesicles were visible (Figure 12 A). Upon pan-glial p24-1 inhibition, a high number of Brp-positive vesicles were visible along the axon (Figure 12 B) revealing massive traffic jam. A high vesicle density was observed in the protrusion area, but also in straight part of the nerve. Thereby, some nerves seemed to be heavily affected while others showed a lower vesicle density.

Regarding the non-uniform distribution of axonal vesicles, we wondered if the transport defects were linked to the axonal out-folding phenotype. To answer this question, we had a look at second instar larvae, which did not display out-foldings yet. In control second instar larval nerves few Brp-positive vesicles were detected (Figure 12 C). In second instar larvae after glial p24-1 inhibition, we could detect a higher density of Brp vesicles than in control.

To summarize the above findings, we found that p24-1 inhibition in glial cells generates transport defects of axonal vesicles from second instar stage on.

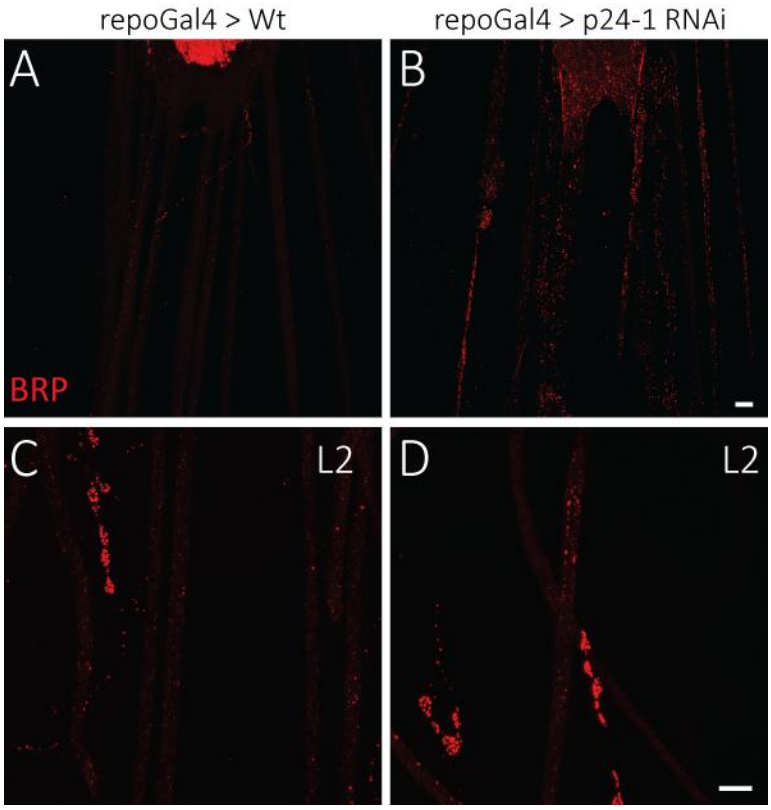

Figure 12: Vesicular traffic jam in axons upon p24-1 inhibition
Anterograde transport of Bruchpilot-positive vesicles (red). (**A**, **C**) In control peripheral nerves of third instar (**A**) and second instar (L2) larval nerves (**C**) few vesicles are visible. Genotype repoGal4CD8GFP/+. (**B**, **D**) Peripheral nerves after p24-1 inhibition in glial cells reveals axonal transport defects in third instar (**B**) and second instar stage (**D**). Genotype repoCD8GFP/p24-1 RNAi. Scale bar 10 µm.

3.3.3 p24-1 phenotype kinetics reveal progressive defects

From previous experiments, in which we analyzed the axonal out-foldings (Figure 6 B) and transport defects of axonal vesicles (Figure 12 B), but also from behavioral observations of the animals, it became obvious that nervous system defects appeared late during larval stages. Therefore, we analyzed the kinetics of the p24-1 phenotype. First, the average number of protrusions per nerve was quantified (Figure 13 A). For that purpose, confocal 3D images of the whole nervous system were generated. We visualized neurons with the HRP antibody. In late second instar stage at 70 hours after egg lay (AEL) nearly no protrusions were detected (mean = 0.05). In mid third instar stage at 96 hours AEL, 1 to 3 nerves per filet preparation were affected (mean = 0.29). In wandering larval stage at 118h AEL on average nearly every nerve was affected (mean = 0.77). As upon p24-1 inhibition larvae did not enter pupal stage and remained in third instar stage, animals were also dissected at 140h AEL. In that prolonged third larval stage we detected the highest number of out-foldings per nerve (mean = 1.94).

Next, the kinetics of the axonal transport was assessed (Figure 13 B). Brp-positive vesicles were stained and counted with help of the software Bitplane Imaris. Vesicle numbers were normalized to those of control animals of corresponding stage. Quantification of Brp-positive vesicles in second instar larvae (70 hours AEL) revealed a 1.39 fold increased vesicle number of p24-1 RNAi versus control. This result confirmed the observations of the vesicle transport defect in peripheral nerves we made in previous experiments (Figure 12 C, D). In mid third instar stage, we observed a 2.11 fold increase of vesicle number compared to control. At 118h and 140h AEL, the increase was even higher compared to control with 3.45 fold and 3.61 fold respectively (Figure 13 B).

In conclusion, the out-folding phenotype and the transport defect after glial p24-1 inhibition display progressive kinetics. While the out-foldings became apparent in the mid to late third instar stages, the axonal transport defects were already detectable in second instar larvae.

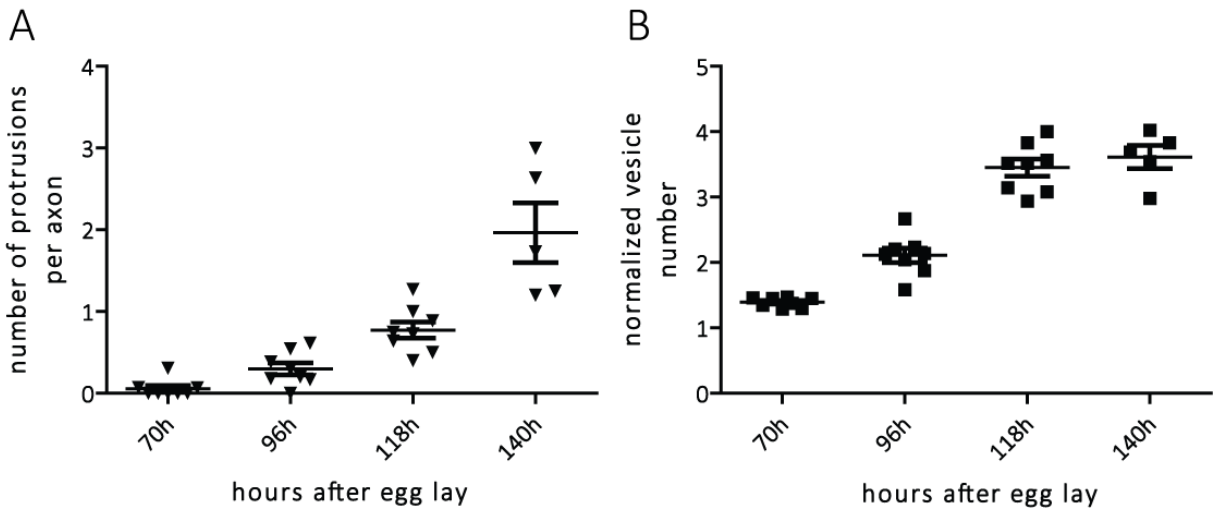

Figure 13: Quantification of out-folding phenotype and transport defects. Larvae were dissected at different stages after p24-1 inhibition in glial cells: second instar stage (70h AEL), mid third instar stage (96h AEL), late third instar stage (118h AEL) and prolonged third instar stage (140h AEL). Genotype of dissected larvae was repo4.3Gal4;repoGal4,CD8GFP/p24-1 RNAi. Tissue was stained for GFP (glia), HRP (neurons) and Bruchpilot (axonal vesicles). Filet preparation was used to analyze the whole PNS, n=8. One-way Anova ($p < 0.0001$) was used to assess statistical significance. (**A**) Quantification of absolute number of axonal out-foldings per PNS indicates increase over time. (**B**) Relative vesicle number showed transport defects already at 70h AEL and a progressive phenotype. Brp-positive vesicles were counted in four 100 µm lone nerve tracts per animal. Numbers were normalized to average vesicle number in control animals of corresponding age.

3.3.4 p24-1 inhibition affects mitochondria appearance

Not only vesicles but also mitochondria are transported along axons. The energy consuming transport process is dependent on mitochondria function. As we could show that transport is affected upon p24-1 inhibition in the glia, we wondered if mitochondria are distributed normally. Therefore, p24-1 was inhibited with the pan-glial driver line repoGal4 and third instar larval peripheral nerves were dissected. Glia was labeled by CD8GFP expression (green), mitochondria were stained with the ATP5α antibody (red) and neurons with the HRP antibody (blue). In control nerves, mitochondria were evenly distributed over the nerve (Figure 14 B). In glial cells they were forming a mesh like structure whereas in axons they were more separated (Figure 14 B'). Upon p24-1 inhibition, the distribution of mitochondria changed (Figure 14 A, A'). There were parts with a high density of the organelles and others with none.

In total, we found less axonal mitochondria upon p24-1 inhibition (96 in p24-1 RNAi and 276 in control axons). Because not only the number but also the size appeared to be changed, we measured the volume of the axonal mitochondria upon glial p24-1 inhibition. This was performed with Bitplane's Imaris software and the mitochondria were analyzed in a nerve section of 75 µm. As indicated in Figure 14 C the mitochondrial volume compared to control was significantly increased (t-test, $p < 0.0001$). P24-1 axonal mitochondria volume showed a mean of 145.5 μm^3, SEM ± 18.64 whereas control mitochondria volume was 59.48 μm^3, SEM ± 5.72. As there were overall fewer volumes detectable, we reasoned that also the number of axonal mitochondria was decreased after p24-1 knockdown. Also in glial cells, the number and size seemed decreased.

In summary, we found that glial and axonal mitochondria size and shape were altered in peripheral nerves upon p24-1 inhibition.

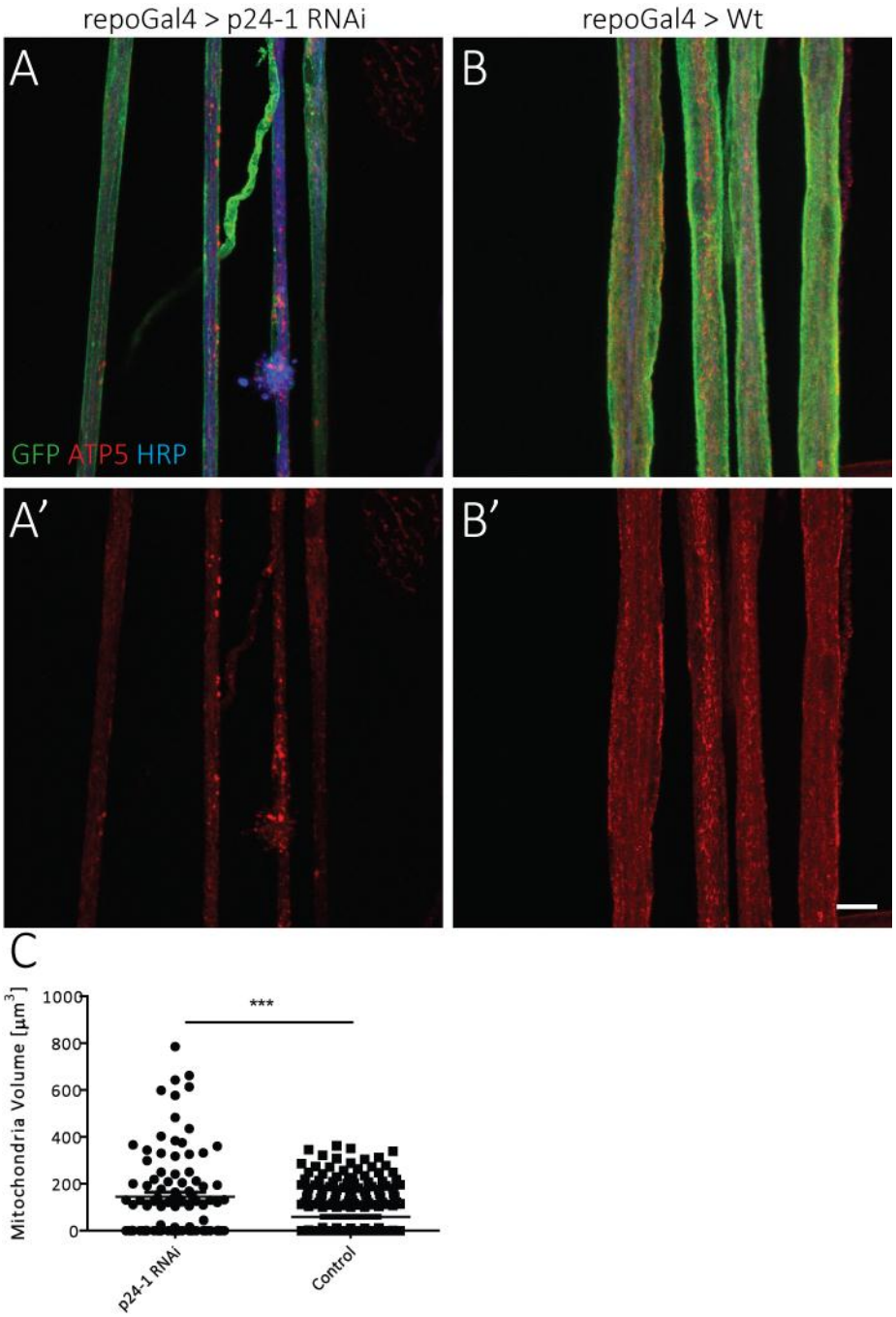

Figure 14: Enlargement of axonal mitochondria upon glial p24-1 inhibition. To examine mitochondria distribution third instar larval peripheral nerves were dissected and stained with for the mitochondrial protein ATP5α (red). Glia membrane was labeled by CD8GFP expression (green) and neurons with the HRP antibody. (**A**) p24-1 inhibition reveals a changed mitochondria size and distribution. (**B**) In control nerves (genotype repoCD8GFP/+) mitochondria are evenly distributed. (**C**) Quantification of mitochondria volume shows significant increase of p24-1 RNAi compared to control ($p < 0.0001$). Significance was determined by t-test. Scale bar 10 µm.

3.3.5 Target defects after glial p24-1 inhibition in photoreceptor cells

Regarding the axonal out-folding phenotype, we decided to consider photoreceptor axons as another class of functional neurons of the peripheral nervous system. Photoreceptor cells (R-cells) grow during larval stages from the eye disc over the optic stalk into the optic lobes. Here they make connections in a distinct pattern. R1-R6 cells terminate in the lamina (asterisk) whereas R7 and R8 cells pass this layer and stop in the medulla (Figure 15 B). Glia membrane was visualized by CD8GFP expression. Neurons were labeled with the HRP antibody and R-cells specifically with the 24B10 antibody.

Inhibition of p24-1 with the pan-glial driver line repoGal4 did not lead to characteristic axonal out-foldings in photoreceptor cells (Figure 15 A). The axons of R-cells showed normal appearance compared to control (compare Figure 15 A' and B') but path-finding seemed to be affected by the p24-1 RNAi expression, since most axons terminated in the lamina (Figure 15 A'). Hence, we concluded that pathfinding of photoreceptor neurons is affected upon p24-1 inhibition.

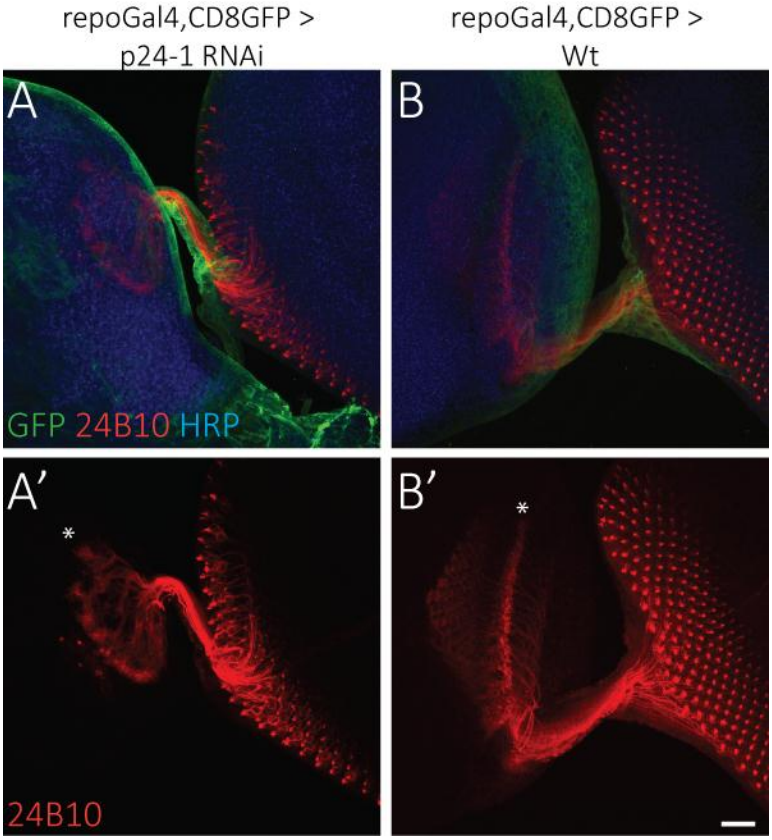

Figure 15: Migration defects of photoreceptor axons. Glial membrane was stained with anti-GFP (green), photoreceptor cells with anti-24B10 (red) and neurons with anti-HRP (blue). (**A**) Migration of photoreceptor axons was disturbed after glial inhibition. All axons terminate in lamina. Genotype repoCD8GFP/p24-1 RNAi. (**B**) Photoreceptor axons grow through the optic stalk and terminate in lamina and medulla. Scale bar 10 µm.

3.3.6 No alterations of the neuro-muscular junction stability after p24-1 inhibition

After observing the motor defects of the third instar larvae upon glial p24-1 inhibition, we wondered if not only the axons but also the neuro-muscular connections are malfunctioning. To examine the appearance of the NMJ, we stained the presynaptic localized protein Bruchpilot and the postsynaptic localized protein Disc large with specific antibodies. Glia membrane was visualized by CD8GFP expression. The presynaptic marker Bruchpilot appeared normally distributed after glial p24-1 inhibition (Figure 16 A) compared to control

NMJ (Figure 16 B). Upon p24-1 inhibition, also the postsynaptic Protein Disc large was localized as in control NMJs (compare Figure 16 C and D). In control animals, the glia membrane was associated to the NMJ and extended fine processes to the synaptic terminals (Figure 16 B, D). However, in p24-1 RNAi animals the glia was retracted from NMJs (Figure 16 A, C).

To summarize this we found that the NMJ morphology appeared unaltered upon p24-1 knockdown but glial processes were retracted from synaptic terminals.

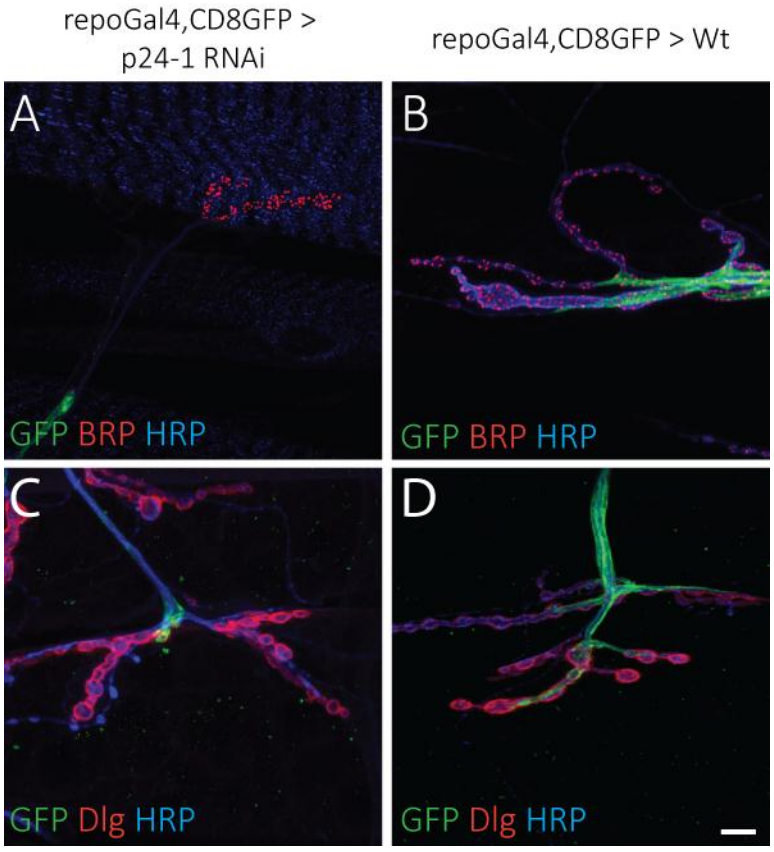

Figure 16: No neuro-muscular junction defects after p24-1 inhibition. Glia membrane was stained with anti-GFP (green), neurons with anti-HRP (blue) and synaptic proteins with anti-Bruchpilot or anti-Disc large (red). (**A**) Glial p24-1 inhibition did not alter the presynaptic marker Brp. (**B**) Control NMJ displays wild-typical presynaptic appearance. (**C**) Normal postsynaptic marker expression after p24-1 inhibition, (**D**) compared to control NMJ. After p24-1 inhibition, glia membrane is retracted from NMJ (**A**, **C**). Scale bar 10 µm.

3.4 Specificity of the p24-1 RNAi phenotype

3.4.1 p24-1 antibody confirmed absence of protein after p24-1 knockdown

To validate the specificity of the p24-1 RNA interference phenotype we made use of a specific antibody against the p24-1 protein (Saleem et al., 2012). Glia was marked with anti-GFP (green), neuronal membrane with anti-HRP in blue and anti-p24-1 was depicted in red. In control animals p24-1 appeared to be present in all tissues visible like muscles, glia and trachea (Figure 17 B). After knockdown in glial cells the p24-1 signal was absent frrom glia (Figure 17 A) and the peripheral nerve didin't show p24-1 protein expression whereas the signal was still detectable in trachea.

Hence, knockdown with the p24-1^{GD12196} RNAi line inhibited the expression of the p24-1 protein completely.

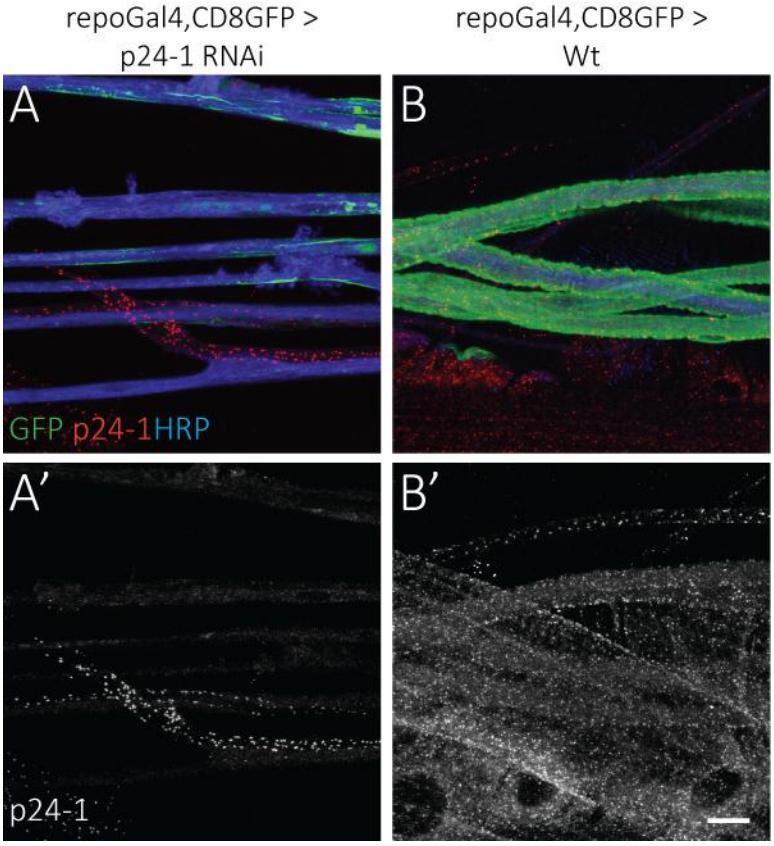

Figure 17: p24-1 Antibody showed p24-1 absence in glia upon p24-1 knockdown Glia was labeled by CD8GFP expression (green), anti-p24-1 (red) and neurons with anti-HRP (blue). (**A**) Glial p24-1 inhibition caused absence of p24-1 signal in glia. (**B**) Control animals showed ubiquitous p24-1 expression. Scale bar 10 µm.

3.4.2 Expression of *Drosophila virilis* p24-1 could not rescue the RNAi induced phenotype

As the experimental setup is based on RNA interference, we sought to rule out off-target effects. To test the specificity of the RNAi construct used in above experiments, we designed an RNAi rescue approach. The two different approaches cross-species RNAi rescue (Kondo et al., 2009) or *Drosophila* RNAi Escape Strategy Construct (RESC) (Schulz et al., 2009) can be used. For cloning of the cross-species RNAi rescue construct, mRNA from wild-type *Drosophila virilis* was isolated. The *p24-1* gene was amplified by PCR from synthesized cDNA and cloned with the Gateway System into the UAS expression vector pUAST containing a HA tag (Figure 18A). The DNA plasmid was further integrated into the *D. melanogaster* genome via ϕC31

integrase mediated site-directed mutagenesis in landing site 51C on the second chromosome (2R). For the generation of the RESC construct first the target sequence of the p24-1^{GD12196} RNAi construct was identified in the *p24-1* gene. This target sequence was then modified *in silico* with silent mutations, making it unlikely for RNA interference to occur. The modified p24-1-string sequence was synthesized by GeneArt by Thermo Fisher Scientific Inc. and cloned into a UAS expression vector with or without GFP tag (Figure 18 A). The pUAST constructs were integrated into the fly genome at landing sites 51D (2nd chromosome, 2R) and 22A (2nd chromosome, 2L) respectively.

Expression of the generated transgenic constructs in glial cells with repoGal4 (Figure 18 B) indicated that p24-1-D.Virilis-HA was localized in a similar pattern as the endogenous D. melanogaster p24-1 (Figure 17B). p24-1-string-GFP revealed a diffuse distribution upon anti-GFP staining (not shown) indicating the gene product was not functional and degraded.

To test the rescue capacity of the p24-1 D. virilis transgenic constructs, it was simultaneously expressed with the p24-1^{GD12196} RNAi construct in glial cells. However, the constructs could not rescue the p24-1 induced neuronal phenotype or lethality, which might be due to degradation of the transcript, off-target effects or malfunctioning of the *D. virilis* p24-1 protein.

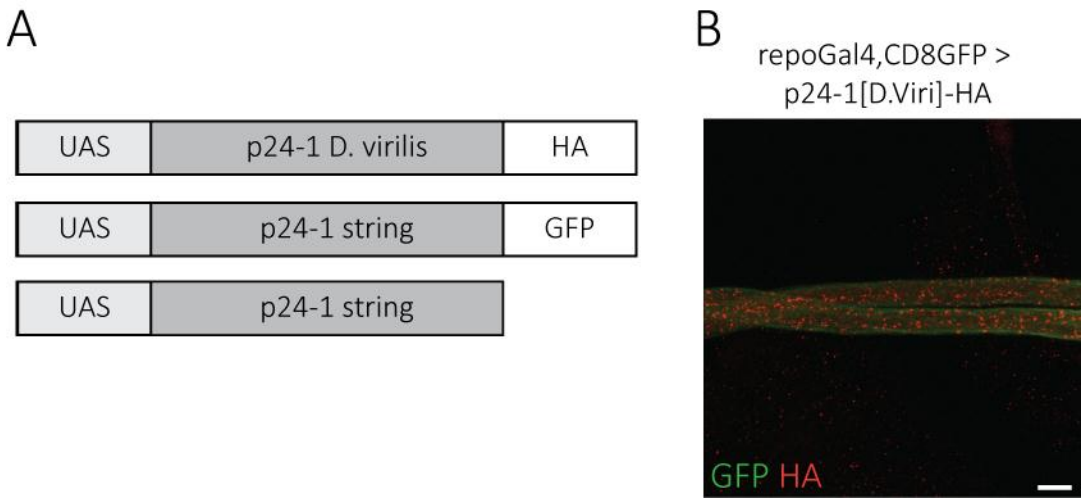

Figure 18: RNAi rescue experiment RNAi rescue constructs were cloned and transgenic fly strains generated. (**A**) Three different pUAST plasmid constructs were generated containing the p24-1 gene of *D. virilis* with HA tag and a *D. melanogaster* p24-1 gene with silent mutations in RNAi target region (p24-1 string) with or without GFP tag. (**B**) The p24-1-D.virilis-HA construct was expressed with repoGal4. Scale bar 10 µm.

3.4.3 Inhibition of other p24 family members reproduces p24-1 phenotype

The p24 family in *Drosophila* consists of nine members (Saleem et al., 2012). For the eight p24 genes (*p24-1, p24-2, éclair, Chop24, CG9308, CG31787, opossum* and *baiser*) RNAi lines were available. To investigate the relevance of the entire p24 family in glial function, we acquired UAS RNAi lines for those members (if available two different lines).

Knockdown in glial cells with the pan-glial driver line repoGal4 showed that p24-1, Chop24 and opossum are required in glial cells (Figure 19A). Inhibition of Chop24 (lines Chopp24^{GD7039} and Chop24^{KK100274}) caused lethality in pupal stages or early adulthood. Induction of the RNA interference with lines p24-1$^{GD\ 12196}$, opm^{GD10168} and opm^{KK101312} led to lethality in third instar larval stage. Pan-glial knockdown of p24-1 RNAi with line KK100594 though, had no detectable effect.

Next, we examined the appearance of the larval nervous system after inhibition of p24 family members. Chop24 did not display alterations of the larval nervous system after glial inhibition like the other viable p24 family members (p24-2, éclair, CG9308, CG31787 and baiser). For p24-1, only glial expression of line GD12196 but not of line KK100594 caused the characteristic axonal out-folding phenotype (Figure 6 B). Glial inhibition of opossum with both available lines (GD10168 and KK101312) displayed the axonal out-folding phenotype (Figure 19B).

The analysis of the p24 family revealed that p24-1 and opossum expression is necessary for glial cells as inhibition caused axonal protrusions and glial degradation in third instar larval PNS and resulted in lethality.

A

p24 family	VDRC ID	RepoGal4 > RNAi
eclair	KK101388	V
eclair	GD5843	V
p24-2	KK109179	V
CG9308	GD6606	V
CG9308	GD6605	V
CHOp24	GD7039	Semi lethal
CHOp24	KK100274	Pupal lethal
CG31787	GD6372	V
p24-1	KK100594	V
p24-1	GD12196	L3 lethal
opossum	GD10168	L3 lethal
opossum	KK101312	L3 lethal
baiser	KK100612	V

B

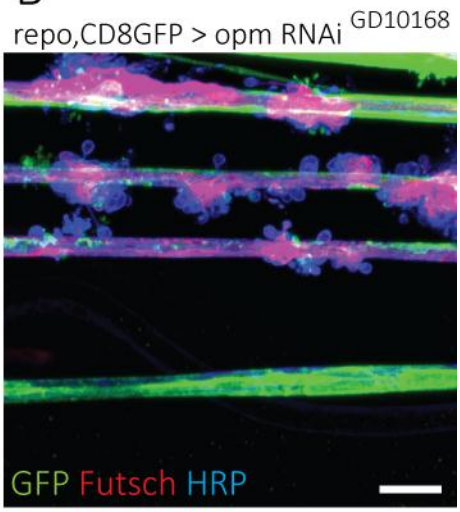

Figure 19: The p24 family member opossum reproduced the p24-1 phenotype. (**A**) UAS-RNAi lines were ordered for all p24 family members. Knockdown was performed with the pan-glial driver line repoGal4. V = viable, semi lethal = flies die as young adults or short after hatching, pupal lethal = animals died during pupal stages, L3 lethal = animals died during third instar larval stage. Chop24, p24-1 and opossum showed lethality after glial knockdown. (**B**) Glial inhibition of opossum (Line GD10168) displayed the axonal out-folding phenotype. Glia was visualized with CD8GFP (green), sensory axons with anti-Futsch (red) and all neurons with anti-HRP (blue). Scale bar 10 µm.

3.5 Identification of p24-1 interaction partners

p24 proteins are components of the secretory pathway and mainly described to transport cargo

from the endoplasmic reticulum (ER) towards the Golgi apparatus (reviewed in Strating and Martens, 2009). The globular GOLD domain, a feature of p24 proteins, serves probably as a selective protein cargo selection motive (Anantharaman and Aravind, 2002).

We hypothesized that p24-1 and opossum are responsible to secrete glial proteins. In *Drosophila,* it has been shown that different combinations of p24 proteins are needed for the secretion of the signaling molecule wingless. It was proposed that either éclair and Chop24 (Port et al., 2011) or p24-1, Chop24 and opossum (Buechling et al., 2011) play a role in

secreting Wg by shuttling the molecule through the ER-Golgi interface. Because of these findings, we also tested if Wg signaling was involved in generating the characteristic axon-glial phenotype. Therefore, we acquired RNAi lines from VDRC for different members of the canonical Wg signaling pathway (wingless^{KK104579}, Frizzled^{KK105493}, armadillo^{KK107344}, catenin^{KK107298} and dishevelled^{KK101525}). RNA interference was induced with the pan-glial driver line repoGal4 but no defects in viability or alterations of the larval nervous system were detected (data not shown). Therefore, we intended to conduct a broader search for p24 interaction partners.

3.5.1 Genetic approach to identify p24-1 interaction partners

To identify p24-1 interaction partners we executed a secondary screening. Since p24-1 and opossum are key players in the secretory pathway, we aimed for candidates, which are secreted. The screening strategy was to inhibit gene functions of a set of candidates via RNA interference in the nervous system. Because p24-1 and opossum inhibition was lethal in third instar larvae, we screened for lethality.

As candidates, we selected all *Drosophila* genes, which were annotated as 'secreted' in the UniProt database (www.uniprot.org). Of those, we selected all candidates for which a UAS-RNAi line from VDRC was available (220 candidates). Additionally, all members of the Immunoglobulin Superfamily were selected for the screen as these proteins are transported through the secretory pathway. Furthermore, several IgSF members are described to be involved in cell communication and adhesion, which we thought might be affected in the absence of p24-1. For the immunoglobulin superfamily, we found another 142 RNAi lines from VDRC.

In total, we screened 362 RNAi lines for lethality with a combined neuronal (n-sybGal4) and glial (repoGal4) driver line (Table 19). 25% of all candidates (95 lines) displayed lethality upon nervous system specific inhibition (Figure 20 A). These positive candidates were re-screened with the single pan-neuronal (n-sybGal4) and pan-glial (repoGal4) driver line only. As depicted, 51% of the candidates showed lethality and were required in neurons (46 lines) and

21% in glia (19 lines) (Figure 20 B). 28% of all lines showed only lethality after pan-neural inhibition (25 lines).

Because p24-1 inhibition resulted in lethality after glia specific knockdown, we first examined the candidates of the secondary screen, which also were lethal upon glial inhibition. For those 19 lines, a detailed confocal analysis of the nervous system was carried out. We found that the three candidates ferritin 1 heavy chain (fer1hch), yolk protein 2 (yp-2) and defective proboscis response 2 (dpr-2) produced the p24-1 nervous system phenotype upon glial inhibition.

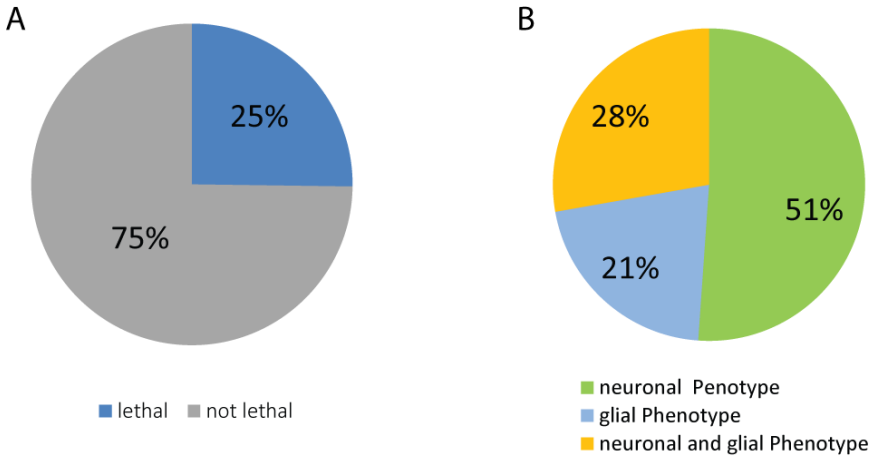

Figure 20: Secondary RNAi screening identifies candidates required for nervous system function. (**A**) Knockdown of 380 candidates (secreted proteins and Immunoglobulin superfamily members) with a combined n-sybGal4 and repoGal4 driver line was performed. 95 lines showed lethality (25%). (**B**) Re-screening of the lethal candidates with single pan-glia (repoGal4) and pan-neuronal (n-sybGal4) driver lines was performed. 51% showed lethality after neuronal inhibition, 21% after glial inhibition and 28% showed lethality only with the combined neuronal and glial driver line

3.6 Ferritin1 heavy chain is necessary for neural function

The genetic approach showed that inhibition of Ferritin 1 heavy chain (Fer1HCH) displayed the same phenotype as p24-1 upon glial inhibition (Figure 21 A). A large study of protein complex networks in *Drosophila* Schneider cells tested interactions of 5000 individual epitope

tagged proteins by mass spectrometry. This biochemical approach revealed a direct interaction between p24-1 and Fer1HCH (Guruharsha et al., 2011). Therefore, we decided to continue with the analysis of Fer1HCH.

3.6.1 Fer1HCH phenotype kinetics show progressive development

Upon glial Fer1HCH inhibition, we could detect the same axonal out-foldings, which were observed upon glial p24-1 inhibition. Glia membrane was labeled by expression of a membrane bound CD8GFP in repo pattern (green), sensory neurons with the Futsch antibody (red) and all neurons with the HRP antibody (blue) (Figure 21 A). The glial membrane was altered in some regions along the peripheral nerves and occasionally absent at the sites of the axonal out-folding. The axonal protrusions were distributed over the whole PNS and could be found in proximal or distal regions (Figure 21 A). The animals developed severe motor defects in third instar stage and remained up to several days in the larval stage until they died.

To characterize the Fer1HCH RNAi phenotype further, the kinetics of the phenotype were determined. Therefore a confocal analysis of the complete PNS was performed. Axons were labeled with the HRP antibody and axonal vesicles with the Bruchpilot antibody. The quantification of axonal protrusions showed a significant increase of protrusions per nerve over time ($p < 0.0001$) (Figure 21 B). At an age of 70 hours (in second larval stage), there were no protrusions detectable yet. The axonal alterations started to develop in mid third instar larval stage (96 hours) when on average 0.75 protrusion per nerve could be found. The protrusions became more frequent at 118 (mean = 2.01 protrusions/axon) and 140 hours (mean = 3.47 protrusions/axon) after egg lay. In addition, we detected transportation defects of axonal vesicles upon glial Fer1HCH inhibition. We stained Bruchpilot-positive vesicles upon Fer1HCH knockdown and quantified the vesicle number in axons of peripheral nerves. The counts were then normalized to numbers of Bruchpilot-positive vesicles of control animals of the corresponding age. We could detect a significant increase ($p < 0.0001$) of vesicles over time compared to control (Figure 21 C). At 70 hours after egg lay, the second instar larvae already showed a 1.51 fold increase of vesicles number compared to control. In subsequent

stages, the axonal vesicle transport defect became stronger and we could detect up to 3.58 fold increase in vesicles during the prolonged third instar larval stage at 140 hours AEL.

Taken together, the characterization of the Fer1HCH RNAi induced phenotype revealed a strong disturbance of the axo-glial architecture. The phenotype kinetics exhibits a progressive increase in the occurrence of axonal out-foldings as well an increase in the number of axonal vesicles in peripheral nerves.

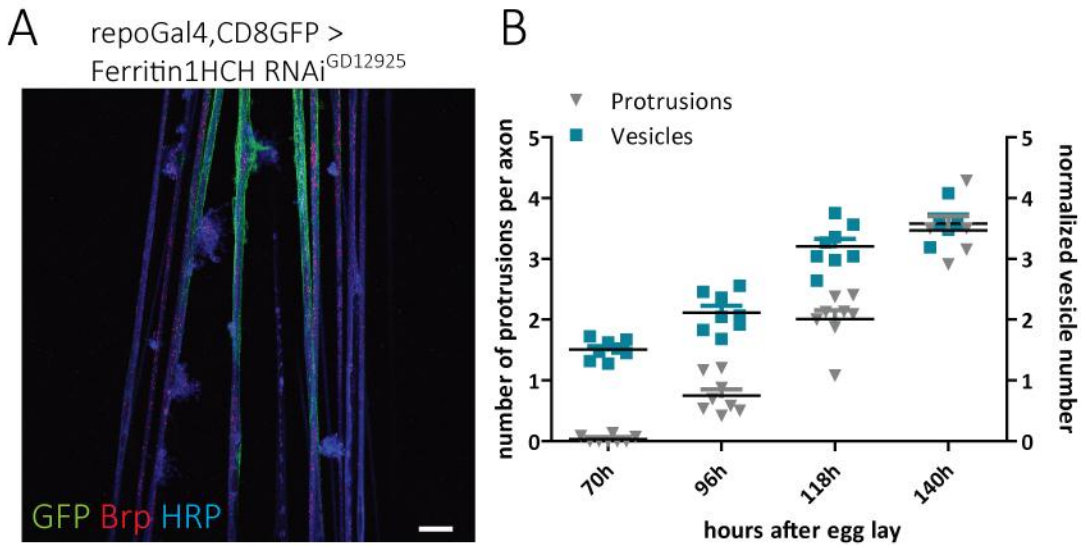

Figure 21: Inhibition of Ferritin 1 heavy chain shows alterations in axo-glial structure with progressive development. Glial inhibition of Fer1HCH revealed axonal failure. (**A**) Confocal analysis of third instar larval PNS shows axonal out-foldings. Glia was labeled by CD8GFP expression, sensory neurons were stained with anti-Futsch and all neurons with anti-HRP. (**B**) For quantification, larvae were dissected at different stages after p24-1 inhibition in glial cells: second instar stage (70h AEL), mid third instar stage (96h AEL), late third instar stage (118h AEL) and prolonged third instar stage (140h AEL). Genotype was repo4.3Gal4;repoGal4,CD8GFP/Fer1HCH RNAi. Tissue was stained for GFP (glia), HRP (neurons) and Bruchpilot (axonal vesicles) in filet preparation, n=8. One-way Anova was used to assess statistical significance. Quantification of absolute number of axonal out-foldings per PNS indicates increase over time. $p < 0.0001$. Quantification of relative vesicle number showed transport defects already at 70h AEL and a progressive phenotype. Brp-positive vesicles were counted in four 100 µm lone nerve tracts per animal. Numbers were normalized to average vesicle number in control animals of corresponding age. Numbers are significantly different ($p < 0.0001$).

3.6.2 Glial inhibition of Fer1HCH indicates axonal transport defect and axonal swellings

To find out in which neural cell type *ferritin1hch* expression is specifically required, an analysis with sub-class specific Gal4 driver lines was performed. To determine the effect on the axon morphology and function, we stained third instar larval peripheral nerves with the HRP antibody to check for axonal protrusions and with the Bruchpilot antibody to check for axonal transport failure (Figure 22).

First, pan-neuronal inhibition of Fer1HCH was tested with n-sybGal4 (Figure 22 B). The animals had no behavioral impairments and no neuronal phenotype could be observed upon knockdown. Expression of Fer1HCH RNAi in wrapping glia cells led to a higher density of Brp-positive vesicles in axons (Figure 22 C) but behavior of the larvae and morphology of the axon was not altered. However, we observed a wrapping defect comparable to p24-1 inhibition with nrv2Gal4 (not shown). A transport defect of axonal vesicles was also visible upon Fer1HCH RNAi expression in subperineurial glia cells with gliotactinGal4 (Figure 22 D). Ferritin inhibition in subperineurial glia was not followed by the characteristic axonal out-foldings, but axonal swellings appeared (triangle, Figure 22 E).These swellings occurred over long stretches of the axon.

In summary, we found that Fer1HCH inhibition in wrapping glia, subperineurial glia and in all glia cells produced a traffic jam of axonal Bruchpilot-positive vesicles, whereas inhibition in neurons had no effect. Axonal out-foldings only occurred upon pan-glial knockdown. Axonal swellings were detected upon Fer1HCH inhibition in subperineurial glia.

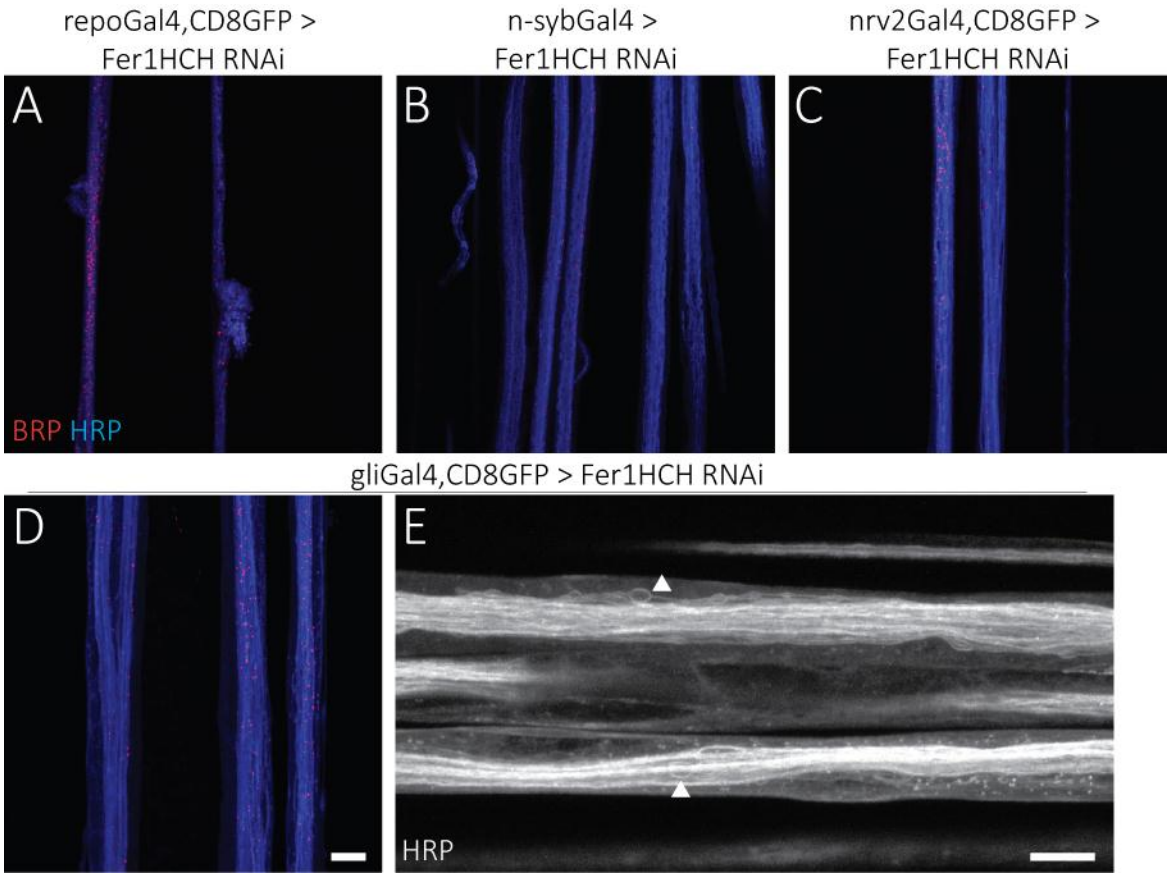

Figure 22: Altered axonal transport upon Feritin1HCH inhibition in glial sub-classes. Fer1HCH RNAi was expressed in wrapping glia, subperineurial glia and neurons. Neurons were labeled with the HRP antibody (blue), axonal vesicles with the Bruchpilot antibody (red), CD8GFP is not shown. (**A**) Inhibition of Fer1HCH with the pan-glial driver repoGal4 led to axonal out-foldings and traffic jam of Brp-positive vesicles. (**B**) Knockdown of Fer1HCH with the pan-neuronal driver line n-sybGal4 had no effect on neurons or axonal transport. (**C**) Inhibition of Fer1HCH in wrapping glia cells with nervana2Gal4 showed transport defects of Brp-positive vesicles. (**D**) Inhibition in subperineurial glia wit gliotactinGal4 led to traffic jam of vesicles and (E) neurons showed axonal swellings. Scale bar 10 µm.

3.7 Ferritin1HCH is secreted by the glia and transferred to neurons

3.7.1 Overexpression study reveals transfer of Ferritin from glia to neuron

For a better characterization of Ferritin1HCH function in glial cells, a transgenic fly line was generated that allowed tissue specific overexpression of Fer1HCH. For this purpose, the *Drosophila fer1hch* gene was cloned into a UAS expression vector pUAST and integrated into the fly genome with the ϕC31 integrase mediated site-specific recombination system. Since no commercial antibody was available to detect Ferritin1HCH, we added a c-terminal HA tag.

To determine the localization upon Fer1HCH overexpression in peripheral nerves, third instar larvae were dissected and stained with an HA antibody (green) to mark Fer1HCH. Neuronal membrane was labeled with the HRP antibody (magenta). Expression with the pan-glial driver line repoGal4 showed that Fer1HCH-HA was expressed (Figure 23 A). The HA signal was present all over the nerve and colocalized with the neuronal marker HRP (Figure 23 A''). The average Pearson's coefficient of P= 0.4414 (n = 3) confirmed the colocalization.

3.7.2 p24-1 is required for Ferritin1HCH secretion

To test, if p24-1 regulated the release of Fer1HCH to neurons, we generated flies that allow simultaneous expression of p24-1 RNAi and Fer1HCH-HA. Expression of both constructs with the pan-glial driver line repoGal4 let to the described axonal out-folding phenotype (Figure 23 B'). HA signal could be detected in a dotted pattern but the HA signal was restricted to glial cells (Figure 22 B). No colocalization of HRP and HA was visible in out-folded areas and straight nerve tracts. The average Pearson's coefficient was P= 0.092.

In summary, we found that inhibition of glial p24-1 expression prevented glial release of Fer1HCH-HA and colocalization with neurons.

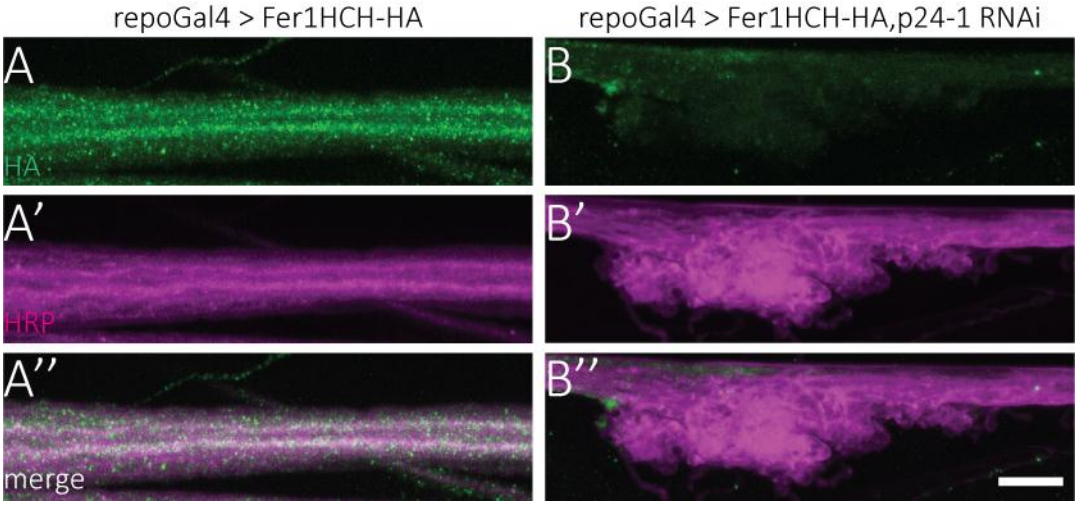

Figure 23: Transfer of Ferritin1HCH from glia to neuron can be blocked by p24-1 inhibition To evaluate the localization of Ferritin1HCH a tagged version of the protein was overexpressed with the pan-glial driver line repoGal4. HA protein was detected with the HA antibody (green), neurons were labeled with the HRP antibody (magenta). (**A**) Expression of Fer1HCH-HA in glial cells shows a spotted distribution and a colocalization of HA and HRP signal. Average Pearson's coefficient P = 0.4414 (n=3) indicated uptake of Ferritin1HCH-HA by neurons. (**B**) Simultaneous block of p24-1 in glial cells inhibits release of Fer1HCH-HA. No colocalization of HA and HRP antibody was detected. Scale bar 10 µm.

3.7.3 Subperineurial and wrapping glia are responsible for Fer1HCH release to neurons

To find out which glial sub-class was responsible for the release of Fer1HCH-HA, we expressed it in wrapping, subperineurial and perineurial glia with the driver lines nervana2Gal4, gliotactinGal4 and C527Gal4 respectively. As a control, Fer1HCH-HA was expressed outside the nervous system in fat body cells with LppGal4. The larval nerves were depicted by a confocal analysis for which neurons were marked with the HRP antibody (magenta) and Fer1HCH-HA with the HA antibody (green).

Figure 24 A shows expression of Fer1HCH-HA in wrapping glia. The HA signal could be found in wrapping glial cells but was also slightly colocalizing with the neuronal HRP signal in some axons. The average Pearson's coefficient was P= 0.24. Upon expression in subperineurial glia, the HA signal was colocalizing with the HRP signal (Figure 24 B) (average Pearson's coefficient P= 0.43) indicating stronger colocalization compared to nervana2Gal4 expression. Upon expression in perineurial glia, there was no colocalization observed (Figure 24 C) indicated by the low Pearson's coefficient (P = 0.07). The weak HA signal was restricted to glial cells.

Expression outside the nervous system with LppGal4 in the fat body led to a dotted HA signal of the Fer1HCH-HA outside the nervous system and eventually with glial cells (Figure 24 D). No colocalization between HRP and HA could be detected (P = -0.612).

In conclusion, we observed a colocalization of Fer1HCH-HA with the neuronal marker HRP after expression in wrapping glia and subperineurial glia. No colocalization was measurable after expression in perineurial glia or fat body.

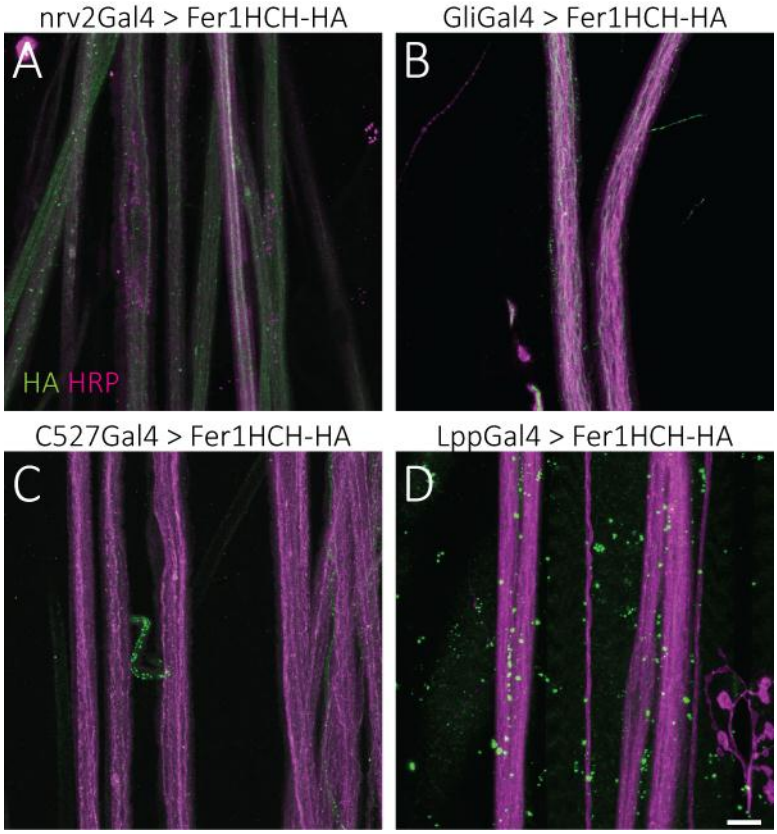

Figure 24: Ferritin1HCH expression in wrapping and subperineurial glia shows colocalization with neurons. To evaluate the localization of Ferritin1HCH a tagged version of the protein was overexpressed with the glial sub-type specific driver lines. For control, the construct was expressed in the fat body with LppGal4. HA protein was detected with the HA antibody (green), neurons were labeled with the HRP antibody (magenta). (**A**) Expression of Fer1HCH-HA in wrapping glial cells with nervana2Gal4 showed colocalization of HA and HRP signal. (B) Expression of Fer1HCH-HA in subperineurial glial cells with gliotactinGal4 showed colocalization of HA and HRP signal. (**C**) Expression in perineurial glia with C527Gal4 showed a weak signal restricted to the glia. (**D**) Expression of Fer1HCH-HA in fat body cells showed a dotted distribution of HA signal and no colocalization was observed. Scale bar 10 µm.

3.7.4 Overexpression of Fer1HCH in cultured primary *Drosophila* cells confirmed transfer

To study the transfer of glially expressed Fer1HCH-HA to neurons, we used cultures of neurons and glia cells. For that purpose, a method was established that allowed us to culture cells isolated from embryos for several days. To label the glia, cells were isolated from embryos expressing a membrane bound CD8GFP (green) under control of the pan-glial driver line repoGal4. Neuronal membrane as before was stained with the HRP antibody (blue). As depicted in Figure 25 A beside other cells, neurons and glia cells were isolated and differentiated *in vitro*. After five days *in vitro* (DIV), glial cells were mostly associated with neurons (Figure 25 A). To test transfer of Fer1HCH-HA cells were isolated from embryos expressing CD8GFP and Fer1HCH-HA under the control of repoGal4. Cells were cultured under same condition as control cells. At five DIV, cells were fixed and stained with the HA antibody (red) as well as for glial and neuronal markers (Figure 25). Fer1HCH-HA was detected in glial cells but also colocalizing with neurons (Figure 25 B, B'). In comparison, there was no HA signal detectable in control cells, which did not express Fer1HCH-HA (Figure 25 A').

In conclusion, the experiment could confirm the transfer of glially expressed Fer1HCH-HA protein to neurons *in vitro*.

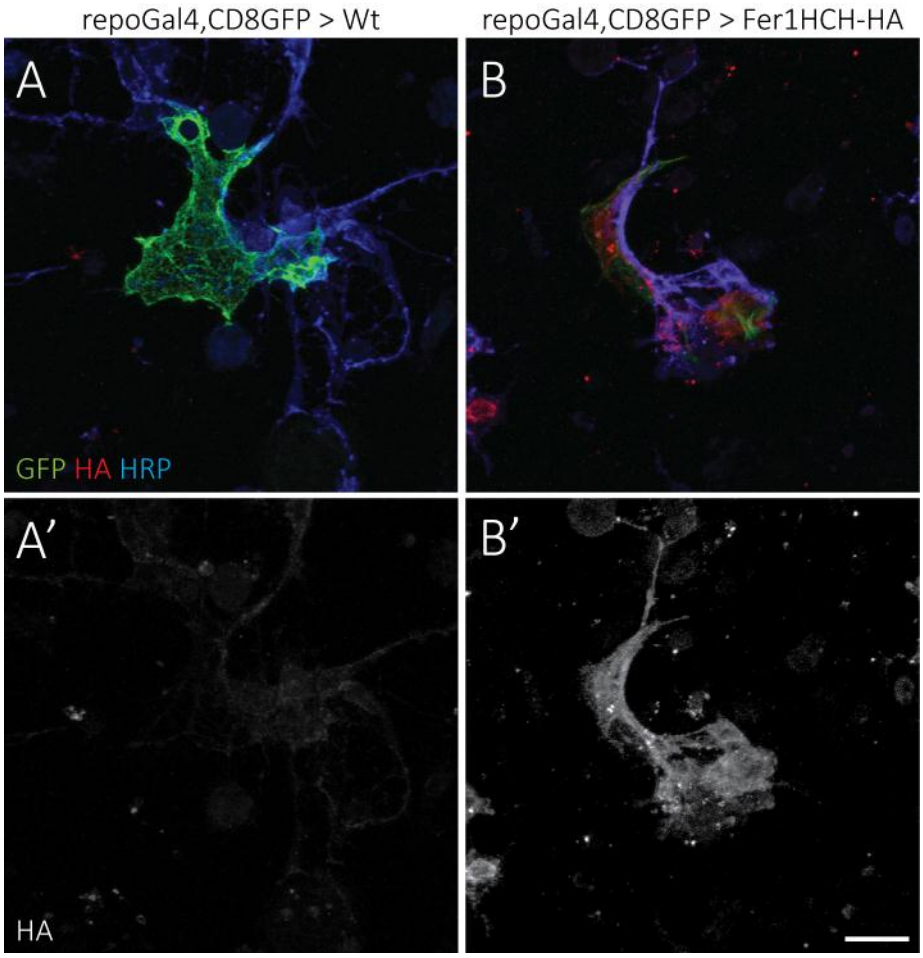

Figure 25: Overexpression of Fer1HCH-HA in cultured primary cells shows colocalization with neuronal marker. Cells were isolated from embryos expressing only CD8GFP (control) or CD8GFP and Fer1HCH-HA in glial cells (green). Neurons were labeled with the HRP antibody (blue), HA protein tag with the HA antibody (red). After five DIV, cells were fixed. (**A**) Control cells did not stain for HA protein. (**B**). Expression of Fer1HCH-HA in glial cells showed localization of HA protein in glial cells as well as with neurons. Scale bar 10 µm.

3.7.5 Ferritin1HCH-HA can integrate into the Ferritin complex

After detecting the Fer1HCH-HA protein colocalizing with the neuronal marker, we wondered if the protein is functional.

Frist, the integration into the ferritin complex was analyzed. Therefore, HA labeled Fer1HCH was expressed in glial cells and brain lysates were subjected to non-reducing SDS

polyacrylamide gel electrophoresis (SDS page) and visualized via western blot. For detection of the protein, the HA antibody was used. As shown in Figure 26 A, several bands were visible. Two strong signal bands appeared at ~33 kDa and 55 kDa. The 33 kDa band corresponded to the Fer1HCH-HA monomer. The size of 55 kDa indicated a dimer of Fer1HCH-HA and the endogenous expressed Ferritin2 light chain (Fer2LCH). That the dimer band showed stronger signal than the monomer band indicated a high degree of stability of the Fer1HCH-Fer2LCH interaction. We also saw several other bands of a higher molecular weight that most likely represent multimers of Fer1HCH-HA and Fer2LCH. It has been described that the ferritin complex consists of 12 Fer1HCH and 12 Fer2LCH subunits which can be detected at a band size of ~240 kDa (Kosmidis et al., 2011). Therefore, the band with the highest molecular weight (~270 kDa) in Figure 26 A corresponded to the whole ferritin complex. The ~ 30 kDa difference was due to the HA protein tag.

In summary, we found that Fer1HCH-HA is integrated into the Ferritin complex.

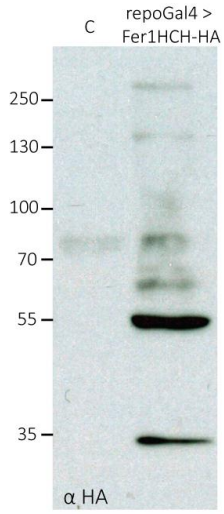

Figure 26: Fer1HCH-HA is not fully functional. To test the functionality of the Fer1HCH-HA, the construct was expressed *in vivo*. (**A**) Fer1HCH-HA was expressed in glial cells. Protein lysates were separated over non-reducing PAGE. Western blot analysis showed HA signal bands of different molecular weights which correspond to dimers and multimers of Fer1HCH-HA and Fer2LCH. Fer1HCH-HA is integrated into the Ferritin complex (~270 kDa).

3.8 Iron accumulation is toxic for glial cells

3.8.1 Iron accumulates upon p24-1 inhibition

As ferritin is described as an iron binding molecule (Granick, 1942) we asked, if the iron homeostasis was changed upon p24-1 inhibition. To answer this question, a staining procedure for *Drosophila* peripheral nerves was established allowing detection of ferrous iron (Fe^{2+}) with the Turnbull's blue staining method. The signal was subsequently enhanced with 3,3' diaminobenzidine (DAB). To test for iron accumulation, p24-1 gene function was inhibited in glial cells and third instar larval peripheral nerves were dissected. As control, the repoGal4 driver line was crossed to wild-type. In control nerves there was only little signal visible (Figure 27 A). Upon expression of p24-1 RNAi in glial cells, we could detect a strong signal along the nerve (Figure 27 B, C). There were accumulations visible that appeared in the outer layers of the nerve. Although the glia and neurons could not be distinguished with this staining method, it is likely that those accumulations are restricted to glial cells.

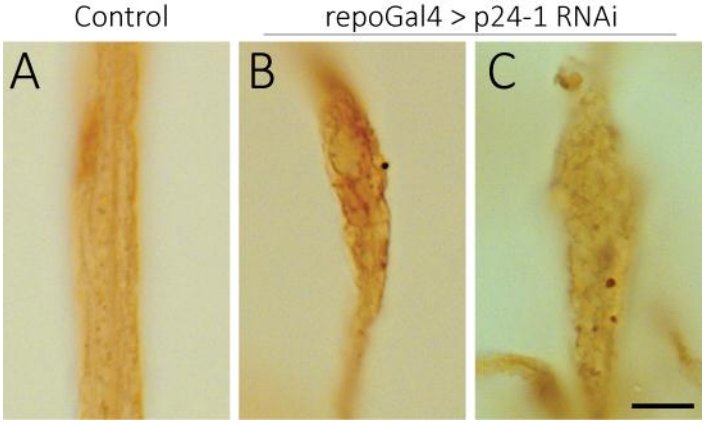

Figure 27: Glial p24-1 inhibition exhibited ferrous iron accumulation. To detect ferrous iron Turnbull's blue stain wit DAB enhancement was applied in third instar peripheral nerves. (**A**) In control nerves (genotype repoGal4/+) only little signal was detected. (**B**, **C**) After p24-1 inhibition in glial cells, (genotype repoGal4/p24-1 RNAi) dark spots were detected mainly in the outer layers of the nerve indicating accumulation of ferrous iron. Scale bar 20 µm.

3.8.2 Phenotype strength can be modulated by ferroptosis inhibitors

After detecting iron accumulation in the PNS, we wondered if this dysfunctional regulation could be modulated by applying drugs that can alter the toxic effect of iron. Ferroptosis has been described to be an iron-dependent form of cell death. The small compound named Ferrostatin-1 as well as different iron chelators were found to rescue from ferroptosis (Dixon et al., 2012). To test the involvement of ferroptosis, we applied the two iron chelators 50 µM bathophenanthroline sulfate (BPS) and 50 µM deferoxamine as well as 150 µM of the inhibitor Ferrostatin-1 to the animals. For control purposes, ddH_2O was applied. To provide more iron 25 mM ferric ammonium citrate (FAC) was used. As readout for the phenotypic strength, the relative number of protrusions per nerve was quantified as well as the normalized number of Brp-positive vesicles. Standard food with inhibitor was supplied over the development, and then the animals were dissected at third instar stage and stained with the neuronal marker HRP and the axonal vesicle marker Bruchpilot.

First, we performed pan-glial inhibition of p24-1 (Figure 28 A). Application of ddH_2O and FAC showed a mean protrusion number of 1.08 and 0.72 respectively. When the chelators BPS and DFO were provided peripheral nerves showed a significant decrease in the number of out-foldings per nerve (BPS mean = 0.22 and DFO mean = 0.14). Also after treatment with ferrostatin-1 we observed a significant decrease of protrusions per nerve (mean = 0.31) compared to water control. One-way Anova revealed a significant difference of the values ($p = 0.0003$) and Bonferroni post-hoc test showed significance between the groups as indicated (* < 0.01, ** < 0.001, *** < 0.0001). Quantification of the vesicle number after glial p24-1 inhibition showed no significant difference between the groups ($p < 0.0001$).

The PNS of animals after pan-glial Fer1HCH inhibition and inhibitor application was considered (Figure 28 B). The quantifications of the axonal protrusions per nerve were significantly different ($p < 0.0001$). Applying ddH2O and FAC led to mean of 1.88 and 2.14 protrusions per nerve respectively. The quantification of the protrusions upon BPS, DFO and Ferrostatin-1 application revealed a strong decrease in the occurrence of the phenotype (BPS mean = 0.136 DFO mean = 0.095, Ferrostatin-1 mean = 0.358). Bonferroni's post-hoc test showed as well a significant difference between the groups as indicated (Figure 28 B). The

vesicle number again was not significantly different between the groups. The quantification of the vesicle number upon p24-1 (Figure 28 C) or Fer1HCH (Figure 28 D) inhibition revealed that there was no difference in strength of the axonal transport defects.

In summary, the inhibitor test showed that the axonal out-folding phenotype, which occurred after p24-1 and fer1HCH knockdown in glial cells, could be alleviated by application of iron chelators and the drug ferrostatin-1. The axonal transport defect of Brp-positive was not changed upon application of inhibitors.

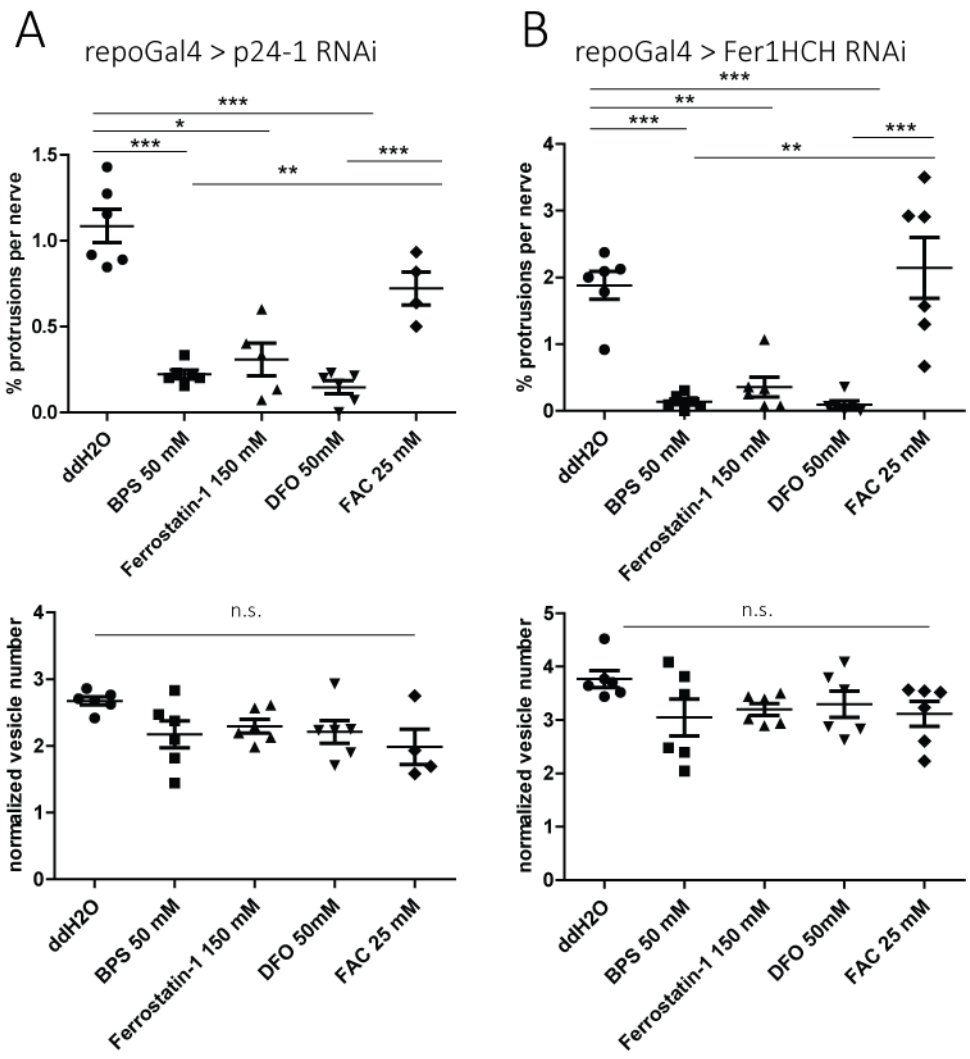

Figure 28: Inhibitors can modulate p24-1 phenotype penetrance. Iron chelators and the small compound Ferrostatin-1 were applied to *Drosophila* third instar larvae. Phenotype strength was quantified as number of protrusions found in nerves and as normalized number of Brp-positive vesicles in 4 x 100 µm nerve sections. Third instar larval tissue was stained for GFP (glia), HRP (neurons) and Bruchpilot (axonal vesicles). Filet preparation were used to analyze the whole PNS, n=6. One-way Anova and Bonferroni post-hoc test was used to assess statistical significance * < 0.001, ** < 0.0001, *** < 0.00001. (**A**) Animals after pan-glial inhibition of p24-1 were analyzed. Quantification of absolute number of axonal out-foldings per larval nerves counted indicates decrease of protrusions after application of BPS, Fer-1 and DFO compared to H2O and FAC. p = 0.0003. The normalized vesicle number was not significantly different between the groups. (**B**) Animals after pan-glial inhibition of Fer1HCH were analyzed. Quantification of absolute number of axonal out-foldings per larval nerves counted indicates significant decrease of protrusions after application of BPS, Ferrostatin-1 and DFO compared to ddH_2O and FAC p < 0.0001. The normalized vesicle number was not significantly different between the groups.

3.8.3 Ferritin1HCH mutant reveals defects in the nervous system

Next, we examined the appearance of peripheral nerves in Ferritin1HCH mutants. For p24-1, there was no lethal allele available. For Fer1HCH, the mutant allele *fer1hch*^{451} was homozygous lethal. It has been described that 43% of the embryos die during embryonic stages and a fraction of mutant animals showed nervous system defects (González-Morales et al., 2015).

We analyzed the peripheral nerves of homozygote mutants, which survived until larval stages (~50%). First instar larvae were dissected and stained with the neuronal marker HRP. In few animals, we found defasciculated axons in peripheral nerves (Figure 29 A). However many animals did not display axonal changes. Ubiquitous expression of Fer1HCH-HA with act5cGal4 in *fer1hch-null* mutant background rescued to some extent and animals survived until second instar stage. When we examined the nerves, we could not find axonal alterations (Figure 29 B). Expression of Fer1HCH-HA in glial cells with the weaker repo4.3Gal4 driver could also not rescue from lethality or PNS alterations. To investigate the appearance of glial cells in mutant animals, a membrane bound CD8GFP (green) was expressed under the glial repo4.3Gal4 driver in homozygous mutant background. In ~ 50% of the analyzed animals, we found an uneven distribution of the CD8GFP signal (Figure 29 C). Because CD8GFP is associated to glial membranes, we speculated about a perturbed synthesis of glial membrane or developmental defects. As wrapping glia is not yet differentiated in first instar larvae, it is likely that subperineurial glia is affected in *fer1hch*^{451} mutants.

To conclude above findings, we found that homozygous *ferritin1hch* mutants displayed developmental defects in neuronal and glial cells.

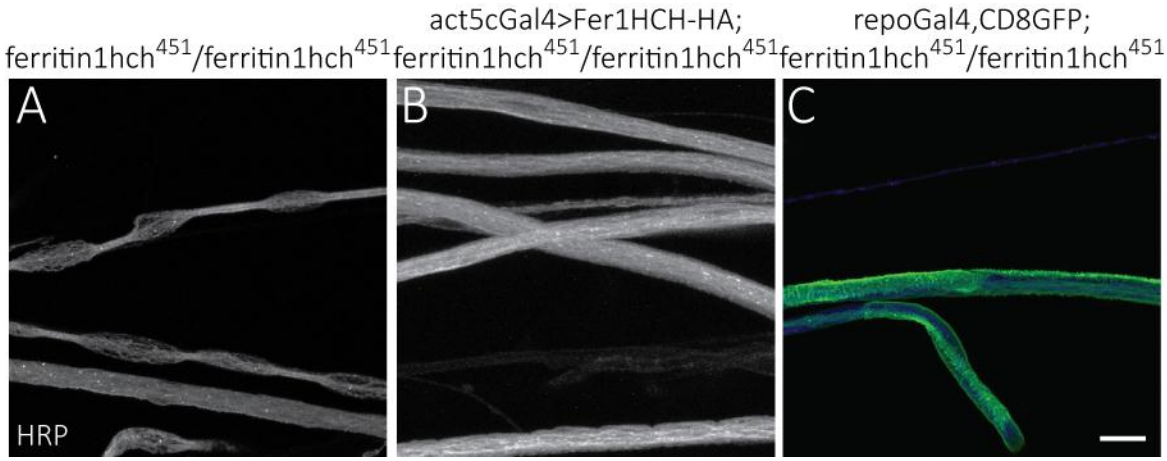

Figure 29: *fer1hch-null* mutant shows alterations of glia and axons. The homozygous lethal *fer1hch*^{451} allele was analyzed. Animals die between embryonic and first instar larval stage. Glia was labeled by repoGal4 > CD8GFP expression and neurons were labeled with the HRP antibody. (**A**) Few homozygous mutants display axonal defasciculation distributed over peripheral nerves. (**B**) Ubiquitous expression of Fer1HCH-HA with the actin5cGal4 driver repressed axonal alterations. (**C**) Labeling of glia membrane reveals glial alterations in *fer1hch*^{451} mutants. Scale bar 10 µm.

3.9 Neuronal transcriptome changes after glial iron blockage

3.9.1 Experimental design of the ribosome profiling experiment

To evaluate the neuronal response upon p24-1 or Fer1HCH inhibition in the glia, we designed a ribosome profiling experiment, which allowed the purification of neuronal translating ribosomes and parallel knockdown in glial cells.

We made use of the binary Q expression system (Potter et al., 2010). First, the ribosomal protein Rpl10ab was amplified from a pUAST-Rpl10ab vector (Thomas et al., 2012) and cloned into a pQUAST expression vector. Either a HA protein tag or a GFP was n-terminally attached. The pQUAST-Rpl10ab-HA/GFP vector was then integrated into the fly genome with help of the ϕC31 site-specific integration system in landing site 22A (2nd chromosome, 2L). Flies harboring the QUAS-Rpl10ab-HA construct were recombined with fly lines containing the UAS-p24-1 RNAi or the UAS-Fer1HCH RNAi constructs, respectively. As a pan-glial driver line repoGal4 was used to express p24-1 RNAi. To drive pan-neuronal expression of the QUAS-HA-

Rpl10ab the fly line n-sybQF.2 was selected. The two drivers RepoGal4 and n-sybQF.2 were recombined in one fly line (Figure 30 A). A similar line was also generated harboring a pQUAST-GFP-Rpl10ab construct.

To verify expression of the newly generated QUAS-Rpl10ab-HA construct in vivo, we first crossed n-sybQF.2 to QUAS-HA-Rpl10ab or QUAS-GFP-Rpl10ab flies. Staining with an HA antibody (green) confirmed expression in neuronal cells (Figure 30 B). Nuclei were labeled with ToPro dye (blue). The Rpl10ab-GFP line was neglected from further applications because expression in glial cells led to lethality of the animals in pupal stages. This indicated that the Rpl10ab-GFP version is not fully functional or even toxic for cells.

Second, we verified expression of the Rpl10ab-HA by western blot. Therefore, lysates of repoGal4 > UAS-Rpl10-HA, n-sybQF.2 > QUAS-HA-Rpl10ab and combined animals repoGal4, n-sybQF.2 >> UAS-p24-1 RNAi, QUAS-HA-Rpl10ab were separated on a SDS page. Western blot detection with the HA antibody reveled expression of HA-Rpl10ab in all three conditions (Figure 30 C). The ribosomal protein Rpl10ab was then immuno-purified over the HA protein tag and RNA was isolated from neuronal ribosomes as described in 2.5.4. After several purification steps the RNA was sequenced

In summary, we created a system that allowed the manipulation of glial cells by the expression of the RNAi construct and the contemporaneous isolation of translating ribosomes. From immune-purified ribosomes, we could successfully isolate neuronal RNA.

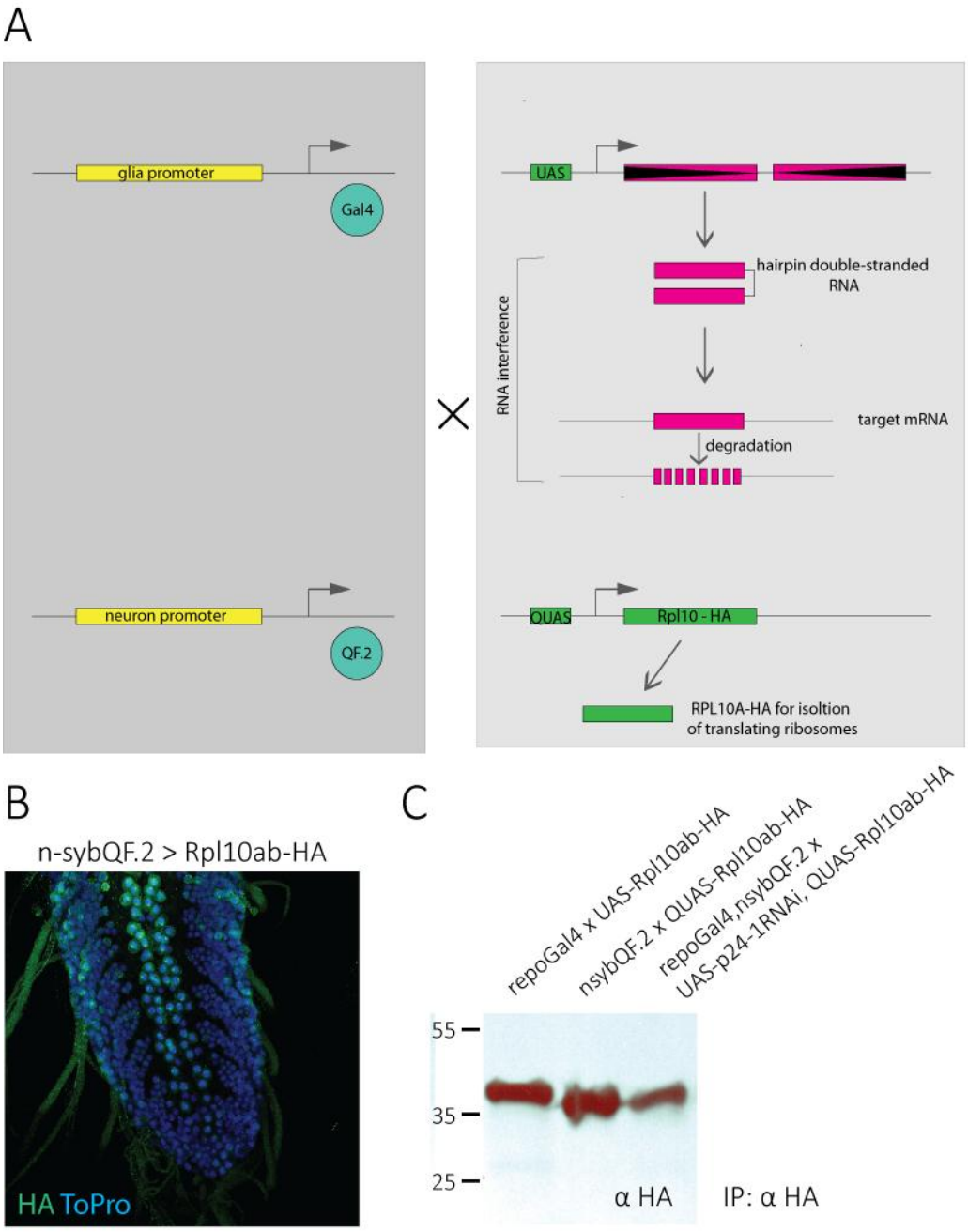

Figure 30: Ribosome profiling experimental design. To determine the neuronal response upon glial p24-1 or Fer1HCH inhibition ribosome profiling was performed. (**A**) A transgenic fly line harboring a QUAS-Rpl10ab-HA construct was combined to a fly line with the p24-1 RNAi construct. The pan-glial repoGal4 driver line was recombined to a pan-neuronal n-sybQF.2 driver line. (**B**) Rpl10ab-HA was successfully expressed in third instar larval brain. HA was labeled with the HA antibody (green), Nuclei were stained with the ToPro dye. (**C**) Lysates of third instar larvae were prepared for repo > UAS-Rpl10ab-HA, n-sybQF.2 > QUAS-Rpl10ab-HA and the combined line repoGal4, n-sybQF.2 >> UAS-p24-1 RNAi, QUAS-Rpl10ab-HA. Separation with reducing SDS page and detection over western blot showed expression of RPL10ab-HA in all three conditions.

3.9.2 RNA sequencing results

The sequencing procedure was performed with an Illumina next-generation sequencing setup (in collaboration with Moritz Rossner, LMU München).We sequenced the whole transcriptome isolated from neurons (with nsybQF.2) and glia (repoGal4) from third instar larvae. We could detect ~7200 transcripts of which 763 were significantly differently expressed (not shown). High expression levels of known neuronal transcripts such as *futsch*, *bruchpilot* and *synapsin* appeared in the probe isolated from n-sybQF.2 > HA-Rpl10ab expressing animals. This confirmed that with this method we were able to isolate cell type specific translating ribosomes.

The comparison of neuronal transcripts isolated from animals, which expressed Fer1HCH RNAi to control revealed 592 differentially, expressed transcripts. The glial inhibition of Fer1HCH causes a down-regulation of iron-responsive transcripts in neurons. These transcripts harbor an iron-response element or need iron as cofactor for Fe-S clusters and heme binding. The results are listed in Table 15.

Table 15: Iron-dependent transcripts are differentially expressed upon glial Fer1HCH inhibition. Neuronal RNA transcripts were sequenced. LSMean shows average number of reads per transcript of three technical samples. Control neuronal (n-syb) versus and neuronal transcripts with glial Fer1HCH RNAi (Fer1HCH) were compared (Fold change). Fold change > 1.8 was considered as significantly changed.

Gene ID	Gene symbol	P-Value	Fold change	LSMean (nsyb)	LSMean (Fer1HCH)
FBgn0013972	Gycalpha99B	5,79E-02	1,05E+01	3,22E+01	3,08E+00
FBgn0000108	Appl	7,09E-02	8,22E+00	1,03E+03	1,25E+02
FBgn0031684	ND-13A	1,35E-01	5,35E+00	2,34E+01	4,37E+00
FBgn0038295	Gyc88E	2,61E-01	3,78E+00	4,31E+00	1,14E+00
FBgn0030733	UQCR-14	3,36E-01	2,62E+00	1,13E+01	4,32E+00
FBgn0062442	Cisd2	3,88E-01	2,57E+00	6,86E+00	2,67E+00
FBgn0036728	UQCR-Q	2,98E-01	2,51E+00	1,68E+01	6,68E+00
FBgn0030718	ND-20	4,55E-01	2,12E+00	7,69E+00	3,62E+00
FBgn0032597	CG17904	4,68E-01	2,03E+00	6,48E+00	3,19E+00
FBgn0017567	ND-23	4,89E-01	1,97E+00	4,38E+00	2,22E+00
FBgn0015222	Fer1HCH	4,42E-01	1,95E+00	1,19E+02	6,11E+01

4 Discussion

The main task of glial cells is the axonal ensheathment. In vertebrates, this is accomplished by oligodendrocytes in the CNS and Schwann cells in the PNS, which form myelin around axons. In a similar manner, *Drosophila* glia cells ensheath peripheral axons to form the blood-brain barrier and to separate single axons. Due to the neuron-glia architecture, all signals, metabolites and other molecules have to be shuttled through the glial layers. Thus, a tight interaction between neuron and glia cells is indispensable. However, our knowledge about this interaction or communication process and the molecules involved remains limited.

4.1 Molecules involved in neuron-glia interactions

4.1.1 Identification of factors affecting neuronal integrity

By conducting an RNAi screen of highly conserved molecules, we sought to uncover glial molecules, which have an impact on function or morphology of neurons. As a system to analyze neuron-glia interactions, we selected the *Drosophila* larval peripheral nerve because of certain advantageous attributes: first, it is easily accessible; second, the organization of the nerves is rather simple since only three glial cell types exist, for which genetic markers are available; third, RNAi efficiency is high during larval stages; fourth glial development is mostly terminated and glial function can be studied (in the sense that cell types are specified, migration is finished and most of the cells only grow in size). For the screening, we selected homologs from a proteome analysis of the axo-glial fraction from mouse and human tissue (Figure 5 A). This guaranteed the exclusive analysis of candidates having human and mouse homologs.

Strikingly, around 40% of the tested candidates showed at least a mild disturbance in the larval segmental nerves (Figure 5 B). This number suggests that the screening setup was

sensitive enough to detect small failures but also indicates that glial cells are susceptible upon genetic manipulations. Confocal analysis allowed us to detect viable defects, since not necessarily all nervous system alterations are lethal. For instance, glial knockdown of the solute carrier NCC69 or the motor protein Khc generates severe defects, but animals are viable (Leiserson and Keshishian, 2011; Schmidt et al., 2012). In other, more global screening approaches looking for vital glia functions, the positive hit rate was between 11 and 13% (Ghosh et al., 2013; Schmidt et al., 2012). Hence, the high positive rate found in this study reveals that many protein functions are highly conserved between the initial vertebrate and the invertebrate candidates.

4.1.2 Glial secretion is necessary for neuronal function

The positive candidates could be clustered regarding their gene function (Figure 5 C). The majority of the candidates are involved in binding and catalytic processes. A smaller number of candidates had transport activity. When we had a closer look on the molecules, we found that several candidates, such as Atlastin, several Syntaxins, Gdi, p24-1 were involved in the secretory pathway. In a global RNAi screen it has been found that especially metabolic pathways were over represented within adult glia (Ghosh et al., 2013). Hence, it is likely that parts of the metabolic products are delivered to neuronal cells. This phenomenon has been described in vertebrates and invertebrates for carbohydrates which are transported over the glial barrier and provided to the neuron (Saab et al., 2013; Volkenhoff et al., 2015).

We found that one candidate, p24-1, which is involved in the secretory pathway, showed the strongest effect on the nervous system upon knockdown with the pan-glial driver line repoGal4. Therefore, we decided to continue with the analysis of p24-1 in the context of neuron-glia interaction.

4.2 Glial p24-1 function is required for the architecture and function of the nervous system

Pan-glial inhibition of p24-1 gene function had a massive impact on the nervous system (Figure 6). We observed a faint CD8GFP signal indicating disturbances of glia membranes. In some areas, we found thickenings of the peripheral nerve. In parts in which the glia membrane was disrupted, the neuronal alterations were evident. Out-foldings of the axons occurred randomly over the PNS and affected sensory as well as motor axons. Single axon labeling in sections, which were beginning to form out-foldings, revealed local instabilities of the axon although glial membranes still covered the nerve (Figure 11). The onset of those alterations was in the third instar stage. With increasing age, also the axonal out-foldings increased in size and occurrence (Figure 13 A). At the end of the larval stage, a considerable amount of axons degraded (Figure 9). Although the glia appeared destructed, we could not detect signs of apoptosis (Figure 10). The attempt to find out in which glial sub-type p24-1 function was required surprisingly did not mirror the axonal phenotype (Figure 7) and had no effect on the larval nervous system at all upon inhibition in neuronal cells (Figure 7 D). Eventually, the Gal4 driver lines just expressed the UAS-RNAi in a too weak fashion or at a too late time point during embryonic and larval development. Labeling the glial sub-types Gal4 independently by GFP exon trap lines revealed a more precise picture of the glial phenotype (Figure 8). Wrapping glia cells did not differentiate in order to separate axon and septate junctions in subperineurial glia were disrupted, meaning that BBB integrity was affected. Thus, p24-1 function is probably required in wrapping glia and subperineurial glia cells.

4.2.1 Specificity of the p24-1 phenotype

The experimental setup of the screen based on the RNA interference technique. This targeted gene silencing allowed for a fast and cell-type specific analysis of a big set of candidate genes. Nevertheless, the method also has its drawbacks since it can generate false-positive and false-negative results. The false-negative rate can be up to 34.7% of the genes but depends strongly on the Gal4 driver line used and the tissue assessed. The false-positive rate for the VDRC GD library was estimated to be below 2% (Dietzl et al., 2007). We discovered the p24-1

phenotype upon induction of RNA interference with the VDRC line p24-1^{GD12196}. Line GD12196 had three off-targets but inhibition of those genes did not cause similar defects or lethality. To ensure the specificity of the RNAi induced phenotype, p-element insertions within the p24-1 locus were investigated, but none of them was a lethal allele showing nervous system defects. To further validate the specificity, tissue was stained with an specific antibody against p24-1 (Saleem et al., 2012) and confirmed that p24-1 protein was absent upon expression of p24-1^{GD12196} (Figure 17) and p24-1^{KK100594}. Another method to confirm RNAi specificity is RESC and inter-species RNAi rescue (Kondo et al., 2009; Schulz et al., 2009). Upon expression of the RESC construct in glial cells, the protein could not be detected in the expected pattern, which might be due to the instability of the transcript. The inter-species rescue construct was localized in the expected pattern but could not rescue from p24-1 induced lethality (Figure 18). Either p24-1 from *D. virilis* was still targeted by the RNAi, the protein was not fully functional across the species or the HA tag inhibited its functionality. Interestingly, it has been shown, that ubiquitous p24-1^{GD12196} and p24-1^{KK10094} knockdown was lethal, while the KK10094 line produced in a milder developmental phenotype than the GD12196 line (Saleem et al., 2012). Hence, the stronger glial phenotype observed in this study might be due to a stronger knockdown.

Because it has been described that the family of p24 proteins possibly function as heterodimers or trimers (Buechling et al., 2011; Port et al., 2011), we tested all p24 family members for their involvement in nervous system integrity. Nine p24 family members are expressed in *Drosophila* melanogaster and for eight RNAi lines were available. Inhibition in the whole animal was described to be lethal for éclair, Chop24, p24-1, opossum and baiser, whereas p24-2 and CG9308 showed weak defects and CG31787 only reduced male fertility (Saleem et al., 2012). Knockdown in glia cells, in contrast, was only lethal for Chop24, p24-1^{GD12196} and opossum. Chop24 RNAi expression in the glia led to lethality during early adult or pupal stages (Figure 19). Pan-glial opossum inhibition with both lines (opm^{GD10168} and opm^{KK101312}) caused lethality in third instar larvae and analyses of the peripheral nerves revealed the axonal out-folding phenotype (Figure 19 B). There was no difference in

phenotype penetrance between p24-1 and opossum. Thus, we reasoned that p24-1 and opossum might function as heterodimers or in the same pathway.

A microarray analysis of the adult *Drosophila* neural transcriptome confirmed that p24-1 is highly expressed in the brain. The comparison revealed that it is 1.65 times more expressed in repo positive cells than in elav positive cells. Opossum is weaker expressed in the adult brain and shows a slight increase (1.1 fold) in glia cells compared to neurons (DeSalvo et al., 2014).

We concluded that the described glial p24-1 phenotype is specific and not due to an off-target effect. Nevertheless, the phenotype should be confirmed by a cell type specific full knockout of p24-1 and opossum. p24-1 function is presumably critical for glia function although it is expressed in other tissues.

4.2.2 p24 proteins in selective secretion

The secretion process has a pivotal role in cell interaction and communication. It depends on multiple sorting and transporting steps. p24 proteins have an important function in the early secretory pathway where they shuttle between the ER to the Golgi compartment, but also show post-Golgi localization (Strating and Martens, 2009). The p24 protein family consists of ~24 kDa type I transmembrane proteins, which are highly conserved across many phyla (e.g. yeast, plants and humans). p24 proteins are equipped with distinct domains. In proximate distance to the hydrophobic transmembrane domain, a short C-terminal domain faces towards the cytosol. Here, several highly conserved motifs allow the interaction with vesicle coat proteins like COP I and COP II (Belden and Barlowe, 2001; Dominguez et al., 1998; Strating and Martens, 2009). At the luminal site near the transmembrane region, p24 proteins have a helical domain which probably mediates interaction between family members (Ciufo and Boyd, 2000). The biggest part is covered by the GOLD domain (Golgi dynamics). This globular domain has been predicted to be necessary for the interactions with cargo molecules (Anantharaman and Aravind, 2002). The molecular structure indicates possible functions as cargo receptor, in vesicle formation and in quality control of secreted proteins (Carney and Bowen, 2004), which was confirmed by studies in yeast. Deletions of all eight p24 proteins did not cause lethality but the transport of secretory and membrane proteins was blocked and ER

resident proteins were secreted instead (Springer et al., 2000). In higher species, p24 proteins have vital functions. Mutations of p23δ1 are embryonically lethal in mice (Denzel et al., 2000). Down-regulation of most p24 proteins in *Drosophila* results in lethality during development (Saleem et al., 2012). Studies indicated that p24 proteins are expressed in a variety of different tissues but they might have cell type specific or temporal expression patterns during developmental stages (Boltz et al., 2007; Saleem et al., 2012). Evidence that p24 proteins might act in concert came from two studies proposing different combinations of p24 proteins are responsible for wingless secretion in the *Drosophila* wing disc (Buechling et al., 2011; Port et al., 2011). Thus, we tested if wingless is possibly involved in generating the p24 nervous system phenotype, but no link between wingless signaling and p24-1 in glial cells could be found. Another example of p24 function can be found in the adult *Drosophila* CNS, where logjam probably in combination with éclair and baiser is involved in the oviposition behavior (Boltz et al., 2007). Hence, as we found in our study that the inhibition generated the same phenotype, it might well be that p24-1 and opossum act together in glial cells. However, a biochemical confirmation is still needed.

4.2.3 Non-cell autonomous effects of p24-1 inhibition

Upon pan-glial p24-1 inhibition, we observed non-cell autonomous effects on axons indicating neuronal dysfunction. They included axonal instabilities with axonal swellings (Figure 11), axonal traffic jam (Figure 12), mitochondria defects (Figure 14), axonal loss (Figure 9) and photoreceptor migration defects (Figure 14). All these ultimate effects together with the knowledge about p24-1's and opossum's critical role in the secretory pathway, revealed that glial cells must secrete proteins, which are necessary for neurons.

One example for a glia-derived neurotrophic factor is dMANF. This factor is secreted from embryonic glia cells. dMANF mutants die during early larval stages and show a reduced number of dopaminergic neurites (Palgi et al., 2009). Interestingly, an example of p24 family members involved in cell interaction can be found in vertebrates. It has been publicized that p24 proteins regulate the transport of GPI-anchored proteins to the plasma membrane, where they eventually function in cell to cell signaling (Takida et al., 2008). This data could be

confirmed in yeast suggesting that GPI-anchored proteins exit the ER upon concentration at the ER exit site (ERES) with support of p24 proteins (Castillon et al., 2009). An example for a GPI-anchored protein with nervous system function is Glial Lazarillo (GLaz). Absence of GLaz in adulthood leads to more lipid peroxidation products, reduces oxidative stress resistance in neural cells and causes neurodegeneration (Sanchez et al., 2006), whereas ubiquitous overexpression improves iron induced oxidative stress resistance (Ruiz et al., 2012). If GLaz secretion is affected by p24 inhibition could be further analyzed. Another study showed that the TNFα-like molecule Gurken, which is required for cell polarity in oogenesis of flies, is secreted with help of Cornichon (cni), a cargo receptor in the early secretory pathway. Surprisingly, the luminal part of cni can be replaced by the GOLD domain of the p24 family member Chop24 without affecting Gurken secretion (Bökel et al., 2006). Most likely cni is responsible for the transport of transmembrane proteins, whereas for example the Chop24 yeast homolog Emp24p is required for the transport of GPI-anchored proteins (Castillon et al., 2009). Evidence of p24 proteins' involvement in neurodegeneration comes from studies of human diseases. Human p24β1 (which corresponds to *D.m. Chop24*) has been found to interact with atlastin and is linked to hereditary spastic paraplegias (Namekawa et al., 2007). Human p23/p24δ1 (which corresponds to *D.m. baiser*) is involved in the secretion of soluble APP and links p24 function to Alzheimer's disease (Vetrivel et al., 2007).

We were interested to identify the molecules, which are secreted by p24 proteins from glial cells during the end of the larval stages. Thus, we conducted a genetic screen (Figure 20). The secondary RNAi screen of secreted and Immunoglobulin superfamily members revealed three candidates, which reproduced the axonal out-folding phenotype upon glial inhibition (Ferritin1HCH, Yolk protein 2 and Dpr-2). This was partially supported by a study in *Drosophila* S2 cells, which identified Ferritin1HCH as one binding partners of p24-1 (Guruharsha et al., 2011). p24 proteins are likely to be involved in the transport of difficult cargo like large oligomeric assemblies (D'Arcangelo et al., 2015). Thus, we propose that Ferritin1HCH is secreted from glia cells with help of p24-1 and opossum.

4.3 Ferritin functions as iron trap and transporter in the glia

The function of Ferritin1HCH in glia cells was analyzed by using RNAi. Strikingly, pan-glial inhibition for all available Fer1HCH lines (Fer1HCH^{GD12925}, Fer1HCH^{GD49536} and Fer1HCH^{KK102406}) was lethal and generated the axonal out-folding phenotype (Figure 21 A). Very similar to p241 knockdown, we could observe disassembly of glial cells and strong morphological and functional defects in neurons. The phenotype kinetics also showed a progressive development from the third instar larval stage on (Figure 21 B, C). Fer1HCH inhibition even revealed a slightly stronger defects since the average protrusion number per axon was around 1 upon p24-1 knockdown and 2 upon Fer1HCH knockdown at 118 hours AEL.

There are three *ferritin* genes encoded in *Drosophila* named *fer1hch*, *fer2lch* and *fer3hch*. Fer1HCH and Fer2LCH are described to assemble in a complex storing iron (Missirlis et al., 2007). Fer3HCH localizes to mitochondria and is homologous to the vertebrate mitochondrial ferritin, but is only present in the testis (Missirlis et al., 2006) and also did not lead to impairments upon glial inhibition. Ubiquitous knockdown of Ferritin has been shown to be lethal for Fer1HCH during first and second instar stages and for Fer2LCH at late pupal stage (Tang and Zhou, 2013b). Pan-glial inhibition of Fer1HCH, as already mentioned, is lethal after a prolonged larval stage. Fer2LCH was lethal in young adults short after eclosion when inhibited in glial cells. This discrepancy in the lethality time points might be either explained by the possibility that the RNAi line did not sufficiently inhibit the gene dosage of Fer2LCH or that Fer1HCH has another independent function. Interestingly, it has been proposed that Fer1HCH alone is also able to bind iron (Pozzi et al., 2015). In our hands, inhibition of Fer1HCH and Fer2LCH gene function in neurons (with n-sybGal4) did not cause any obvious defects during larval stages (Figure 22 B). However during aging, Fer1HCH inhibition in neurons triggered degeneration in the eye and brain vacuolization (Tang and Zhou, 2013b). This study also revealed that down-regulation of either Fer1HCH or Fer2LCH led to the inhibition of the other ferritin subunit on protein levels indicating a mechanism ensuring a constant ratio of Fer1HCH and Fer2LCH protein.

The RNA interference data were confirmed by a study, which analyzed ferritin-null mutants. Homozygous animals for the *fer1hch*^{451} or the *fer2lch*^{35} mutant allele died during development (González-Morales et al., 2015). These Animals, which showed lethality during embryonic stages (36 % for *fer2lch*^{35} and 43 % for *fer1hch*^{451}) displayed cuticular phenotypes like germband retraction or dorsal closure defects. Also defects in the CNS were described, which included holes and twisted VNC, misguided axons or loss of parts of the PNS (González-Morales et al., 2015). As around 50% of homozygous mutant animals survive the embryonic stages, we analyzed the appearance of the peripheral nerves of *fer1hch*^{451} in first instar stage (Figure 29). Some rare cases showed axonal defects (Figure 29 A), but more apparent were defects in glial cells. The uneven distribution of CD8GFP localized membrane indicated that eventually the cell differentiation or the lipid synthesis might be affected. Hence, those defects are most likely not due to toxic effects but rather a consequence of iron deficiency in all tissues. Ubiquitous expression of a tagged Ferritin1HCH construct partially rescued the mutant's survival until the second instar stage and PNS defects were absent (Figure 29 B). However, these results also showed that the Fer1HCH construct was not fully functional. Although Fer1HCH-HA was at least partially integrated into the ferritin complex (Figure 26), the protein tag itself might hinder proper Fer1HCH function in either iron binding, complex formation or secretion. In contrast, expression of an untagged Fer1HCH including an IRE could rescue the survival to early adulthood (Tang and Zhou, 2013b).

4.3.1 Functions of iron in the nervous system

Ferritin is highly expressed in the nervous system of vertebrates and invertebrates. In adult *Drosophila* for instance, Fer1HCH is among the 50 highest expressed genes of surface glia cells (DeSalvo et al., 2014). In vertebrates, Fer1HCH is also highly expressed and 3 fold more enriched in oligodendrocytes compared to neurons. The highest expression can be observed in microglia (6.5 times more enriched than in oligodendrocytes) (Sharma et al., 2015). However the quantity of Ferritin transcripts is not directly linked to the protein amount, as they can be stored and their translation is regulated over the iron-response system (Pantopoulos, 2004). In *Drosophila,* the inhibition of Ferritin in neurons did not have an effect

during larval stages. Thus, we conclude that glia is the main iron mediator within the nervous system. In that regard it might be interesting to investigate, if a feedback loop exists that would allow the neuron to send signals when it requires iron.

In both systems, iron is an indispensable factor for the function of respiratory chain and citric acid cycle (TCA, *tricarboxylic acid cycle*) proteins. Complex I (NADH dehydrogenase) contains eight ISCs, Complex II (succinate dehydrogenase) has three, Complex III (cytochrome bc1 complex) and aconitase each contain one ISC (Lill et al., 2012; Rouault, 2016). Thus, restricting iron will also inhibit performance of the TCA cycle and the mitochondrial respiratory chain. Interestingly, blockage of Complex I function in *Drosophila* glia causes neuronal loss as well as mitochondrial enlargement and motor dysfunction (Hegde et al., 2014).

The autosomal recessive inherited disease Friedreich's ataxia (FRDA) demonstrates that iron is indispensable for the neuronal survival. The disease is caused by a mutation in the *frataxin* locus, which affects PNS and CNS neurons and is characterized by accumulation of iron in mitochondria, dysfunction of respiratory chain proteins as well as depleted aconitase function (Bulteau et al., 2004; Delatycki et al., 1999, 2000). Frataxin acts as an iron chaperone and is described to be involved in Fe/S cluster assembly and delivery to apo-proteins (Anderson et al., 2005; Shan and Cortopassi, 2012).

Another evidence of how iron could be utilized in the *Drosophila* nervous system comes from a study showing iron involvement in the stability or formation of septate junction in the epithelium. Transferrin 2 (Tsf2, also described as Melanotransferrin) is a component of septate junctions and its function relies on iron binding, since versions of Tsf2 with a mutated iron binding site are not able to form apicolateral septate junctions (Tiklová et al., 2010). As septate junctions are a major component of subperineurial glia cells, it would be interesting to investigate the iron dependence of glial septate junctions. In accordance, Tsf2 has been shown to be expressed in the adult *Drosophila* brain (DeSalvo et al., 2014) and we observed rupture of the BBB upon blockage of iron secretion.

Another possible function of iron in the nervous system might be linked to the synthesis of extracellular collagen. This matrix protein is produced by perineurial glia cells and represents a main component of the neural lamella surrounding CNS and PNS (Edwards et al., 1993).

Maintenance of the BBB integrity might be linked to the composition of the ECM (Gould et al., 2005; Vahedi et al., 2007). The two enzymes lysyl hydroxylase and collagen prolyl 4-hydroxylase are critical for the synthesis of collagen. They are localized in the ER lumen using ferric iron as cofactor. Close observation of the TEM micrographs of p24-1 inhibited nerves revealed a thin and in other parts even missing neural lamella (Figure 9). This might give evidence on how the BBB integrity could be disrupted upon p24-1 or Fer1HCH inhibition in glial cells.

How iron is utilized and distributed in vertebrates is also not entirely clear, although it is known that iron deficiency leads to hypo-myelination in humans and animal models (Beard and Connor, 2003; Lozoff and Georgieff, 2006; Ortiz et al., 2004; Yu et al., 1986). Oligodendrocytes are the cells in the brain, which stain the strongest for ferric iron (Connor and Menzies, 1996). Myelination in developing oligodendrocytes is an energy consuming process, which requires import of the metabolites lactate, glucose and ketone bodies (Vannucci and Simpson, 2003). Lactate is utilized to fuel mitochondria which produce ATP over oxidative phosphorylation (Bittar et al., 1996). Glucose also can be used for energy production over glycolysis and the pentose phosphate pathway. Glycolysis and breakdown of ketone bodies serve as a source of acetyl-CoA, which is required for fatty acid synthesis. Myelin membranes consist by 75% of lipids such as cholesterol, phospholipids, plasmalogen and galactolipids (Jahn et al., 2009). Iron-dependent enzymes needed for lipid synthesis (fatty acid synthesis) and degradation (lipid dehydrogenases) are highly expressed in oligodendrocytes (Cammer, 1984; Tansey et al., 1988). Also the synthesis of the abundant lipid cholesterol is described to be dependent on iron (Graham et al., 2010; Ong and Halliwell, 2004). Interestingly, cholesterol is required and even rate-limiting for myelination (Saher et al., 2005). We also observed defects in wrapping glia maturation upon inhibition of p24-1 and Fer1HCH with repoGal4 and nrv2Gal4 (Figure 7, Figure 8). Wrapping glia produce large amounts of membrane during larval stages to enwrap and separate axons (Stork et al., 2008). It has been shown that synthesis of sphingolipids is critical for the maturation of wrapping glia (Ghosh et al., 2013). Hence, the reduced iron availability might explain the observed wrapping defects.

4.4 Iron homeostasis in the nervous system of *Drosophila* is regulated by glia

4.4.1 Iron transport over the blood-brain barrier

The BBB in *Drosophila* shields axons from the potassium-rich hemolymph to allow efficient nerve signal propagation (Auld et al., 1995), but at the same time also inhibits diffusion of nutrients from the hemolymph to the axon. Upon expression of Ferritin1HCH-HA in the glia, we were able to detect the protein in axons (Figure 23 A). Thus, we concluded that iron might be transferred via Fer1HCH from glial cells to neurons. This transfer can be inhibited by a blockage of Fer1HCH secretion through glial p24-1 knockdown (Figure 23 B). The protein transfer could also be confirmed in primary *Drosophila* cells *in vitro* (Figure 25). The same phenomenon has also been described in a recent study. Expression of tagged Fer1HCH or Fer1LCH constructs in hemocytes resulted in Ferritin accumulation in different tissues (González-Morales et al., 2015). Interestingly, transfer of iron loaded Fer1HCH was also observed in vertebrates. It has been publicized that murine oligodendrocytes (which have the highest demand on iron) take up Ferritin 1HCH with help of the receptor Tim-2 (Todorich et al., 2008). Although Transferrin is present in the ISF, oligodendrocytes have low amounts of Transferrin receptor (Roskams and Connor, 1994). Ferritin might be produced by microglia, which are likely to secrete Ferritin (Zhang et al., 2006) and thereby serve as an alternative iron source in the brain (Todorich et al., 2011). The Ferritin complex in vertebrates can be composed of different ratios between light and heavy chains, which differ between tissues. Heavy chain rich Ferritin complex is found in tissues with a high iron turnover like muscle and brain (Arosio et al., 2009; Harrison and Arosio, 1996). Even though vertebrate Ferritin does not harbor a secretion signal, numerous reports exist of cells releasing Ferritin. Eventually, it is actively secreted through the lysosomal secretory pathway (Cohen et al., 2010), but the exact mechanism remains elusive. Still, human plasma Ferritin is taken as a measure for body iron stores. Low serum Ferritin levels correlate with iron depletion and elevated levels with inflammation or high iron stores (Cook et al., 1974; Punnonen et al., 1997; Wang et al., 2010). That oligodendrocytes require Ferritin heavy chain has also been demonstrated using the Fer1HCH mouse mutant. Homozygous animals were embryonically lethal (Ferreira et al.,

2000). Heterozygous animals, which have 20% of normal levels of Fer1HCH, showed altered myelinogenesis (less cholesterol and myelin proteins) and resembled models of dietary iron deficiency (Ortiz et al., 2004). In conclusion, Ferritin heavy chain has an important function in transporting and distributing iron in the nervous system of vertebrates and invertebrates.

4.4.2 Iron accumulation causes ferroptosis in glia

We found that glial inhibition of p24-1 led to ferrous iron accumulations (Figure 27). These accumulations are in general considered toxic, whereas Ferritin-bound iron is harmless. Free ferrous iron generates reactive oxygen species (ROS) via the Fenton reaction (Halliwell, 1992; Prousek, 2007). This is followed by impairment of ROS sensitive proteins such as kinases, transcription factors and glucose transporters and causes lipid peroxidation and mitochondrial dysfunction, which finally results in cell death (Keller et al., 1997; Salvador, 2010). In accordance with our findings, iron accumulation can also be observed in a human disease called Neuroferritinopathy. This dominant inherited disease is caused by a missense mutation in the C-terminus of Ferritin light chain making the Ferritin complex less capable to sequester iron (Friedman et al., 2011). Consequently, iron is accumulating in deep brain regions, which leads to clinical symptoms in adulthood such as dystonia, dementia, ataxia and parkinsonism (Lehn et al., 2012). We observed glial degeneration upon inhibition of p24-1 and Fer1HCH (Figure 6 and Figure 21). Degeneration and axonal out-foldings could be significantly reduced when we applied iron chelators and Ferrostatin-1 (Figure 28). This implies that iron accumulation in glial cells causes ferroptosis. Ferroptosis, a form of iron-dependent and non-apoptotic cell death, is characterized by iron accumulation and ROS production leading to the blebbing of plasma membrane, rounding of the cell and smaller mitochondria (Dixon et al., 2012). We failed to detect markers of apoptosis like Tunnel positive cells (Figure 10), cleaved caspase 3 or phospho-histone 3 stain (not shown), which is in accordance to the morphological features observed during ferroptosis. This shows that disturbing the iron transport and storage in glial cells leads to toxic iron accumulations causing ferroptosis, which can be prevented by chelators and ferrostatins.

4.4.3 Glia regulates metabolic support of neurons

Metabolic support of axons is conserved between vertebrates and invertebrates: both supply lactate or pyruvate to axons (Saab et al., 2013; Volkenhoff et al., 2015). Surprisingly, post-myelinating oligodendrocytes can solely survive on glycolysis, whereas neurons rely mainly on mitochondrial energy production by oxidative phosphorylation (Fünfschilling et al., 2012; Hall et al., 2012). This discrepancy might be due to the different energy needs during the developmental stages of the cells. Although the brain represents a minor part of the total body mass, it uses about 20% of the oxygen and 25% of the glucose available. This energy is used to maintain ion gradients and allow action potentials, recycling of neurotransmitters and transport cargo in an anterograde and retrograde fashion (Alle et al., 2009; Attwell and Laughlin, 2001; Hirokawa and Takemura, 2005). For example, the maintenance of the resting potential through the ATP dependent Na+/K+ pump can consume up to 54% of the total energy of the neuron (Howarth et al., 2012). This energy demand is thought to be met by ATP production of mitochondria and by glycolytic enzymes directly associated with ion pumps (Mercer and Dunham, 1981; Paul et al., 1979). Although oxidative phosphorylation in mitochondria is 15 times more efficient than glycolysis, it depends on the availability of adenosine diphosphate (ADP) (Erecinska and Wilson, 1978).

In *Drosophila*, fast axonal transport in long axons might partially rely on a newly described mechanism. Transport vesicles in neurons carry the glycolytic enzyme GAPDH, which is used for on-board ATP production (Zala et al., 2013). Upon glial Fer1HCH inhibition, we observed an axonal transport defect, which could be measured even before any signs of glial or axonal failure appeared (Figure 21 C). Bruchpilot-loaded vesicles have to move over very long distances from the VNC to the NMJ. We reasoned, that impaired neuronal mitochondria function decreased the transportation rate because less ATP is available. Our hypothesis is strengthened by the observation that reduction of the out-folding phenotype through iron chelators did not restore the vesicle transport defect (Figure 28). Furthermore, via ribosome profiling, we detected a significant down-regulation of mitochondrial iron-responsive transcripts and other transcripts, which rely on iron as cofactor (Table 15). This indicates that blockage of iron secretion from glia cells mimics iron deficiency in the neuron.

Positioning of mitochondria within the cell seems important. The vertebrate node of Ranvier is an area with high ATP demand (Waxman and Ritchie, 1993) and indeed, mitochondria stop at these sites when the axon is electrically active. In silent phases they reside at mitochondria stationary sites distributed throughout the axon (Ohno et al., 2011). During growth of neurons, the biogenesis of new mitochondria is increased. As the functions of major components of the respiratory chain rely on iron, also iron import is required during growth. Interestingly, a study in vertebrate nerves showed that mitochondrial biosynthesis does occur in the axon, which is relevant especially for long peripheral axons (Amiri and Hollenbeck, 2008) and might explain why we observed transfer of iron to the axon. 99% of the neuronal cytoplasm is contained in the axon (Pilling et al., 2006). As some cytosolic proteins are translated locally, the cytosolic ISC protein assembly machinery requires import of iron, too. Surprisingly, *in vivo* it is not clear how iron enters the neuron since most studies are conducted *in vitro* (without oligodendrocytes), where TfR was observed in dendritic areas (Parton et al., 1992). Oligodendrocytes express Transferrin, which can even be found in compacted myelin areas (Lin and Connor, 1989). If they release iron loaded Transferrin to axonal myelinated sites has to be clarified in future studies. Briefly, the possible iron delivery path in *Drosophila* is depicted in Figure 31.

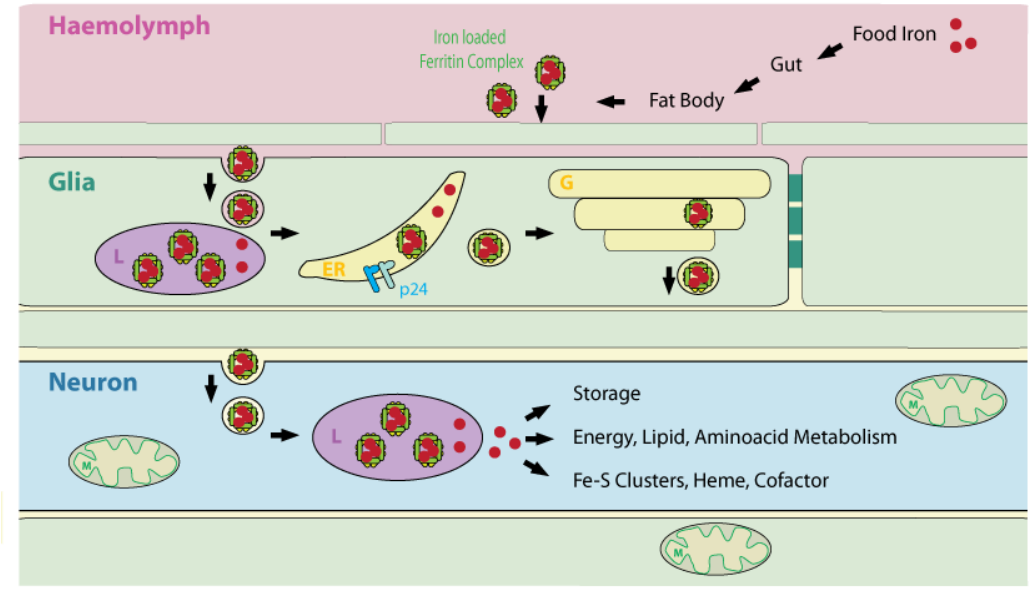

Figure 31: Possible iron delivery pathway in the *Drosophila* nervous system. Food iron is taken up over the gut and loaded on Ferritin secreted to the hemolymph. Ferritin-iron can be taken up by glial cells over a not yet identified mechanism and can be transported via the lysosome to the ER. Here, Ferritin is loaded with iron, transported with the help of p24-1 and opossum to the Golgi and further released to the neuron. Neurons can take up Ferritin and use iron for storage, mitochondria function or ISC assembly.

4.4.4 Iron homeostasis in neurodegenerative disease

Any kind of dysregulation in the iron homeostasis of the nervous system will cause pathological conditions: iron deficiency leads to myelin alterations, whereas overload is related to neurodegenerative disease (Lee et al., 2006; Todorich et al., 2009). Compared to other organs, the brain iron content is high and some structures in the brain show higher iron amounts than others (Hasan et al., 2012). Iron contents are age-related, meaning that iron accumulates during aging (Hardy et al., 2005). In diseases such as Alzheimer's (AD), Parkinson's (PD) and multiple sclerosis iron patterns are changed and iron accumulates (Wong and Duce, 2014).

PD patients are characterized by a loss of dopaminergic neurons and formation of filamentous inclusions of α synuclein between neurons (Parkinson, 2002). In the course of the disease, iron accumulates in the substantia nigra (SN) as well as in dopaminergic neurons within the SN and oxidative damage is observed (Halliwell, 1992; Lin and Beal, 2006; Zecca et al., 2004). There is evidence that ISC biosynthesis might be affected in the pathophysiology of PD. Inhibition of respiratory chain Complex I shows similar features as PD (Betarbet et al., 2000; Horowitz and Greenamyre, 2010), which could lead to further downstream effects. Recently it has been proposed that there might be another link between iron and PD. In a *Drosophila* model of the disease it was demonstrated that mutant α synuclein (A53T and A30P) but not wild-type versions form toxic aggregates (Zhu et al., 2016) when exposed to free iron. In accordance with that finding, it is known that application of iron chelators can protect SN neurons in a mouse PD model (Kaur et al., 2003). AD is a common, age-related neurodegenerative disease, which is characterized by extracellular amyloid β plaques and neurofibrillary tangles (Selkoe, 1996). Magnetic resonance imaging also reveals elevated iron levels in AD patients (Bartzokis et al., 2000). Toxic Aβ plaques are derived from cleavage of the transmembrane protein precursor (APP). Interestingly, APP mRNA contains an IRE in the 5'UTR (Rogers et al., 2002) and the protein possesses ferroxidase activity (Duce et al., 2010). Insoluble iron is localized in Aβ plaques of patients where it probably induces self-aggregation and oligomerization of Aβ peptide (Huang et al., 2004; Lovell et al., 1998).

Once iron enters the brain it has to be stored inside and accumulates over life-time (Salvador, 2010). Because the brain has a high metabolic activity and consumes a major fraction of the body's oxygen, it also produces elevated amounts of ROS. These factors make the brain highly susceptible to iron-catalyzed oxidative damages (Napoli et al., 2006; Yan et al., 1997; Zecca et al., 2004). Therefore, iron even has the potential as a biomarker for diseases such as AD and PD, which are problematic to diagnose and treat (Schenck and Zimmerman, 2004).

5 Conclusion and Outlook

In summary, we could identify in two screening approaches that the p24-1 protein seems to be required for the secretion of the iron binding protein Ferritin 1 heavy chain from glial cells. It is likely that Fer1HCH is secreted from glial cells and taken up by the neurons. As iron is indispensable for the function of the nervous system, we suggest that glia regulate the import of iron into the nervous system. In this study, we could also show that upon blockage of iron release from glial cells, iron accumulates and causes ferroptosis-dependent cell death. Ferroptosis inhibitors and iron chelators can prevent this cell death. The deficiency of neuronal iron upon glial iron blockage could be detected in a transcriptome analysis, which revealed a down-regulation of iron responsive transcripts.

In summary, we identified a new mechanism of iron transport into the nervous system and found another example of metabolic support of the axon by glial cells.

In further experiments, it will be interesting to identify the iron transport route within the vertebrate nervous system. Transferrin, which is described to be the main iron shuttle in vertebrates, is highly expressed in oligodendrocytes. Thus, closer investigation on how iron is transported to a myelinated axon will be intriguing.

Bibliography

Abbott, N.J., Rönnbäck, L., and Hansson, E. (2006). (Review) Astrocyte–endothelial interactions at the blood–brain barrier. Nat. Rev. Neurosci. *7*, 41–53.

Aguzzi, A., Barres, B.A., and Bennett, M.L. (2013). Microglia: scapegoat, saboteur, or something else? Science *339*, 156–161.

Alle, H., Roth, A., and Geiger, J.R.P. (2009). Energy-efficient action potentials in hippocampal mossy fibers. Neuroforum *15*, 130–131.

Allen, N.J. (2014). Astrocyte regulation of synaptic behavior. Annu. Rev. Cell Dev. Biol. *30*, 439–463.

Allen, N.J., and Barres, B. a (2005). Signaling between glia and neurons: focus on synaptic plasticity. Curr. Opin. Neurobiol. *15*, 542–548.

Altenhein, B., Cattenoz, P.B., and Giangrande, A. (2015). The early life of a fly glial cell. Wiley Interdiscip. Rev. Dev. Biol. *5*.

Amiri, M., and Hollenbeck, P.J. (2008). Mitochondrial biogenesis in the axons of vertebrate peripheral neurons. Dev. Neurobiol. *68*, 1348–1361.

Anantharaman, V., and Aravind, L. (2002). The GOLD domain, a novel protein module involved in Golgi function and secretion. Genome Biol. *3*, research0023.

Anderson, P.R., Kirby, K., Hilliker, A.J., and Phillips, J.P. (2005). RNAi-mediated suppression of the mitochondrial iron chaperone, frataxin, in Drosophila. Hum. Mol. Genet. *14*, 3397–3405.

Arosio, P., Ingrassia, R., and Cavadini, P. (2009). Ferritins: a family of molecules for iron storage, antioxidation and more. Biochim. Biophys. Acta *1790*, 589–599.

Attwell, D., and Laughlin, S.B. (2001). An energy budget for signaling in the grey matter of the brain. J. Cereb. Blood Flow Metab. *21*, 1133–1145.

Auld, V.J., Fetter, R.D., Broadie, K., and Goodman, C.S. (1995). Gliotactin, a novel transmembrane protein on peripheral glia, is required to form the blood-nerve barrier in drosophila. Cell *81*, 757–767.

Awasaki, T., Lai, S.-L., Ito, K., and Lee, T. (2008). Organization and postembryonic development of glial cells in the adult central brain of Drosophila. J. Neurosci. *28*, 13742–13753.

Awasaki, T., Huang, Y., O'Connor, M.B., and Lee, T. (2011). Glia instruct developmental neuronal remodeling through TGF-beta signaling. Nat Neurosci *14*, 821–823.

Ball, R.W., Warren-Paquin, M., Tsurudome, K., Liao, E.H., Elazzouzi, F., Cavanagh, C., An, B.S., Wang, T.T., White, J.H., and Haghighi, A.P. (2010). Retrograde BMP signaling controls synaptic growth at the nmj by regulating trio expression in motor neurons. Neuron *66*, 536–549.

Bartzokis, G., Sultzer, D., Cummings, J., Holt, L.E., Hance, D.B., Henderson, V.W., and Mintz, J. (2000). In vivo evaluation of brain iron in Alzheimer disease using magnetic resonance imaging. Arch. Gen. Psychiatry *57*, 47–53.

Bate, M., and Arias, A.M. (1993). The development of Drosophila melanogaster (Cold Spring Harbor Laboratory Press).

Baumgartner, S., Littleton, J.T., Broadie, K., Bhat, M.A., Harbecke, R., Lengyel, J.A., Chiquet-Ehrismann, R., Prokop, A., and Bellen, H.J. (1996). A Drosophila neurexin is required for septate junction and blood-nerve barrier formation and function. Cell *87*, 1059–1068.

Beard, J.L., and Connor, J.R. (2003). Iron Status and Neural Functioning. Annu. Rev. Nutr. *23*, 41–58.

Bélanger, M., Allaman, I., and Magistretti, P.J. (2011). Brain energy metabolism: focus on astrocyte-neuron metabolic cooperation. Cell Metab. *14*, 724–738.

Belden, W.J., and Barlowe, C. (2001). Distinct Roles for the Cytoplasmic Tail Sequences of Emp24p and Erv25p in Transport between the Endoplasmic Reticulum and Golgi Complex. J. Biol. Chem. *276*, 43040–43048.

Bergmann, A., Tugentman, M., Shilo, B.Z., and Steller, H. (2002). Regulation of cell number by MAPK-dependent control of apoptosis: A mechanism for trophic survival signaling. Dev. Cell *2*, 159–170.

Betarbet, R., Sherer, T.B., Mackenzie, G., Garcia-osuna, M., Panov, A. V, and Greenamyre, J.T. (2000). Chronic systemic pesticide exposure reproduces features of Parkinson's disease. Nat. Neurosci. *3*, 1301–1306.

Bettedi, L., Aslam, M.F., Szular, J., Mandilaras, K., and Missirlis, F. (2011). Iron depletion in the intestines of Malvolio mutant flies does not occur in the absence of a multicopper oxidase. J. Exp. Biol. *214*, 971–978.

Bhat, M.A., Rios, J.C., Lu, Y., Garcia-Fresco, G.P., Ching, W., Martin, M.S., Li, J., Einheber, S., Chesler, M., Rosenbluth, J., et al. (2001). Axon-glia interactions and the domain organization of myelinated axons requires Neurexin IV/Caspr/Paranodin. Neuron *30*, 369–383.

Bischof, J., Maeda, R.K., Hediger, M., Karch, F., and Basler, K. (2007). An optimized transgenesis system for Drosophila using germ-line-specific phiC31 integrases. Proc. Natl. Acad. Sci. U. S. A. *104*, 3312–3317.

Bischof, J., Björklund, M., Furger, E., Schertel, C., Taipale, J., and Basler, K. (2013). A versatile platform for creating a comprehensive UAS-ORFeome library in Drosophila. Development *140*, 2434–2442.

Bittar, P.G., Charnay, Y., Pellerin, L., Bouras, C., and Magistretti, P.J. (1996). Selective distribution of lactate dehydrogenase isoenzymes in neurons and astrocytes of human brain. J. Cereb. Blood Flow Metab. *16*, 1079–1089.

Bloch, B., Popovici, T., Levin, M.J., Tuil, D., and Kahn, A. (1985). Transferrin gene expression visualized in oligodendrocytes of the rat brain by using in situ hybridization and immunohistochemistry. Proc. Natl. Acad. Sci. U. S. A. *82*, 6706–6710.

Bökel, C., Dass, S., Wilsch-Bräuninger, M., and Roth, S. (2006). Drosophila Cornichon acts as cargo receptor for ER export of the TGFalpha-like growth factor Gurken. Development *133*, 459–470.

Boltz, K. a, Ellis, L.L., and Carney, G.E. (2007). Drosophila melanogaster p24 genes have developmental, tissue-specific, and sex-specific expression patterns and functions. Dev. Dyn. *236*, 544–555.

Brand, A.H., and Perrimon, N. (1993). Targeted gene expression as a means of altering cell fates and generating dominant phenotypes. Development *118*, 401–415.

Brankatschk, M., and Eaton, S. (2010). Lipoprotein particles cross the blood-brain barrier in Drosophila. J. Neurosci. *30*, 10441–10447.

BrosiusLutz, A., and Barres, B.A. (2014). Contrasting the Glial Response to Axon Injury in the Central and Peripheral Nervous Systems. Dev. Cell *28*, 7–17.

Buechling, T., Chaudhary, V., Spirohn, K., Weiss, M., and Boutros, M. (2011). p24 proteins are required for secretion of Wnt ligands. EMBO Rep. *12*, 1265–1272.

Bulteau, A.-L., O'Neill, H. a, Kennedy, M.C., Ikeda-Saito, M., Isaya, G., and Szweda, L.I. (2004). Frataxin acts as an iron chaperone protein to modulate mitochondrial aconitase activity. Science *305*, 242–245.

Burnette, W.N. (1981). "Western Blotting": Electrophoretic transfer of proteins from sodium dodecyl sulfate-polyacrylamide gels to unmodified nitrocellulose and radiographic detection with antibody and radioiodinated protein A. Anal. Biochem. *112*, 195–203.

Cammer, W. (1984). Oligodendroglia (Boston, MA: Springer US).

Campbell, G., Göring, H., Lin, T., Spana, E., Andersson, S., Doe, C.Q., and Tomlinson, a (1994). RK2, a glial-specific homeodomain protein required for embryonic nerve cord condensation and viability in Drosophila. Development *120*, 2957–2966.

Carlson, S.D., Juang, J., Hilgers, S.L., and Garment, M.B. (2000). Blood Barriers of the Insect. Annu. Rev. Entomol. *45*, 151–174.

Carney, G.E., and Bowen, N.J. (2004). p24 proteins, intracellular trafficking, and behavior: Drosophila melanogaster provides insights and opportunities. Biol. Cell *96*, 271–278.

Casano, A.M., and Peri, F. (2015). Microglia: Multitasking specialists of the brain. Dev. Cell *32*, 469–477.

Castillon, G. a, Watanabe, R., Taylor, M., Schwabe, T.M.E., and Riezman, H. (2009). Concentration of GPI-anchored proteins upon ER exit in yeast. Traffic *10*, 186–200.

Chell, J.M., and Brand, A.H. (2010). Nutrition-responsive glia control exit of neural stem cells from quiescence. Cell *143*, 1161–1173.

Chen, T.T., Li, L., Chung, D.-H., Allen, C.D.C., Torti, S. V, Torti, F.M., Cyster, J.G., Chen, C.-Y., Brodsky, F.M., Niemi, E.C., et al. (2005). TIM-2 is expressed on B cells and in liver and kidney and is a receptor for H-ferritin endocytosis. J. Exp. Med. *202*, 955–965.

Chotard, C., and Salecker, I. (2004). Neurons and glia: team players in axon guidance. Trends Neurosci. *27*, 655–661.

Ciufo, L.F., and Boyd, A. (2000). Identification of a lumenal sequence specifying the assembly of Emp24p into p24 complexes in the yeast secretory pathway. J. Biol. Chem. *275*, 8382–8388.

Clarke, L.E., and Barres, B.A. (2013). Emerging roles of astrocytes in neural circuit development. Nat. Rev. Neurosci. *14*, 311–321.

Cohen, L.A., Gutierrez, L., Weiss, A., Leichtmann-Bardoogo, Y., Zhang, D.L., Crooks, D.R., Sougrat, R., Morgenstern, A., Galy, B., Hentze, M.W., et al. (2010). Serum ferritin is derived primarily from macrophages through a nonclassical secretory pathway. Blood *116*, 1574–1584.

Connor, J.R., and Menzies, S.L. (1996). Relationship of iron to oligodendrocytes and myelination. Glia *17*, 83–93.

Connor, J.R., Menzies, S.L., St Martin, S.M., and Mufson, E.J. (1990). Cellular distribution of transferrin, ferritin, and iron in normal and aged human brains. J. Neurosci. Res. *27*, 595–611.

Cook, J.D., Lipschitz, D.A., Miles, L.E.M., and Finch, C.A. (1974). Serum ferritin as a measure of iron stores in normal subjects. Am. J. Clin. Nutr. *27*, 681–687.

D'Arcangelo, J.G., Crissman, J., Pagant, S., ??opi??, A., Latham, C.F., Snapp, E.L., and Miller, E.A. (2015). Traffic of p24 proteins and COPII coat composition mutually influence membrane scaffolding. Curr. Biol. *25*, 1296–1305.

Dautry-Varsat, A., Ciechanover, A., and Lodish, H.F. (1983). pH and the recycling of transferrin during receptor-mediated endocytosis. Proc. Natl. Acad. Sci. *80*, 2258–2262.

Delatycki, M.B., Camakaris, J., Brooks, H., Evans-Whipp, T., Thorburn, D.R., Williamson, R., and Forrest, S.M. (1999). Direct evidence that mitochondrial iron accumulation occurs in Friedreich ataxia. Ann. Neurol. *45*, 673–675.

Delatycki, M.B., Williamson, R., and Forrest, S.M. (2000). Friedreich ataxia: an overview. J. Med. Genet. *37*, 1–8.

Denzel, a, Otto, F., Girod, a, Pepperkok, R., Watson, R., Rosewell, I., Bergeron, J.J., Solari, R.C., and Owen, M.J. (2000). The p24 family member p23 is required for early embryonic development. Curr. Biol. *10*, 55–58.

DeSalvo, M.K., Hindle, S.J., Rusan, Z.M., Orng, S., Eddison, M., Halliwill, K., and Bainton, R.J. (2014). The Drosophila surface glia transcriptome: Evolutionary conserved blood-brain barrier processes. Front. Neurosci. *8*, 1–22.

Dietzl, G., Chen, D., Schnorrer, F., Su, K.-C., Barinova, Y., Fellner, M., Gasser, B., Kinsey, K., Oppel, S., Scheiblauer, S., et al. (2007). A genome-wide transgenic RNAi library for conditional gene inactivation in Drosophila. Nature *448*, 151–156.

Dixon, S.J., and Stockwell, B.R. (2014). The role of iron and reactive oxygen species in cell death. Nat. Chem. Biol. *10*, 9–17.

Dixon, S.J., Lemberg, K.M., Lamprecht, M.R., Skouta, R., Zaitsev, E.M., Gleason, C.E., Patel, D.N., Bauer, A.J., Cantley, A.M., Yang, W.S., et al. (2012). Ferroptosis: an iron-dependent form of nonapoptotic cell death. Cell *149*, 1060–1072.

Doherty, J., Logan, M.A., Taşdemir, O.E., and Freeman, M.R. (2009). Ensheathing glia function as phagocytes in the adult Drosophila brain. J. Neurosci. *29*, 4768–4781.

Dominguez, M., Dejgaard, K., Füllekrug, J., Dahan, S., Fazel, A., Paccaud, J.P., Thomas, D.Y., Bergeron, J.J.M., and Nilsson, T. (1998). gp25L/emp24/p24 protein family members of the cis-Golgi network bind both COP I and II coatomer. J. Cell Biol. *140*, 751–765.

Duce, J.A., Tsatsanis, A., Cater, M.A., James, S.A., Robb, E., Wikhe, K., Leong, S.L., Perez, K., Johanssen, T., Greenough, M.A., et al. (2010). Iron-Export Ferroxidase Activity of β-Amyloid Precursor Protein is Inhibited by Zinc in Alzheimer's Disease. Cell *142*, 857–867.

Edenfeld, G., Stork, T., and Klämbt, C. (2005). Neuron-glia interaction in the insect nervous system. Curr. Opin. Neurobiol. *15*, 34–39.

Edenfeld, G., Volohonsky, G., Krukkert, K., Naffin, E., Lammel, U., Grimm, A., Engelen, D., Reuveny, A., Volk, T., and Kl??mbt, C. (2006). The Splicing Factor Crooked Neck Associates with the RNA-Binding Protein HOW to Control Glial Cell Maturation in Drosophila. Neuron *52*, 969–980.

Edwards, J.S., Swales, L.S., and Bate, M. (1993). The differentiation between neuroglia and connective tissue sheath in insect ganglia revisited: the neural lamella and perineurial sheath cells are absent in a mesodermless mutant of Drosophila. J. Comp. Neurol. *333*, 301–308.

Enneking, E.-M., Kudumala, S.R., Moreno, E., Stephan, R., Boerner, J., Godenschwege, T. a, and Pielage, J. (2013). Transsynaptic coordination of synaptic growth, function, and stability by the L1-type CAM Neuroglian. PLoS Biol. *11*, e1001537.

Erecinska, M., and Wilson, D.F. (1978). Oxygen Transport to Tissue — III (Boston, MA: Springer US).

Ferreira, C., Bucchini, D., Martin, M.E., Levi, S., Arosio, P., Grandchamp, B., and Beaumont, C. (2000). Early embryonic lethality of H ferritin gene deletion in mice. J. Biol. Chem. *275*, 3021–3024.

Fields, R.D. (2002). New Insights into Neuron-Glia Communication. Science (80-.). *298*, 556–562.

Franzdóttir, S.R., Engelen, D., Yuva-Aydemir, Y., Schmidt, I., Aho, A., and Klämbt, C. (2009). Switch in FGF signalling initiates glial differentiation in the Drosophila eye. Nature *460*, 758–761.

Freeman, M.R. (2015). Drosophila central nervous system glia. Cold Spring Harb. Perspect. Biol. *7*.

Friedman, A., Arosio, P., Finazzi, D., Koziorowski, D., and Galazka-Friedman, J. (2011). Ferritin as an important player in neurodegeneration. Park. Relat. Disord. *17*, 423–430.

Fuentes-Medel, Y., Ashley, J., Barria, R., Maloney, R., Freeman, M., and Budnik, V. (2012). Integration of a retrograde signal during synapse formation by glia-secreted TGF-β ligand. Curr. Biol. *22*, 1831–1838.

Fünfschilling, U., Supplie, L.M., Mahad, D., Boretius, S., Saab, A.S., Edgar, J., Brinkmann, B.G., Kassmann, C.M., Tzvetanova, I.D., Möbius, W., et al. (2012). Glycolytic oligodendrocytes maintain myelin and long-term axonal integrity. Nature *485*, 517–521.

Genova, J.L., and Fehon, R.G. (2003). Neuroglian, Gliotactin, and the Na+/k+ ATPase are essential for septate junction function in Drosophila. J. Cell Biol. *161*, 979–989.

Gerber, B., and Stocker, R.F. (2007). The drosophila larva as a model for studying chemosensation and chemosensory learning: A review. Chem. Senses *32*, 65–89.

Ghosh, A., Manrique-Hoyos, N., Voigt, A., Schulz, J.B., Kreutzfeldt, M., Merkler, D., and Simons, M. (2011). Targeted ablation of oligodendrocytes triggers axonal damage. PLoS One *6*, e22735.

Ghosh, A., Kling, T., Snaidero, N., Sampaio, J.L., Shevchenko, A., Gras, H., Geurten, B., Göpfert, M.C., Schulz, J.B., Voigt, A., et al. (2013). A Global In Vivo Drosophila RNAi Screen Identifies a Key Role of Ceramide Phosphoethanolamine for Glial Ensheathment of Axons. PLoS Genet. *9*, e1003980.

Ghosh, M.C., Zhang, D.-L., and Rouault, T. a (2015). Iron misregulation and neurodegenerative disease in mouse models that lack iron regulatory proteins. Neurobiol. Dis.

Gibson, E.M., Purger, D., Mount, C.W., Goldstein, A.K., Lin, G.L., Wood, L.S., Inema, I., Miller, S.E., Bieri, G., Zuchero, J.B., et al. (2014). Neuronal activity promotes oligodendrogenesis and adaptive myelination in the mammalian brain. Science *344*, 1252304.

Gillespie, M.J., and Stein, R.B. (1983). The relationship between axon diameter, myelin thickness and conduction velocity during atrophy of mammalian peripheral nerves. Brain Res. *259*, 41–56.

Gilmour, D.T., Maischein, H.M., and Nüsslein-Volhard, C. (2002). Migration and function of a glial subtype in the vertebrate peripheral nervous system. Neuron *34*, 577–588.

Ginhoux, F., Lim, S., Hoeffel, G., Low, D., and Huber, T. (2013). Origin and differentiation of microglia. Front. Cell. Neurosci. *7*, 45.

Gomez-Marin, A., and Louis, M. (2012). Active sensation during orientation behavior in the Drosophila larva: More sense than luck. Curr. Opin. Neurobiol. *22*, 208–215.

González-Morales, N., Mendoza-Ortíz, M.Á., Blowes, L.M., Missirlis, F., and Riesgo-Escovar, J.R. (2015). Ferritin Is Required in Multiple Tissues during Drosophila melanogaster Development. PLoS One *10*, e0133499.

Gould, D.B., Phalan, F.C., Breedveld, G.J., van Mil, S.E., Smith, R.S., Schimenti, J.C., Aguglia, U., van der Knaap, M.S., Heutink, P., and John, S.W.M. (2005). Mutations in Col4a1 cause perinatal cerebral hemorrhage and porencephaly. Science *308*, 1167–1171.

Gozzelino, R., and Arosio, P. (2016). Iron homeostasis in health and disease. Int. J. Mol. Sci. *17*, 2–14.

Graham, R.M., Chua, A.C.G., Carter, K.W., Delima, R.D., Johnstone, D., Herbison, C.E., Firth, M.J., O'Leary, R., Milward, E.A., Olynyk, J.K., et al. (2010). Hepatic iron loading in mice increases cholesterol biosynthesis. Hepatology *52*, 462–471.

Granderath, S., Bunse, I., and Klämbt, C. (2000). gcm and pointed synergistically control glial transcription of the Drosophila gene loco. Mech. Dev. *91*, 197–208.

Granick, S. (1942). FERRITIN: I. PHYSICAL AND CHEMICAL PROPERTIES OF HORSE SPLEEN FERRITIN. J. Biol. Chem. *146*, 451–461.

Green, C.H., Burnet, B., and Connolly, K.J. (1983). Organization and patterns of inter- and intraspecific variation in the behaviour of Drosophila larvae. Anim. Behav. *31*, 282–291.

Gunshin, H., Mackenzie, B., Berger, U. V., Gunshin, Y., Romero, M.F., Boron, W.F., Nussberger, S., Gollan, J.L., and Hediger, M.A. (1997). Cloning and characterization of a mammalian proton-coupled metal-ion transporter. Nature *388*, 482–488.

Guruharsha, K.G., Rual, J.-F., Zhai, B., Mintseris, J., Vaidya, P., Vaidya, N., Beekman, C., Wong, C., Rhee, D.Y., Cenaj, O., et al. (2011). A protein complex network of Drosophila melanogaster. Cell *147*, 690–703.

Hall, C.N., Klein-Flugge, M.C., Howarth, C., and Attwell, D. (2012). Oxidative Phosphorylation, Not Glycolysis, Powers Presynaptic and Postsynaptic Mechanisms Underlying Brain Information Processing. J. Neurosci. *32*, 8940–8951.

Halliwell, B. (1992). Reactive oxygen species and the central nervous system. J. Neurochem. *59*, 1609–1623.

Han, J., Seaman, W.E., Di, X., Wang, W., Willingham, M., Torti, F.M., and Torti, S. V. (2011). Iron uptake mediated by binding of H-ferritin to the TIM-2 receptor in mouse cells. PLoS One *6*.

Harding, C., Heuser, J., and Stahl, P. (1983). Receptor-mediated endocytosis of transferrin and recycling of the transferrin receptor in rat reticulocytes. J. Cell Biol. *97*, 329–339.

Hardy, P.A., Gash, D., Yokel, R., Andersen, A., Ai, Y., and Zhang, Z. (2005). Correlation of R2 with total iron concentration in the brains of rhesus monkeys. J. Magn. Reson. Imaging *21*, 118–127.

Harrison, P.M., and Arosio, P. (1996). The ferritins: molecular properties, iron storage function and cellular regulation. Biochim. Biophys. Acta *1275*, 161–203.

Hartenstein, V. (1993). Atlas of Drosophila Development. Atlas Drosoph. Dev. 1–57.

Hartenstein, V. (2011). Morphological diversity and development of glia in Drosophila. Glia *59*, 1237–1252.

Hasan, K.M., Walimuni, I.S., Kramer, L. a, and Narayana, P. a (2012). Human brain iron mapping using atlas-based T2 relaxometry. Magn. Reson. Med. *67*, 731–739.

Hegde, V.R., Vogel, R., and Feany, M.B. (2014). Glia are critical for the neuropathology of complex I deficiency in Drosophila. Hum. Mol. Genet. 1–24.

Hentze, M.W., Muckenthaler, M.U., Galy, B., and Camaschella, C. (2010). Two to tango: regulation of Mammalian iron metabolism. Cell *142*, 24–38.

Herculano-Houzel, S. (2014). The glia/neuron ratio: How it varies uniformly across brain structures and species and what that means for brain physiology and evolution. Glia *62*, 1377–1391.

Hidalgo, A., Kinrade, E.F. V, and Georgiou, M. (2001). The Drosophila Neuregulin Vein Maintains Glial Survival during Axon Guidance in the CNS. Dev. Cell *1*, 679–690.

Hidalgo, A., Learte, A.R., McQuilton, P., Pennack, J., and Zhu, B. (2006). Neurotrophic and gliatrophic contexts in Drosophila. Brain. Behav. Evol. *68*, 173–180.

Hidalgo, A., Kato, K., Sutcliffe, B., McIlroy, G., Bishop, S., and Alahmed, S. (2011). Trophic neuron-glia interactions and cell number adjustments in the fruit fly. Glia *59*, 1296–1303.

von Hilchen, C.M., Hein, I., Technau, G.M., and Altenhein, B. (2010). Netrins guide migration of distinct glial cells in the Drosophila embryo. Development *137*, 1251–1262.

von Hilchen, C.M., Bustos, A.E., Giangrande, A., Technau, G.M., and Altenhein, B. (2013). Predetermined embryonic glial cells form the distinct glial sheaths of the Drosophila peripheral nervous system. Development *140*, 3657–3668.

Hirokawa, N., and Takemura, R. (2005). Molecular motors and mechanisms of directional transport in neurons. Nat. Rev. Neurosci. *6*, 201–214.

Holtmaat, A., and Svoboda, K. (2009). Experience-dependent structural synaptic plasticity in the mammalian brain. Nat. Rev. Neurosci. *10*, 647–658.

Horowitz, M.P., and Greenamyre, J.T. (2010). Mitochondrial iron metabolism and its role in neurodegeneration. J. Alzheimer's Dis. *20*.

Hortsch, M., Bieber, A.J., Patel, N.H., and Goodman, C.S. (1990). Differential splicing generates a nervous system-Specific form of drosophila neuroglian. Neuron *4*, 697–709.

Hortsch, M., Nagaraj, K., and Godenschwege, T.A. (2009). The interaction between L1-type proteins and ankyrins--a master switch for L1-type CAM function. Cell. Mol. Biol. Lett. *14*, 57–69.

Howarth, C., Gleeson, P., and Attwell, D. (2012). Updated energy budgets for neural computation in the neocortex and cerebellum. J. Cereb. Blood Flow Metab. *32*, 1222–1232.

Huang, L.Y.M., Gu, Y., and Chen, Y. (2013). Communication between neuronal somata and satellite glial cells in sensory ganglia. Glia *61*, 1571–1581.

Huang, X., Atwood, C.S., Moir, R.D., Hartshorn, M.A., Tanzi, R.E., and Bush, A.I. (2004). Trace metal contamination initiates the apparent auto-aggregation, amyloidosis, and oligomerization of Alzheimer's A?? peptides. J. Biol. Inorg. Chem. *9*, 954–960.

Hummel, T., Krukkert, K., Roos, J., Davis, G., and Klämbt, C. (2000). Drosophila Futsch/22C10 is a MAP1B-like protein required for dendritic and axonal development. Neuron *26*, 357–370.

Hummel, T., Attix, S., Gunning, D., and Zipursky, S.L. (2002). Temporal control of glial cell migration in the Drosophila eye requires gilgamesh, hedgehog, and eye specification genes. Neuron *33*, 193–203.

Jacob, C. (2015). Transcriptional control of neural crest specification into peripheral glia. Glia *63*, 1883–1896.

Jacobs, J.R. (2000). The Midline Glia of Drosophila: A molecular genetic model for the developmental functions of Glia. Prog. Neurobiol. *62*, 475–508.

Jahn, O., Tenzer, S., and Werner, H.B. (2009). Myelin proteomics: Molecular anatomy of an insulating sheath. Mol. Neurobiol. *40*, 55–72.

Jan, Y.-N., and Jan, L.Y. (2010). Branching out: mechanisms of dendritic arborization. Nat. Rev. Neurosci. *11*, 316–328.

Jessen, K.R., and Mirsky, R. (2016). The repair Schwann cell and its function in regenerating nerves. J. Physiol. *0*, 1–11.

Jones, B.W. (2005). Transcriptional control of glial cell development in Drosophila. Dev. Biol. *278*, 265–273.

Jones, B.W., Fetter, R.D., Tear, G., and Goodman, C.S. (1995). glial cells missing: a genetic switch that controls glial versus neuronal fate. Cell *82*, 1013–1023.

Kasischke, K. a, Vishwasrao, H.D., Fisher, P.J., Zipfel, W.R., and Webb, W.W. (2004). Neural activity triggers neuronal oxidative metabolism followed by astrocytic glycolysis. Science *305*, 99–103.

Kaur, D., Yantiri, F., Rajagopalan, S., Kumar, J., Mo, J.Q., Boonplueang, R., Viswanath, V., Jacobs, R., Yang, L., Beal, M.F., et al. (2003). Genetic or pharmacological iron chelation prevents MPTP-induced neurotoxicity in vivo: A novel therapy for Parkinson's disease. Neuron *37*, 899–909.

Keller, J.N., Mark, R.J., Bruce, A.J., Blanc, E., Rothstein, J.D., Uchida, K., Waeg, G., and Mattson, M.P. (1997). 4-hydroxynonenal, an aldehydic product of membrane lipid peroxidation, impairs glutamate transport and mitochondrial function in synaptosomes. Neuroscience *80*, 685–696.

Keller, L.C., Cheng, L., Locke, C.J., Müller, M., Fetter, R.D., and Davis, G.W. (2011). Glial-derived prodegenerative signaling in the Drosophila neuromuscular system. Neuron *72*, 760–775.

Kerr, K.S., Fuentes-Medel, Y., Brewer, C., Barria, R., Ashley, J., Abruzzi, K.C., Sheehan, A., Tasdemir-Yilmaz, O.E., Freeman, M.R., and Budnik, V. (2014). Glial Wingless/Wnt Regulates Glutamate Receptor Clustering and Synaptic Physiology at the Drosophila Neuromuscular Junction. J. Neurosci. *34*, 2910–2920.

Keshishian, H., Broadie, K., Chiba, A., and Bate, M. (1996). The drosophila neuromuscular junction: a model system for studying synaptic development and function. Annu. Rev. Neurosci. *19*, 545–575.

Kidd, T., Bland, K.S., and Goodman, C.S. (1999). Slit is the midline repellent for the robo receptor in Drosophila. Cell *96*, 785–794.

Kim, S.N., Jeibmann, A., Halama, K., Witte, H.T., Wälte, M., Matzat, T., Schillers, H., Faber, C., Senner, V., Paulus, W., et al. (2014). ECM stiffness regulates glial migration in Drosophila and mammalian glioma models. Development 3233–3242.

Klaes, A., Menne, T., Stollewerk, A., Scholz, H., and Kl??mbt, C. (1994). The Ets transcription factors encoded by the Drosophila gene pointed direct glial cell differentiation in the embryonic CNS. Cell *78*, 149–160.

Klämbt, C., and Goodman, C.S. (1991). The diversity and pattern of glia during axon pathway formation in the Drosophila embryo. Glia *4*, 205–213.

Kohsaka, H., Okusawa, S., Itakura, Y., Fushiki, A., and Nose, A. (2012). Development of larval motor circuits in Drosophila. Dev. Growth Differ. *54*, 408–419.

Kolodziej, P.A., Timpe, L.C., Mitchell, K.J., Fried, S.R., Goodman, C.S., Jan, L.Y., and Jan, Y.N. (1996). frazzled Encodes a Drosophila member of the DCC immunoglobulin subfamily and is required for CNS and motor axon guidance. Cell *87*, 197–204.

Kondo, S., Booker, M., and Perrimon, N. (2009). Cross-species RNAi rescue platform in Drosophila melanogaster. Genetics *183*, 1165–1173.

Kosmidis, S., Botella, J. a, Mandilaras, K., Schneuwly, S., Skoulakis, E.M.C., Rouault, T. a, and Missirlis, F. (2011). Ferritin overexpression in Drosophila glia leads to iron deposition in the optic lobes and late-onset behavioral defects. Neurobiol. Dis. *43*, 213–219.

Laemmli, U.K. (1970). Cleavage of structural proteins during the assembly of the head of bacteriophage T4. Nature *227*, 680–685.

Landgraf, M., Sánchez-Soriano, N., Technau, G.M., Urban, J., and Prokop, A. (2003). Charting the Drosophila neuropile: A strategy for the standardised characterisation of genetically amenable neurites. Dev. Biol. *260*, 207–225.

Lang, M., Braun, C.L., Kanost, M.R., and Gorman, M.J. (2012). Multicopper oxidase-1 is a ferroxidase essential for iron homeostasis in Drosophila melanogaster. Proc. Natl. Acad. Sci. U. S. A. *109*, 13337–13342.

Learte, A.R., Forero, M.G., and Hidalgo, A. (2008). Gliatrophic and gliatropic roles of PVF/PVR signaling during axon guidance. Glia *56*, 164–176.

Lee, B.P., and Jones, B.W. (2005). Transcriptional regulation of the Drosophila glial gene repo. Mech. Dev. *122*, 849–862.

Lee, T., and Luo, L. (1999). Mosaic analysis with a repressible cell marker for studies of gene function in neuronal morphogenesis. Neuron *22*, 451–461.

Lee, D.W., Andersen, J.K., and Kaur, D. (2006). Iron dysregulation and neurodegeneration: the molecular connection. Mol Interv *6*, 89–97.

Lee, T., Lee, a, and Luo, L. (1999). Development of the Drosophila mushroom bodies: sequential generation of three distinct types of neurons from a neuroblast. Development *126*, 4065–4076.

Lee, T., Marticke, S., Sung, C., Robinow, S., and Luo, L. (2000). Cell-autonomous requirement of the USP/EcR-B ecdysone receptor for mushroom body neuronal remodeling in Drosophila. Neuron *28*, 807–818.

Lehn, A., Boyle, R., Brown, H., Airey, C., and Mellick, G. (2012). Neuroferritinopathy. Parkinsonism Relat. Disord. *18*, 909–915.

Leiserson, W.M., and Keshishian, H. (2011). Maintenance and regulation of extracellular volume and the ion environment in Drosophila larval nerves. Glia *59*, 1312–1321.

Leiserson, W.M., Harkins, E.W., and Keshishian, H. (2000). Fray, a Drosophila serine/threonine kinase homologous to mammalian PASK, is required for axonal ensheathment. Neuron *28*, 793–806.

Levy, F., Bulet, P., and Ehret-Sabatier, L. (2004). Proteomic analysis of the systemic immune response of Drosophila. Mol. Cell. Proteomics *3*, 156–166.

Lill, R., and Mühlenhoff, U. (2006). Iron-sulfur protein biogenesis in eukaryotes: components and mechanisms. Annu. Rev. Cell Dev. Biol. *22*, 457–486.

Lill, R., Hoffmann, B., Molik, S., Pierik, A.J., Rietzschel, N., Stehling, O., Uzarska, M.A., Webert, H., Wilbrecht, C., and Mühlenhoff, U. (2012). The role of mitochondria in cellular iron-sulfur protein biogenesis and iron metabolism. Biochim. Biophys. Acta - Mol. Cell Res. *1823*, 1491–1508.

Limmer, S., Weiler, A., Volkenhoff, A., Babatz, F., and Klämbt, C. (2014). The drosophila blood-brain barrier: Development and function of a glial endothelium. Front. Neurosci. *8*, 1–19.

Lin, H.H., and Connor, J.R. (1989). The development of the transferrin-transferrin receptor system in relation to astrocytes, MBP and galactocerebroside in normal and myelin-deficient rat optic nerves. Dev. Brain Res. *49*, 281–293.

Lin, M.T., and Beal, M.F. (2006). Mitochondrial dysfunction and oxidative stress in neurodegenerative diseases. Nature *443*, 787–795.

Liu, H., and Naismith, J.H. (2008). An efficient one-step site-directed deletion, insertion, single and multiple-site plasmid mutagenesis protocol. BMC Biotechnol. *8*, 91.

Lovell, M.A., Robertson, J.D., Teesdale, W.J., Campbell, J.L., and Markesbery, W.R. (1998). Copper, iron and zinc in Alzheimer's disease senile plaques. J. Neurol. Sci. *158*, 47–52.

Lozoff, B., and Georgieff, M.K. (2006). Iron Deficiency and Brain Development. Semin. Pediatr. Neurol. *13*, 158–165.

Mahr, A., and Aberle, H. (2006). The expression pattern of the Drosophila vesicular glutamate transporter: A marker protein for motoneurons and glutamatergic centers in the brain. Gene Expr. Patterns *6*, 299–309.

Mandilaras, K., Pathmanathan, T., and Missirlis, F. (2013). Iron absorption in Drosophila melanogaster. Nutrients *5*, 1622–1647.

Manrique-Hoyos, N. (2012). Neurodegenration in toxin-mediated demyelinating animal models of Multiple Sclerosis. Georg-August University of Goettingen.

Margeta, M.A., and Shen, K. (2010). Molecular mechanisms of synaptic specificity. Mol. Cell. Neurosci. *43*, 261–267.

Matzat, T., Sieglitz, F., Kottmeier, R., Babatz, F., Engelen, D., and Klämbt, C. (2015). Axonal wrapping in the Drosophila PNS is controlled by glia-derived neuregulin homolog Vein. Development *142*, 1336–1345.

McCarthy, R.C., and Kosman, D.J. (2013). Ferroportin and exocytoplasmic ferroxidase activity are required for brain microvascular endothelial cell iron efflux. J. Biol. Chem. *288*, 17932–17940.

Mckenzie, I.A., Ohayon, D., Li, H., Faria, J.P. De, Emery, B., Tohyama, K., and Richardson, W.D. (2014). Motor skill learning requires active central myelination. Science (80-.). *346*, 318–322.

Mercer, R.W., and Dunham, P.B. (1981). Membrane-bound ATP fuels the Na/K pump. Studies on membrane-bound glycolytic enzymes on inside-out vesicles from human red cell membranes. J. Gen. Physiol. *78*, 547–568.

Meyron-Holtz, E.G., Moshe-Belizowski, S., and Cohen, L. a (2011). A possible role for secreted ferritin in tissue iron distribution. J. Neural Transm. *118*, 337–347.

Mi, H., Muruganujan, A., Casagrande, J.T., and Thomas, P.D. (2013). Large-scale gene function analysis with the PANTHER classification system. Nat. Protoc. *8*, 1551–1566.

Michailov, G. V, Sereda, M.W., Brinkmann, B.G., Fischer, T.M., Haug, B., Birchmeier, C., Role, L., Lai, C., Schwab, M.H., and Nave, K.-A. (2004). Axonal neuregulin-1 regulates myelin sheath thickness. Science *304*, 700–703.

Miller, D., Hannon, C., and Ganetzky, B. (2012). A mutation in Drosophila Aldolase causes temperature-sensitive paralysis, shortened lifespan, and neurodegeneration. J. Neurogenet. *26*, 317–327.

Missirlis, F., Holmberg, S., Georgieva, T., Dunkov, B.C., Rouault, T. a, and Law, J.H. (2006). Characterization of mitochondrial ferritin in Drosophila. Proc. Natl. Acad. Sci. U. S. A. *103*, 5893–5898.

Missirlis, F., Kosmidis, S., Brody, T., Mavrakis, M., Holmberg, S., Odenwald, W.F., Skoulakis, E.M.C., and Rouault, T. a (2007). Homeostatic mechanisms for iron storage revealed by genetic manipulations and live imaging of Drosophila ferritin. Genetics *177*, 89–100.

Moos, T. (2002). Brain iron homeostasis. Dan. Med. Bull. *49*, 279–301.

Morrison, B.M., Lee, Y., and Rothstein, J.D. (2013). Oligodendroglia: Metabolic supporters of axons. Trends Cell Biol. *23*, 644–651.

Namekawa, M., Muriel, M.P., Janer, A., Latouche, M., Dauphin, A., Debeir, T., Martin, E., Duyckaerts, C., Prigent, A., Depienne, C., et al. (2007). Mutations in the SPG3A gene encoding the GTPase atlastin interfere with vesicle trafficking in the ER/Golgi interface and Golgi morphogenesis. Mol. Cell. Neurosci. *35*, 1–13.

Napoli, E., Taroni, F., and Cortopassi, G.A. (2006). Frataxin, iron-sulfur clusters, heme, ROS, and aging. Antioxid. Redox Signal. *8*, 506–516.

Nave, K.A. (2010). Myelination and the trophic support of long axons. Nat Rev Neurosci *11*, 275–283.

Nave, K.-A., and Trapp, B.D. (2008). Axon-glial signaling and the glial support of axon function. Annu. Rev. Neurosci. *31*, 535–561.

Nemeth, E., Tuttle, M.S., Powelson, J., Vaughn, M.B., Donovan, A., Ward, D.M., Ganz, T., and Kaplan, J. (2004). Hepcidin regulates cellular iron efflux by binding to ferroportin and inducing its internalization. Science *306*, 2090–2093.

Nichol, H., Law, J.H., and Winzerling, J.J. (2002). Iron metabolism in insects. Annu. Rev. Entomol. *47*, 535–559.

Noordermeer, J.N., Kopczynski, C.C., Fetter, R.D., Bland, K.S., Chen, W.Y., and Goodman, C.S. (1998). Wrapper, a novel member of the Ig superfamily, is expressed by midline glia and is required for them to ensheath commissural axons in Drosophila. Neuron *21*, 991–1001.

Ohgami, R.S., Campagna, D.R., McDonald, A., and Fleming, M.D. (2006). The Steap proteins are metalloreductases. Blood *108*, 1388–1394.

Ohno, N., Kidd, G.J., Mahad, D., Kiryu-Seo, S., Avishai, A., Komuro, H., and Trapp, B.D. (2011). Myelination and axonal electrical activity modulate the distribution and motility of mitochondria at CNS nodes of Ranvier. J. Neurosci. *31*, 7249–7258.

Ong, W.Y., and Halliwell, B. (2004). Iron, atherosclerosis, and neurodegeneration: A key role for cholesterol in promoting iron-dependent oxidative damage? Ann. N. Y. Acad. Sci. *1012*, 51–64.

Ortiz, E., Pasquini, J.M., Thompson, K., Felt, B., Butkus, G., Beard, J., and Connor, J.R. (2004). Effect of manipulation of iron storage, transport, or availability on myelin composition and brain iron content in three different animal models. J. Neurosci. Res. *77*, 681–689.

Ou, J., He, Y., Xiao, X., Yu, T.M., Chen, C., Gao, Z., and Ho, M.S. (2014). Glial cells in neuronal development: Recent advances and insights from Drosophila melanogaster. Neurosci. Bull. *30*, 584–594.

Palgi, M., Lindström, R., Peränen, J., Piepponen, T.P., Saarma, M., and Heino, T.I. (2009). Evidence that DmMANF is an invertebrate neurotrophic factor supporting dopaminergic neurons. Proc. Natl. Acad. Sci. U. S. A. *106*, 2429–2434.

Pantopoulos, K. (2004). Iron metabolism and the IRE/IRP regulatory system: an update. Ann. N. Y. Acad. Sci. *1012*, 1–13.

Paradkar, P.N., Zumbrennen, K.B., Paw, B.H., Ward, D.M., and Kaplan, J. (2009). Regulation of mitochondrial iron import through differential turnover of mitoferrin 1 and mitoferrin 2. Mol. Cell. Biol. *29*, 1007–1016.

Parkinson, J. (2002). An essay on the shaking palsy. 1817. J. Neuropsychiatry Clin. Neurosci. *14*, 223–236; discussion 222.

Parton, R.G., Simons, K., and Dotti, C.G. (1992). Axonal and dendritic endocytic pathways in cultured neurons. J. Cell Biol. *119*, 123–137.

Patel, B.N., Dunn, R.J., Jeong, S.Y., Zhu, Q., Julien, J.-P., and David, S. (2002). Ceruloplasmin regulates iron levels in the CNS and prevents free radical injury. J. Neurosci. *22*, 6578–6586.

Paul, R.J., Bauer, M., and Pease, W. (1979). Vascular smooth muscle: aerobic glycolysis linked to sodium and potassium transport processes. Science (80-.). *206*, 1414–1416.

Pellerin, L., Bouzier-Sore, A.K., Aubert, A., Serres, S., Merle, M., Costalat, R., and Magistretti, P.J. (2007). Activity-dependent regulation of energy metabolism by astrocytes: An update. Glia *55*, 1251–1262.

Pereanu, W., Shy, D., and Hartenstein, V. (2005). Morphogenesis and proliferation of the larval brain glia in Drosophila. Dev. Biol. *283*, 191–203.

Pham, D.Q.D., and Winzerling, J.J. (2010). Insect ferritins: Typical or atypical? Biochim. Biophys. Acta *1800*, 824–833.

Pilling, A.D., Horiuchi, D., Lively, C.M., and Saxton, W.M. (2006). Kinesin-1 and Dynein are the primary motors for fast transport of mitochondria in Drosophila motor axons. Mol. Biol. Cell *17*, 2057–2068.

Port, F., Hausmann, G., and Basler, K. (2011). A genome-wide RNA interference screen uncovers two p24 proteins as regulators of Wingless secretion. EMBO Rep. *12*, 1144–1152.

Potter, C.J., Tasic, B., Russler, E. V., Liang, L., and Luo, L. (2010). The Q system: A repressible binary system for transgene expression, lineage tracing, and mosaic analysis. Cell *141*, 536–548.

Pozzi, C., Di Pisa, F., Bernacchioni, C., Ciambellotti, S., Turano, P., and Mangani, S. (2015). Iron binding to human heavy-chain ferritin. Acta Crystallogr. D. Biol. Crystallogr. *71*, 1909–1920.

Prousek, J. (2007). Fenton chemistry in biology and medicine. Pure Appl. Chem. *79*, 2325–2338.

Punnonen, K., Irjala, K., and Rajamäki, a (1997). Serum transferrin receptor and its ratio to serum ferritin in the diagnosis of iron deficiency. Blood *89*, 1052–1057.

Reese, T., and Karnovsky, M. (2005). From the Archive: Endothelial tigh junctions form the blood-brain barrier. J. Cell Biol. *169*, 378–379.

Rodrigues, F., Schmidt, I., and Klämbt, C. (2011). Comparing peripheral glial cell differentiation in Drosophila and vertebrates. Cell. Mol. Life Sci. *68*, 55–69.

Rodrigues, V., Cheah, P.Y., Ray, K., and Chia, W. (1995). malvolio, the Drosophila homologue of mouse NRAMP-1 (Bcg), is expressed in macrophages and in the nervous system and is required for normal taste behaviour. EMBO J. *14*, 3007–3020.

Rogers, J.T., Randall, J.D., Cahill, C.M., Eder, P.S., Huang, X., Gunshin, H., Leiter, L., McPhee, J., Sarang, S.S., Utsuki, T., et al. (2002). An iron-responsive element type II in the 5′-untranslated region of the Alzheimer's amyloid precursor protein transcript. J. Biol. Chem. *277*, 45518–45528.

Roskams, a J., and Connor, J.R. (1994). Iron, transferrin, and ferritin in the rat brain during development and aging. J. Neurochem. *63*, 709–716.

Rouault, T. a (2006). The role of iron regulatory proteins in mammalian iron homeostasis and disease. Nat. Chem. Biol. *2*, 406–414.

Rouault, T. a (2013). Iron metabolism in the CNS: implications for neurodegenerative diseases. Nat. Rev. Neurosci. *14*, 551–564.

Rouault, T.A. (2015). Mammalian iron-sulphur proteins: novel insights into biogenesis and function. Nat. Rev. Mol. Cell Biol. *16*, 45–55.

Rouault, T.A. (2016). Mitochondrial iron overload: Causes and consequences. Curr. Opin. Genet. Dev. *38*, 31–37.

Rowitch, D.H., and Kriegstein, A.R. (2010). Developmental genetics of vertebrate glial-cell specification. Nature *468*, 214–222.

Ruiz, M., Wicker-Thomas, C., Sanchez, D., and Ganfornina, M.D. (2012). Grasshopper Lazarillo, a GPI-anchored Lipocalin, increases Drosophila longevity and stress resistance, and functionally replaces its secreted homolog NLaz. Insect Biochem. Mol. Biol. *42*, 776–789.

Saab, A.S., Tzvetanova, I.D., and Nave, K.A. (2013). The role of myelin and oligodendrocytes in axonal energy metabolism. Curr. Opin. Neurobiol. *23*, 1065–1072.

Saher, G., Brügger, B., Lappe-Siefke, C., Möbius, W., Tozawa, R., Wehr, M.C., Wieland, F., Ishibashi, S., and Nave, K.-A. (2005). High cholesterol level is essential for myelin membrane growth. Nat. Neurosci. *8*, 468–475.

Saleem, S., Schwedes, C.C., Ellis, L.L., Grady, S.T., Adams, R.L., Johnson, N., Whittington, J.R., and Carney, G.E. (2012). Drosophila melanogaster p24 trafficking proteins have vital roles in development and reproduction. Mech. Dev. *129*, 177–191.

Salvador, G. a (2010). Iron in neuronal function and dysfunction. Biofactors *36*, 103–110.

Salzer, J.L. (2015). Schwann cell myelination. Cold Spring Harb. Perspect. Biol. *7*.

Salzer, J.L., Brophy, P.J., and Peles, E. (2008). Molecular domains of myelinated axons in the peripheral nervous system. Glia *56*, 1532–1540.

Sanchez, D., López-Arias, B., Torroja, L., Canal, I., Wang, X., Bastiani, M.J., and Ganfornina, M.D. (2006). Loss of glial lazarillo, a homolog of apolipoprotein D, reduces lifespan and stress resistance in Drosophila. Curr. Biol. *16*, 680–686.

Schenck, J.F., and Zimmerman, E. a (2004). High-field magnetic resonance imaging of brain iron: birth of a biomarker? NMR Biomed. *17*, 433–445.

Schmidt, I., Thomas, S., Kain, P., Risse, B., Naffin, E., and Klämbt, C. (2012). Kinesin heavy chain function in Drosophila glial cells controls neuronal activity. J. Neurosci. *32*, 7466–7476.

Schulz, J.G., David, G., and Hassan, B. a (2009). A novel method for tissue-specific RNAi rescue in Drosophila. Nucleic Acids Res. *37*, e93.

Schummers, J., Yu, H., and Sur, M. (2008). Tuned responses of astrocytes and their influence on hemodynamic signals in the visual cortex. Science *320*, 1638–1643.

Seeger, M., Tear, G., Ferres-Marco, D., and Goodman, C.S. (1993). Mutations affecting growth cone guidance in Drosophila: genes necessary for guidance toward or away from the midline. Neuron *10*, 409–426.

Seidl, A.H. (2014). Regulation of conduction time along axons. Neuroscience *276*, 126–134.

Selkoe, D.J. (1996). Amyloid beta-protein and the genetics of Alzheimer's Disease. J. Biol. Chem. *271*, 18295–18298.

Sepp, K.J., and Auld, V.J. (1999). Conversion of lacZ enhancer trap lines to GAL4 lines using targeted transposition in Drosophila melanogaster. Genetics *151*, 1093–1101.

Sepp, K.J., Schulte, J., and Auld, V.J. (2000). Developmental dynamics of peripheral glia in Drosophila melanogaster. Glia *30*, 122–133.

Sepp, K.J., Schulte, J., and Auld, V.J. (2001). Peripheral glia direct axon guidance across the CNS/PNS transition zone. Dev. Biol. *238*, 47–63.

Shan, Y., and Cortopassi, G. (2012). HSC20 interacts with frataxin and is involved in iron-sulfur cluster biogenesis and iron homeostasis.

Shandala, T., Takizawa, K., and Saint, R. (2003). The dead ringer/retained transcriptional regulatory gene is required for positioning of the longitudinal glia in the Drosophila embryonic CNS. Development *130*, 1505–1513.

Sharma, K., Schmitt, S., Bergner, C.G., Tyanova, S., Kannaiyan, N., Manrique-Hoyos, N., Kongi, K., Cantuti, L., Hanisch, U.-K., Philips, M.-A., et al. (2015). Cell type– and brain region–resolved mouse brain proteome. Nat. Neurosci. *18*, 1–16.

Shigemoto-Mogami, Y., Hoshikawa, K., Goldman, J.E., Sekino, Y., and Sato, K. (2014). Microglia enhance neurogenesis and oligodendrogenesis in the early postnatal subventricular zone. J. Neurosci. *34*, 2231–2243.

Silies, M., and Klämbt, C. (2010). APC/C(Fzr/Cdh1)-dependent regulation of cell adhesion controls glial migration in the Drosophila PNS. Nat. Neurosci. *13*, 1357–1364.

Silies, M., and Klämbt, C. (2011). Adhesion and signaling between neurons and glial cells in Drosophila. Curr. Opin. Neurobiol. *21*, 11–16.

Silies, M., Yuva-Aydemir, Y., Rut Franzdottir, S., and Klämbt, C. (2014). The eye imaginal disc as a model to study the coordination of neuronal and glial development. Fly (Austin). *4*, 71–79.

Simons, M., and Nave, K. (2015). Oligodendrocytes: Myelination and Axonal Support. Cold Spring Harb. Perspect. Biol. *8*, 1–16.

Snaidero, N., Möbius, W., Czopka, T., Hekking, L.H.P., Mathisen, C., Verkleij, D., Goebbels, S., Edgar, J., Merkler, D., Lyons, D.A., et al. (2014). Myelin membrane wrapping of CNS axons by PI(3,4,5)P3-dependent polarized growth at the inner tongue. Cell *156*, 277–290.

Spéder, P., and Brand, A.H. (2014). Gap junction proteins in the blood-brain barrier control nutrient-dependent reactivation of Drosophila neural stem cells. Dev. Cell *30*, 309–321.

Springer, S., Chen, E., Duden, R., Marzioch, M., Rowley, A., Hamamoto, S., Merchant, S., and Schekman, R. (2000). The p24 proteins are not essential for vesicular transport in Saccharomyces cerevisiae. Proc. Natl. Acad. Sci. U. S. A. *97*, 4034–4039.

Squarzoni, P., Oller, G., Hoeffel, G., Pont-Lezica, L., Rostaing, P., Low, D., Bessis, A., Ginhoux, F., and Garel, S. (2014). Microglia Modulate Wiring of the Embryonic Forebrain. Cell Rep. *8*, 1271–1279.

Stebbings, L.A., Todman, M.G., Phillips, R., Greer, C.E., Tam, J., Phelan, P., Jacobs, K., Bacon, J.P., and Davies, J.A. (2002). Gap junctions in Drosophila: Developmental expression of the entire innexin gene family. Mech. Dev. *113*, 197–205.

Stephan, R. (2008). Functional studies of the abelson interactor gene during the development of Drosophila melanogaster. Westfälische Wilhelms-Universität Münster.

Stork, T., Engelen, D., Krudewig, A., Silies, M., Bainton, R.J., and Klämbt, C. (2008). Organization and function of the blood-brain barrier in Drosophila. J. Neurosci. *28*, 587–597.

Stork, T., Thomas, S., Rodrigues, F., Silies, M., Naffin, E., Wenderdel, S., and Klämbt, C. (2009). Drosophila Neurexin IV stabilizes neuron-glia interactions at the CNS midline by binding to Wrapper. Development *136*, 1251–1261.

Stork, T., Bernardos, R., and Freeman, M.R. (2012). Analysis of glial cell development and function in Drosophila. Cold Spring Harb. Protoc. *7*, 1–17.

Strating, J.R.P.M., and Martens, G.J.M. (2009). The p24 family and selective transport processes at the ER-Golgi interface. Biol. Cell *101*, 495–509.

Stratoulias, V., and Heino, T.I. (2015). Analysis of the conserved neurotrophic factor MANF in the Drosophila adult brain. Gene Expr. Patterns *18*, 8–15.

Subbarao, K., Forrest, S., Ackley, D.H., Perelson, A.S., Bush, R.M., Bender, C.A., Cox, N.J., Galvani, A.P., Bush, R.M., Murphy, A.M., et al. (2006). Structure of Dual Function Iron Regulatory Protein 1 Complexed with Ferritin IRE-RNA. Science *314*, 1903–1909.

Suzuki, A., Stern, S.A., Bozdagi, O., Huntley, G.W., Walker, R.H., Magistretti, P.J., and Alberini, C.M. (2011). Astrocyte-neuron lactate transport is required for long-term memory formation. Cell *144*, 810–823.

Takida, S., Maeda, Y., and Kinoshita, T. (2008). Mammalian GPI-anchored proteins require p24 proteins for their efficient transport from the ER to the plasma membrane. Biochem. J. *409*, 555–562.

Tandara, L., and Salamunic, I. (2012). Iron metabolism: current facts and future directions. Biochem Med *22*, 311–328.

Tang, X., and Zhou, B. (2013a). Iron homeostasis in insects: Insights from Drosophila studies. IUBMB Life *65*, 863–872.

Tang, X., and Zhou, B. (2013b). Ferritin is the key to dietary iron absorption and tissue iron detoxification in Drosophila melanogaster. FASEB J. *27*, 288–298.

Tansey, F.A., Thampy, K.G., and Cammer, W. (1988). Acetyl-CoA carboxylase in rat brain . II . *43*, 131–138.

Taveggia, C. (2016). Schwann cells–axon interaction in myelination. Curr. Opin. Neurobiol. *39*, 24–29.

Tessier-Lavigne, M., and Goodman, C.S. (1996). The molecular biology of axon guidance. Science *274*, 1123–1133.

Thomas, A., Lee, P.-J., Dalton, J.E., Nomie, K.J., Stoica, L., Costa-Mattioli, M., Chang, P., Nuzhdin, S., Arbeitman, M.N., and Dierick, H. a (2012). A versatile method for cell-specific profiling of translated mRNAs in Drosophila. PLoS One *7*, e40276.

Tiklová, K., Senti, K.-A., Wang, S., Gräslund, A., and Samakovlis, C. (2010). Epithelial septate junction assembly relies on melanotransferrin iron binding and endocytosis in Drosophila. Nat. Cell Biol. *12*, 1071–1077.

Todorich, B., Zhang, X., Slagle-Webb, B., Seaman, W.E., and Connor, J.R. (2008). Tim-2 is the receptor for H-ferritin on oligodendrocytes. J. Neurochem. *107*, 1495–1505.

Todorich, B., Pasquini, J.M., Garcia, C.I., Paez, P.M., and Connor, J.R. (2009). Oligodendrocytes and myelination: the role of iron. Glia *57*, 467–478.

Todorich, B., Zhang, X., and Connor, J.R. (2011). H-ferritin is the major source of iron for oligodendrocytes. Glia *59*, 927–935.

Tsacopoulos, M., and Magistretti, P.J. (1996). Metabolic coupling between glia and neurons. J. Neurosci. *16*, 877–885.

Urbán, N., and Guillemot, F. (2014). Neurogenesis in the embryonic and adult brain: same regulators, different roles. Front. Cell. Neurosci. *8*, 396.

Vahedi, K., Kubis, N., Boukobza, M., Arnoult, M., Massin, P., Tournier-Lasserve, E., and Bousser, M.G. (2007). COL4A1 mutation in a patient with sporadic, recurrent intracerebral hemorrhage. Stroke *38*, 1461–1464.

Vannucci, S.J., and Simpson, I. a (2003). Developmental switch in brain nutrient transporter expression in the rat. Am. J. Physiol. Endocrinol. Metab. *285*, E1127–E1134.

Vetrivel, K.S., Gong, P., Bowen, J.W., Cheng, H., Chen, Y., Carter, M., Nguyen, P.D., Placanica, L., Wieland, F.T., Li, Y.-M., et al. (2007). Dual roles of the transmembrane protein p23/TMP21 in the modulation of amyloid precursor protein metabolism. Mol. Neurodegener. *2*, 4.

Virchow, R.L.K. (1871). Die Cellularpathologie in ihrer Begründung auf physiologische und pathologische Gewebelehre (Berlin, Unter den Linden: Verlag von August Hirschfeld).

Volkenhoff, A., Weiler, A., Letzel, M., Stehling, M., Klämbt, C., and Schirmeier, S. (2015). Glial glycolysis is essential for neuronal survival in drosophila. Cell Metab. *22*, 437–447.

Volterra, A., and Meldolesi, J. (2005). Astrocytes, from brain glue to communication elements: the revolution continues. Nat. Rev. Neurosci. *6*, 626–640.

Wang, W., Knovich, M.A., Coffman, L.G., Torti, F.M., and Torti, S. V (2010). Serum ferritin: Past, present and future. Biochim. Biophys. Acta *1800*, 760–769.

Waxman, S.G., and Ritchie, J.M. (1993). Molecular dissection of the myelinated axon. Ann. Neurol. *33*, 121–136.

Wong, B.X., and Duce, J.A. (2014). The iron regulatory capability of the major protein participants in prevalent neurodegenerative disorders. Front. Pharmacol. *5 APR*.

Xiao, G., Wan, Z., Fan, Q., Tang, X., and Zhou, B. (2014). The metal transporter ZIP13 supplies iron into the secretory pathway in Drosophila melanogaster. Elife *3*, e03191.

Xiong, W.C., Okano, H., Patel, N.H., Blendy, J.A., and Montell, C. (1994). repo encodes a glial-specific homeo domain protein required in the Drosophila nervous system. Genes Dev. *8*, 981–994.

Yan, L.J., Levine, R.L., and Sohal, R.S. (1997). Oxidative damage during aging targets mitochondrial aconitase. Proc. Natl. Acad. Sci. U. S. A. *94*, 11168–11172.

Yoshiga, T., Georgieva, T., Dunkov, B.C., Harizanova, N., Ralchev, K., and Law, J.H. (1999). Drosophila melanogaster transferrin: Cloning, deduced protein sequence, expression during the life cycle, gene localization and up-regulation on bacterial infection. Eur. J. Biochem. *260*, 414–420.

Yu, G.S., Steinkirchner, T.M., Rao, G.A., and Larkin, E.C. (1986). Effect of prenatal iron deficiency on myelination in rat pups. Am. J. Pathol. *125*, 620–624.

Yuasa, Y. (2003). Drosophila homeodomain protein REPO controls glial differentiation by cooperating with ETS and BTB transcription factors. Development *130*, 2419–2428.

Zala, D., Hinckelmann, M.-V., Yu, H., Lyra da Cunha, M.M., Liot, G., Cordelières, F.P., Marco, S., and Saudou, F. (2013). Vesicular glycolysis provides on-board energy for fast axonal transport. Cell *152*, 479–491.

Zecca, L., Youdim, M.B.H., Riederer, P., Connor, J.R., and Crichton, R.R. (2004). Iron, brain ageing and neurodegenerative disorders. Nat. Rev. Neurosci. *5*, 863–873.

Zhang, X., Surguladze, N., Slagle-Webb, B., Cozzi, A., and Connor, J.R. (2006). Cellular iron status influences the functional relationship between microglia and oligodendrocytes. Glia *54*, 795–804.

Zhu, Z.J., Wu, K.C., Yung, W.H., Qian, Z.M., and Ke, Y. (2016). Differential interaction between iron and mutant alpha-synuclein causes distinctive Parkinsonian phenotypes in Drosophila. Biochim. Biophys. Acta - Mol. Basis Dis. *1862*, 518–525.

Zuchero, J.B., and Barres, B.A. (2013). Intrinsic and extrinsic control of oligodendrocyte development. Curr. Opin. Neurobiol. *23*, 914–920.

I

Appendix

Table 16: Primer designed and used in this study. Note that primers used for generation of pENTR plasmids for Gateway based cloning contain a CACC sequence for site directed insertion. Primers were synthesized by AGCT Lab (Core facility, MPI experimental medicine).

Cloning Primer	Sequence 5' - 3'	Description
pENTR_p24-1 for	CACCATGAACACACAAATCGTTGTATT	cloning Primer #1 forward, pENTR_p24-1
pENTR_p24-1 S rev	CTACAGCCGCCCGTAGTGTGC	cloning Primer #1 reverse, pENTR_p24-1_Stop
pENTR_p24-1 OS rev	CAGCCGCCCGTAGTGTGCCTG	cloning Primer #1 reverse, pENTR_p24-1_ohneStop
pENTR_p24-1 D_OUT rev	CAGCACCATAATCTGGACGAGAC	cloning Primer #1 reverse, pENTR_p24-1 delta outside
pENTR_p24-1 sb_Gold rev	CCGCTGATTGAGATCTTCGGC	cloning Primer #1 reverse, pENTR_p24-1 GOLD soluble
pENTR_Fer1HC O.S. rev	CAGGGTCTTGTCGAACAGGAAC	cloning Primer #1 reverse, pENTR_Ferritin1HC ohne Stop
pENTR_Fer1HC for	CACCATGGTGAAACTAATTGCTAGCC	cloning Primer #1 forward, pENTR_Ferritin1HC Iso A-D
pENTR_Fer1HC rev	TTACAGGGTCTTGTCGAACAGGA	cloning Primer #1 reverse, pENTR_Ferritin1HC
MUTA Fer1HC FLAG for	GATGACTACAAAGACGATGACGACAAGTTCAAGTGCTCCCTGGCTGTTCCTGAGATTACCAAG	mutagenesis Primer #1 forward, pENTR_Ferritin1HC FLAG
MUTA Fer1HC FLAG rev	GAACTTGTCGTCATCGTCTTTGTAGTCATCTCCATAGGCCTGGGCCACCACGGCC	mutagenesis Primer #1 reverse, pENTR_Ferritin1HC FLAG
attB land site for	GTCGACGATGTAGGTCACGGTC	cloning primer forward attB landing site
attB land site rev	GTCGACATGCCCGCCGTG	cloning primer reverse attB landing site
attB land site rev	CATCAAGTCTAGACTAGTAAAGACGCTGGGGC	cloning primer reverse Rpl10a with XbaI and linker
MUTA FLAG-HA for	CACGACTACAAAGACGATGACGACAAGCGCGGTGGAGGCCGCATCTTTTACCCATACGATGTTCC	mutagenesis Primer FLAG HA pUAST attB
MUTA FLAG-HA rev	GCGCTTGTCGTCATCGTCTTTGTAGTCGTGGAGATCCATTCTAGCAGATATCACCACTTTGTACAAGAAAGCTGAACG	mutagenesis Primer FLAG HA pUAST attB rev
Rpl10ab-XbaI rev	CATCAAGTCTAGACTAGTAAAGACGCTGGGGC	cloning primer reverse Rpl10a with XbaI and linker
GFP for with Eco for	GTTACAGAATTCCACCATGGTGAGCAAGGGCGA	cloning primer forward GFP with EcoRI , Kozak and linker, GFP-Rpl10ab
HA for with Eco for	GTTACAGAATTCCACCATGTACCCATACGACGTCCC	cloning primer forward HA with EcoRI , Kozak and linker, HA-Rpl10ab
pENTR_p24-1Viri for	CACCATGCGCGACGAGCAGCTGAATAA	cloning Primer #1 forward, pENTR_p24-1 D.viri
pENTR_p24-1Viri S rev	TTACAGGCGACCATAGCGCGC	cloning Primer #1 reverse, pENTR_p24-1Viri mit Stop

pENTR_p24-1Viri o.S. rev	CAGGCGACCATAGCGCGC	cloning Primer #1 reverse, pENTR_p24-1Viri mit ohneStop

PCR Primer	Sequence 5' - 3'	Description
QF2 for	ATGCCGACGGACACGCCGACG	PCR primer forward QF2 and QF2w
QF2 rev	GAGGCCGTAGCCGTGGCGGTAGG	PCR primer reverse QF2 and QF2w
LandSite 51D rev	CAGGTAGTTGAGGAGCTAACGTC	PCR Primer for genomic localization of landing site 51D reverse
LandSite 22A rev	GCCGTGCAAAGACAGCTCTCG	PCR Primer for genomic localization of landing site 22A reverse
LandSite 51C rev	GAGCCACAATGAGCTGGAGTAGC	PCR Primer for genomic localization of landing site 51C reverse
PCR p24-1 for	GAACCCCAGACCTATCGTGCGGCG	PCR Primer #1 forward, p24-1
PCR p24-1 rev	TGACGCCCTTCTATTGAAACGCTTTGTG	PCR Primer #1 reverse, p24-1
UAS for	CGGAGTACTGTCCTCCGAG	PCR primer forward UAS
repo for	ATGAAGCTACTGTCTTCTATCG	PCR primer Gal4 for
repo rev	AAGAGCATCCCTGGGCATAAA	PCR primer Gal4 rev
UAS for	CGGAGTACTGTCCTCCGAG	PCR primer forward UAS
PCR p24-1 for	GAACCCCAGACCTATCGTGCGGCG	PCR Primer #1 forward, p24-1
PCR p24-1 rev	TGACGCCCTTCTATTGAAACGCTTTGTG	PCR Primer #1 reverse, p24-1

Table 17: Fly transformation plasmids generated in this work. Note that different strategies (Gateway system, conventional cloning and PCR site directed insertion) were used to generate plasmids. pUAST and pQUAST harbor an *ampicillin resistance* gene for selection. The attB landing can be used for site directed insertion into the fly genome.

Plasmid	Cloning strategy
pUASTattB-p24-1	Gateway with pENTR-p24-1
pUASTattB-p24-1-GFP	Gateway with pENTR-p24-1 w/o stop
pUASTattB-p24-1-ΔOUT-HA	Gateway with pENTR-p24-1 Δout w/o stop
pUASTattB-p24-1-ΔOUT-GFP	Gateway with pENTR-p24-1 Δout w/o stop
pUASTattB-p24-1-HA	Gateway with pENTR-p24-1 w/o stop
pUASTattB-Myc-p24-1	Gateway with pENTR-p24-1
pUASTattB-p24-1 stringDNA-GFP	Gateway with pENTR-p24-1 stringDNA w/o stop
pUASTattB-p24-1 [*D.Viri*]-HA	Gateway with pENTR-p24-1 [*D.virilis*] w/o stop
pUASTattB-RfA-FLAG-HA	PCR site directed insertion of FLAG-HA
pUASTattB-p24-1 FLAG-HA	Gateway with pENTR-p24-1 w/o stop
pUASTattB-p24-1-ΔOUT-FLAG-HA	Gateway with pENTR-p24-1 Δout w/o stop
pUASTattB-Fer1HCH-GFP	Gateway with pENTR-Fer1HCH w/o stop
pUASTattB-Fer1HCH-HA	Gateway with pENTR-Fer1HCH w/o stop
pUASTattB-SP-FLAG-Fer1HCH	PCR site directed insertion of FLAG between signal peptide and ORF
pQUASTattB	Conventional cloning of attB in *StuI* restriction site
pQUASTattb-GFP-Rpl10ab	Conventional cloning of GFP-RPL10ab with *EcoI* and *XbaI* in MCS
pQUAST-attb-HA-Rpl10ab	Conventional cloning of HA-RPL10ab with *EcoI* and *XbaI* in MCS

Table 18: Screened RNAi lines. PNS defects observed upon confocal analysis are indicated (X).

Gene ID	Gene name	VDRC ID	PNS defect
FBgn0037092	M6	101757	
FBgn0261822	Bsg	2789	
FBgn0011708	Syx5	108928	x
FBgn0036211	CG5946	110688	x
FBgn0002543	robo2	11823	
FBgn0004456	mew	109608	
FBgn0250874	ttm50	5587	x
FBgn0000108	Appl	42673	x
FBgn0039734	Tace	2733	
FBgn0037710	CG9393	44400	
FBgn0026438	Eaat2	104371	
FBgn0051547	CG31547	105911	
FBgn0004868	Gdi	26537	x
FBgn0036843	CG6812	8534	
FBgn0037240	Cont	40613	x
FBgn0029870	Marf	40478	
FBgn0051229	CG31229	9660	
FBgn0031500	CG17221	25229	x
FBgn0033020	COX4L	106700	
FBgn0002921	Atpalpha	12330	
FBgn0015399	kek1	36252	x
FBgn0035032	ATPsynF	13324	
FBgn0029687	Vap-33A	30404	x
FBgn0033451	CG1665	9958	
FBgn0039213	atl	6719	x
FBgn0000071	Ama	22944	x
FBgn0013997	Nrx-IV	9039	x
FBgn0051619	nolo	33102	
FBgn0035523	CG1311	39695	
FBgn0031392	AIF	2544	
FBgn0030341	p24-1	12196	x
FBgn0083950	CG34114	103456	x
FBgn0261260	mgl	103661	
FBgn0000497	ds	36219	

Gene ID	Gene name	VDRC ID	PNS defect
FBgn0035587	Gdap1	106485	
FBgn0261862	whd	4047	x
FBgn0032949	Lamp1	7309	
FBgn0034753	CG2852	15069	x
FBgn0010473	tutl	3064	
FBgn0025678	CaBP1	43148	
FBgn0038038	CG5167	6092	
FBgn0032833	COX4	3923	x
FBgn0028692	Rpn2	44135	x
FBgn0015623	Cpr	44232	
FBgn0013343	Syx1A	33112	x
FBgn0005666	bt	46253	x
FBgn0030887	CG6867	37416	x
FBgn0031981	CG7466	42462	x
FBgn0023537	CG17896	107006	
FBgn0030035	CG11190	14821	
FBgn0023549	Mct1	106773	
FBgn0027865	Tsp96F	3422	
FBgn0265296	Dscam2	1100	
FBgn0036509	CG7739	51521	x
FBgn0024947	NTPase	7265	x
FBgn0050491	CG30491	12817	
FBgn0004619	GluRIA	44439	
FBgn0033906	CG8331	105290	
FBgn0263219	Dscam4	25365	
FBgn0036821	CG3961	37305	
FBgn0250876	Sema-5c	9428	x
FBgn0034368	CG5482	4991	
FBgn0265140	Meltrin	3704	x
FBgn0027786	Mtch	106996	
FBgn0032679	bsf	22837	
FBgn0034645	ND-B12	8837	x
FBgn0029131	Debcl	47517	x
FBgn0262870	axo	107491	x

Gene ID	Gene name	VDRC ID	PNS defect
FBgn0259214	PMCA	101743	x
FBgn0026439	Eaat1	109401	
FBgn0039688	Kul	28347	x
FBgn0259110	mmd	103449	x
FBgn0014868	Ost48	105881	
FBgn0005631	robo1	42241	
FBgn0039709	Cad99C	27211	
FBgn0039140	Miro	106683	x
FBgn0021764	sdk	9437	
FBgn0053113	Rtnl1	7866	
FBgn0011259	Sema-1a	36147	x
FBgn0051072	Lerp	1251	
FBgn0042135	CG18812	39224	
FBgn0037239	CG11739	44562	x
FBgn0025608	Faf2	107414	x
FBgn0004919	gol	37435	x
FBgn0025741	PlexA	4740	
FBgn0030883	CG7772	30431	
FBgn0263006	SERCA	4474	
FBgn0019886	Letm1	6662	
FBgn0037756	CG8507	42640	
FBgn0000447	Dhod	51061	
FBgn0053303	CG33303	107778	
FBgn0039689	CIA30	14861	
FBgn0010051	Itp-r83A	106982	x
FBgn0259714	DIP-epsilon	23490	x
FBgn0033324	CG14744	40829	
FBgn0265042	Irk1	28431	
FBgn0266758	Esyt2	28418	
FBgn0264975	Nrg	27202	
FBgn0000635	Fas2	36351	
FBgn0034997	CG3376	12226	x
FBgn0026409	Mpcp	8366	x
FBgn0036279	Ncc69	106499	x
FBgn0283499	InR	992	
FBgn0000464	Lar	36270	x

Gene ID	Gene name	VDRC ID	PNS defect
FBgn0035798	frac	104254	
FBgn0028671	Vha100-1	22925	
FBgn0267828	Fatp	9406	
FBgn0032850	Kua	101360	x
FBgn0028331	l(1)G0289	1054	
FBgn0035600	Cyt-c1	9180	
FBgn0261985	Ptpmeg	38652	x
FBgn0260743	GC1	106319	
FBgn0033095	CG3409	37141	x
FBgn0003360	sesB	48582	x
FBgn0038837	CG3822	4085	x
FBgn0032536	Ance-3	43198	
FBgn0035519	CG1309	37227	
FBgn0001250	if	5600	x
FBgn0265187	CG44252	3528	
FBgn0039528	dsd	1106	
FBgn0011455	ND-SGDH	11381	x
FBgn0050404	Tango11	29385	
FBgn0038975	Nrx-1	36328	
FBgn0035473	mge	109502	x
FBgn0034497	CG9090	44297	x
FBgn0267849	Syx7	107264	x
FBgn0036702	CG6512	8515	x
FBgn0030703	MSBP	45185	x
FBgn0015031	cype	13403	
FBgn0039830	ATPsynC	106834	
FBgn0039651	Cyt-c1L	106229	
FBgn0035588	CG10672	18661	
FBgn0004242	Syt1	8875	x
FBgn0028369	kirre	3111	
FBgn0019957	ND-42	110787	
FBgn0031401	papi	2554	
FBgn0024189	sns	109442	
FBgn0023529	CG2918	18440	
FBgn0011592	fra	16923	
FBgn0013675	mt:CoII	109401	

Table 19: Screen list of secreted and IgSF candidates. Lethality observed upon neuronal + glial (NG), glial (G) and neuronal (N) is indicated (X).

Gene ID	Gene name	VDRC ID	NG	G	N
FBgn0034920	CG5597	12875			
FBgn0261822	Bsg	105293			
FBgn0010238	Lac	107450	x	x	
FBgn0013433	beat-Ia	4543			
FBgn0034730	ppk12	105131			
FBgn0002543	robo2	11823			
FBgn0259716	CG42370	110244			
FBgn0001257	ImpL2	106543	x		x
FBgn0039431	plum	101135			
FBgn0025878	wrapper	105314	x		x
FBgn0031016	kek5	47768			
FBgn0024189	sns	877			
FBgn0083950	CG34114	103456			
FBgn0037240	Cont	40613	x	x	
FBgn0015399	kek1	101166			
FBgn0036146	CG14141	43017			
FBgn0000071	Ama	22944			
FBgn0052311	zormin	104689			
FBgn0051619	nolo	104736	x		
FBgn0267728	otk2	106266			
FBgn0032006	Pvr	105353	x	x	
FBgn0000636	Fas3	100642	x		x
FBgn0041097	robo3	44702			
FBgn0030723	dpr18	983			
FBgn0028482	bdl	109857			
FBgn0032629	beat-IIIc	109015			
FBgn0052057	dpr10	103511			
FBgn0038092	beat-Vb	106502			
FBgn0259245	DIP-beta	106021			
FBgn0038282	dpr9	38690			
FBgn0005631	robo1	100624			
FBgn0265607	beat-IIIa	45866			
FBgn0261871	dpr2	29742	x	x	
FBgn0085420	DIP-delta	42353			
FBgn0036145	CG7607	9208			
FBgn0000633	fas	102073	x		x
FBgn0265002	CG44153	44494			
FBgn0021764	sdk	106217			
FBgn0053543	CG33543	17859			
FBgn0028644	beat-Ic	105066	x		x
FBgn0003137	Ppn	108005			
FBgn0053512	dpr4	102905			
FBgn0003495	spz	105017			
FBgn0051361	dpr17	100978	x		x

Gene ID	Gene name	VDRC ID	NG	G	N
FBgn0014007	Ptp69D	104761	x		x
FBgn0033159	Dscam1	108835			
FBgn0039584	beat-VI	105798	x		x
FBgn0038494	beat-IIb	104935			
FBgn0010473	tutl	108746			
FBgn0052791	DIP-alpha	104044			
FBgn0261046	Dscam3	6685			
FBgn0029082	hbs	105913	x		x
FBgn0038084	beat-Vc	102793	x		x
FBgn0005592	btl	110277			
FBgn0052311	zormin	101304	x		x
FBgn0032479	CG16974	100366	x		x
FBgn0265296	Dscam2	1100			
FBgn0005666	bt	46253	x		
FBgn0267911	trol	110494			
FBgn0259245	DIP-beta	49553			
FBgn0030887	CG6867	37416			
FBgn0051708	DIP-zeta	107866			
FBgn0030174	CG15312	101286			
FBgn0034724	babos	36304			
FBgn0037107	CG7166	107945			
FBgn0040388	boi	108265			
FBgn0031627	CG15630	107797			
FBgn0085382	CG34353	102326			
FBgn0265002	CG44153	102832			
FBgn0037908	dpr5	102228			
FBgn0035170	dpr20	101673	x		
FBgn0034788	CG13532	105696			
FBgn0085400	CG34371	22710			
FBgn0000547	ed	104279			
FBgn0086604	CG12484	104814			
FBgn0034013	unc-5	110155			
FBgn0051431	CG31431	104697	x		x
FBgn0029974	dpr14	102040			
FBgn0053202	dpr11	23243			
FBgn0030466	CG15744	1096			
FBgn0038087	beat-Va	102698	x		x
FBgn0051774	fred	101138	x		x
FBgn0028645	beat-Ib	101662			
FBgn0004839	otk	104688	x		x
FBgn0083949	CG34113	101967			
FBgn0037993	dpr15	46245			
FBgn0017590	klg	108818			

Gene ID	Gene name	VDRC ID	NG	G	N
FBgn0034286	dpr13	107676	x		x
FBgn0034723	CG13506	104632			
FBgn0053481	dpr7	106546	x		x
FBgn0039089	beat-IV	52413			
FBgn0259245	DIP-beta	107402	x		x
FBgn0250908	beat-VII	102329			
FBgn0011828	Pxn	107180	x	x	
FBgn0037736	CG12950	106353			
FBgn0003285	rst	27223			
FBgn0028370	kek3	6354			
FBgn0263219	Dscam4	23488			
FBgn0264975	Nrg	107991	x	x	
FBgn0051646	DIP-theta	100781			
FBgn0000635	Fas2	103807	x		x
FBgn0053519	Unc-89	106267			
FBgn0038156	CG14372	16636			
FBgn0000464	Lar	107996			
FBgn0037295	dpr16	102628	x		
FBgn0011592	fra	16923			
FBgn0053516	dpr3	6692	x		
FBgn0031756	CG13992	2642			
FBgn0051814	CG31814	102224	x		
FBgn0051806	CG31806	107474			
FBgn0262509	nrm	104295			
FBgn0039862	kek6	109681	x		x
FBgn0040823	dpr6	103521			
FBgn0031872	ihog	102602			
FBgn0035410	CG14964	43603			
FBgn0086906	sls	47298	x	x	
FBgn0053202	dpr11	107548	x		x
FBgn0052600	dpr8	106791			
FBgn0263219	Dscam4	25365			
FBgn0015400	kek2	4745			
FBgn0011260	Sema-2a	15810			
FBgn0016061	side	1283			
FBgn0034083	lbk	106679			
FBgn0031837	DIP-iota	18054			
FBgn0085414	dpr12	44740			
FBgn0053516	dpr3	106517	x		x
FBgn0036454	CG17839	100149			
FBgn0028369	kirre	109585			
FBgn0259213	CG42313	103687			
FBgn0032484	kek4	105647			
FBgn0040726	dpr1	33816			
FBgn0266801	CG45263	102322			
Fbgn0032233	dpr19	110059			
FBgn0039617	DIP-gamma	104056	x		x
FBgn0003984	vn	109437	x		
FBgn0001114	Glt	15428			

Gene ID	Gene name	VDRC ID	NG	G	N
FBgn0003034	SP	109175	x		x
FBgn0264810	Pburs	102690	x		
FBgn0004360	Wnt2	104338			
FBgn0025583	IM2	46291			
FBgn0027109	NPF	108772			
FBgn0002563	Lsp1beta	35584			
FBgn0032144	CG17633	13283	x		
FBgn0015584	Acp53Ea	52435			
FBgn0034329	IM1	8812			
FBgn0043577	PGRP-SB2	106538			
FBgn0014411	Vps26	110384	x	x	x
FBgn0025456	CREG	108999			
FBgn0039298	to	100079			
FBgn0011581	Ms	108760	x		x
FBgn0011746	ana	9287			
FBgn0031701	TotM	106727			
FBgn0002863	Acp95EF	6853			
FBgn0014076	Vm32E	102810			
FBgn0005391	Yp2	50156	x	x	
FBgn0004240	DptA	104287	x	x	
FBgn0043575	PGRP-SC2	104578	x		x
FBgn0040813	Nplp2	15305			
FBgn0003865	tsg	108750			
FBgn0036713	Mip	106076			
FBgn0020277	lush	102307	x		x
FBgn0010388	Dro	105251			
FBgn0040717	Nplp4	104662			
FBgn0030099	CG12056	108336			
FBgn0000594	Est-P	30870			
FBgn0000278	CecB	103148			
FBgn0000592	Est-6	35607			
FBgn0034328	IM23	15385			
FBgn0262728	Pal2	102238			
FBgn0001112	Gld	108361	x		x
FBgn0011279	Obp69a	39523			
FBgn0011694	EbpII	103004			
FBgn0010225	Gel	37865			
FBgn0004009	wg	13352			
FBgn0038134	wntD	107727			
FBgn0264089	sli	108853	x	x	
FBgn0036565	CG5235	108305			
FBgn0015585	Acp63F	106565			
FBgn0023178	Pdf	50750			
FBgn0039678	Obp99a	100475	x	x	x
FBgn0011293	a10	11478			
FBgn0010359	gammaTry	31016			
FBgn0003751	trk	51240			
FBgn0044050	Ilp3	106512			
FBgn0010295	ng3	102175	x	x	x

Gene ID	Gene name	VDRC ID	NG	G	N
Fbgn0039722	Capa	101705	x		x
FBgn0002121	l(2)gl	109604			
FBgn0261534	l(2)34Fc	12405			
FBgn0004045	Yp1	13343			
FBgn0087002	apolpp	100944			
FBgn0015001	iotaTry	43206			
FBgn0041579	AttC	101213			
FBgn0015773	NetA	108577			
FBgn0011259	Sema-1a	104505			
FBgn0043578	PGRP-SB1	101298			
FBgn0004034	y	106068			
FBgn0000808	gd	14892			
FBgn0267327	Acp33A	109126			
FBgn0030310	PGRP-SA	5594			
FBgn0064237	Idgf5	100977			
FBgn0000658	fj	6774			
FBgn0034468	Obp56a	100850			
FBgn0035092	Nplp1	107116			
FBgn0030695	PGRP-LE	23664			
FBgn0000533	ea	102357			
FBgn0000427	dec-1	22940			
FBgn0028396	TotA	106548			
FBgn0000277	CecA2	9715			
FBgn0015583	Acp29AB	100995			
FBgn0010357	betaTry	102898			
FBgn0034470	Obp56d	100671			
FBgn0000299	Col4a1	104536	x		x
FBgn0034803	CG9849	12852			
FBgn0010296	ng4	104038	x		x
FBgn0016122	Acer	3324			
FBgn0003450	snk	107337			
FBgn0013767	Crz	106876			
FBgn0000715	FMRFa	37965			
FBgn0010385	Def	102437			
FBgn0003390	shf	14803			
FBgn0069242	eca	101388			
FBgn0010453	Wnt4	104671	x		x
FBgn0267327	Acp33A	50979			
FBgn0029838	CG4666	109818			
FBgn0010114	hig	109863	x		
FBgn0011281	Obp83a	102733			
FBgn0002856	Acp26Ab	107536			
FBgn0028374	Hug	107771			
FBgn0011554	etaTry	33233			
FBgn0000359	Cp36	14824			
FBgn0033367	PPO2	107772			
FBgn0020416	Idgf1	12414			

Gene ID	Gene name	VDRC ID	NG	G	N
FBgn0003979	Vm26Aa	101812			
FBgn0004569	aos	47180	x		
FBgn0261987	Pxt	104446	x	x	
FBgn0004644	hh	1402			
FBgn0283462	IMPPP	12843			
FBgn0067905	IM14	110032			
FBgn0011669	Mst57Db	29219			
FBgn0010294	ng2	109556	x	x	x
FBgn0020509	Acp62F	107475	x		x
FBgn0044048	Ilp5	105004	x		
FBgn0002562	Lsp1alpha	101101			
FBgn0011591	fng	51977			
FBgn0001254	ImpE2	100148	x		x
FBgn0041581	AttB	52342			
FBgn0000500	Dsk	106592			
FBgn0003313	sala	100432	x		x
FBgn0044028	Notum	103775			
FBgn0004552	Akh	105063			
FBgn0002564	Lsp1gamma	38129			
FBgn0045866	bai	100612	x		x
FBgn0044046	Ilp7	105024			
FBgn0002926	ndl	102818			
FBgn0011559	Acp36DE	105453			
FBgn0030251	CG2145	110580			
FBgn0050031	CG30031	38031			
FBgn0014865	Mtk	109740			
FBgn0035806	PGRP-SD	107879			
FBgn0004956	upd1	3282			
FBgn0030926	psh	18543			
FBgn0011283	Obp28a	103254			
FBgn0020414	Idgf3	12423			
FBgn0023496	Lip1	105572	x		
FBgn0002565	Lsp2	109979			
FBgn0036141	wls	103812			
FBgn0025615	Torsin	110073			
FBgn0003866	tsh	16892			
FBgn0011653	mas	103955	x		
FBgn0039685	Obp99b	109839			
FBgn0040323	GNBP1	107100	x		x
FBgn0004047	Yp3	46785			
FBgn0011282	Obp84a	1849			
FBgn0034475	Obp56h	102562			
FBgn0031381	Npc2a	106771			
FBgn0036545	GXIVsPLA2	100558			
FBgn0011695	EbpIII	100157			
FBgn0086782	amn	5606			
FBgn0044811	TotF	101199			

Gene ID	Gene name	VDRC ID	NG	G	N
FBgn0011670	Mst57Dc	106728			
FBgn0038901	Burs	102204	x		x
FBgn0044810	TotX	100514	x		x
FBgn0042201	Nplp3	105584			
FBgn0000564	Eh	44967	x		
FBgn0011668	Mst57Da	40694			
FBgn0016031	lama	107629	x		x
FBgn0000358	Cp19	110305			
FBgn0003980	Vm26Ab	103228	x		x
FBgn0000719	fog	101125	x	x	
FBgn0030501	BthD	45975	x	x	
FBgn0044047	Ilp6	102465	x		x
FBgn0002855	Acp26Aa	41193			
FBgn0010194	Wnt5	101621			
FBgn0005590	scw	21400			
FBgn0040736	IM3	104908			
FBgn0011294	a5	100657			
FBgn0028418	Lk	14091			
FBgn0031902	Wnt6	104020	x		x
FBgn0267348	LanB2	104013	x		x
FBgn0000356	Cp16	104999	x	x	x
FBgn0038838	TotB	51123			
FBgn0283509	Phm	104028			
FBgn0011555	thetaTry	102026			
FBgn0037976	Tk	103662	x		x
FBgn0040322	GNBP2	104094			
FBgn0003863	alphaTry	103292			
FBgn0031414	eys	107636			
FBgn0012037	Ance	41219			
FBgn0031903	Wnt10	100867	x	x	
FBgn0003983	Vm34Ca	102199	x	x	
FBgn0032048	Dh31	50295			
FBgn0015591	AstA	103215	x		x
FBgn0283461	Drs	2703			
FBgn0040321	GNBP3	37255			

Gene ID	Gene name	VDRC ID	NG	G	N
FBgn0261363	PPO3	50737			
FBgn0263597	Acp98AB	102677	x		x
FBgn0025879	Timp	109427			
FBgn0000221	brn	45457			
FBgn0024913	Actbeta	108663			
FBgn0261800	LanB1	23119			
FBgn0011556	zetaTry	108756			
FBgn0004181	Ebp	100183	x	x	
FBgn0015586	Acp76A	108698			
FBgn0031109	Obp19a	9387			
FBgn0011280	Obp19d	46707			
FBgn0000357	Cp18	102367			
FBgn0015774	NetB	100840	x	x	x
FBgn0044049	Ilp4	105516	x		x
FBgn0000094	Anp	109202			
FBgn0044812	TotC	106379			
FBgn0000355	Cp15	13860			
FBgn0010403	Obp83b	102252	x		x
FBgn0010425	epsilonTry	30807			
FBgn0026415	Idgf4	104968			
FBgn0015222	Fer1HCH	12925	x	x	
FBgn0002526	LanA	18873			
FBgn0004577	Pxd	48588			
FBgn0023415	Acp32CD	102687			
FBgn0039774	CDase	110671			
FBgn0029708	CG3556	30230			
FBgn0033327	PGRP-SC1b	51237			
FBgn0013763	Idgf6	100906			
FBgn0027095	Manf	100814			
FBgn0003867	tsl	14429			
FBgn0044051	Ilp1	5198			
FBgn0036046	Ilp2	102158	x		x
FBgn0043576	PGRP-SC1a	43201			
FBgn0037906	PGRP-LB	104557	x		x
FBgn0002933	ng1	109143	x	x	x